

1993

Fluid inclusion geochemistry and rare earth element distributions in the Oka carbonatite, Quebec.

Weining, Liu
University of Windsor

Follow this and additional works at: <http://scholar.uwindsor.ca/etd>

Recommended Citation

Liu, Weining, "Fluid inclusion geochemistry and rare earth element distributions in the Oka carbonatite, Quebec." (1993). *Electronic Theses and Dissertations*. Paper 2128.

This online database contains the full-text of PhD dissertations and Masters' theses of University of Windsor students from 1954 forward. These documents are made available for personal study and research purposes only, in accordance with the Canadian Copyright Act and the Creative Commons license—CC BY-NC-ND (Attribution, Non-Commercial, No Derivative Works). Under this license, works must always be attributed to the copyright holder (original author), cannot be used for any commercial purposes, and may not be altered. Any other use would require the permission of the copyright holder. Students may inquire about withdrawing their dissertation and/or thesis from this database. For additional inquiries, please contact the repository administrator via email (scholarship@uwindsor.ca) or by telephone at 519-253-3000ext. 3208.



National Library
of Canada

Acquisitions and
Bibliographic Services Branch

395 Wellington Street
Ottawa, Ontario
K1A 0N4

Bibliothèque nationale
du Canada

Direction des acquisitions et
des services bibliographiques

395, rue Wellington
Ottawa (Ontario)
K1A 0N4

Your file *Votre référence*

Our file *Notre référence*

NOTICE

The quality of this microform is heavily dependent upon the quality of the original thesis submitted for microfilming. Every effort has been made to ensure the highest quality of reproduction possible.

If pages are missing, contact the university which granted the degree.

Some pages may have indistinct print especially if the original pages were typed with a poor typewriter ribbon or if the university sent us an inferior photocopy.

Reproduction in full or in part of this microform is governed by the Canadian Copyright Act, R.S.C. 1970, c. C-30, and subsequent amendments.

AVIS

La qualité de cette microforme dépend grandement de la qualité de la thèse soumise au microfilmage. Nous avons tout fait pour assurer une qualité supérieure de reproduction.

S'il manque des pages, veuillez communiquer avec l'université qui a conféré le grade.

La qualité d'impression de certaines pages peut laisser à désirer, surtout si les pages originales ont été dactylographiées à l'aide d'un ruban usé ou si l'université nous a fait parvenir une photocopie de qualité inférieure.

La reproduction, même partielle, de cette microforme est soumise à la Loi canadienne sur le droit d'auteur, SRC 1970, c. C-30, et ses amendements subséquents.

**FLUID INCLUSION GEOCHEMISTRY AND RARE EARTH ELEMENT
DISTRIBUTIONS IN THE OKA CARBONATITE, QUEBEC**

by
Weining Liu

**A Thesis
Submitted to the Faculty of Graduate Studies and Research
through the Department of Geology in
Partial Fulfillment of the Requirements for the
Degree of Master of Science at the
University of Windsor**

**Windsor, Ontario, Canada
1992**



National Library
of Canada

Acquisitions and
Bibliographic Services Branch

395 Wellington Street
Ottawa, Ontario
K1A 0N4

Bibliothèque nationale
du Canada

Direction des acquisitions et
des services bibliographiques

395, rue Wellington
Ottawa (Ontario)
K1A 0N4

Your file *Votre référence*

Our file *Notre référence*

The author has granted an irrevocable non-exclusive licence allowing the National Library of Canada to reproduce, loan, distribute or sell copies of his/her thesis by any means and in any form or format, making this thesis available to interested persons.

L'auteur a accordé une licence irrévocable et non exclusive permettant à la Bibliothèque nationale du Canada de reproduire, prêter, distribuer ou vendre des copies de sa thèse de quelque manière et sous quelque forme que ce soit pour mettre des exemplaires de cette thèse à la disposition des personnes intéressées.

The author retains ownership of the copyright in his/her thesis. Neither the thesis nor substantial extracts from it may be printed or otherwise reproduced without his/her permission.

L'auteur conserve la propriété du droit d'auteur qui protège sa thèse. Ni la thèse ni des extraits substantiels de celle-ci ne doivent être imprimés ou autrement reproduits sans son autorisation.

ISBN 0-315-83026-3

Canada

Name _____

Dissertation Abstracts International is arranged by broad, general subject categories. Please select the one subject which most nearly describes the content of your dissertation. Enter the corresponding four-digit code in the spaces provided.

Geochemistry

SUBJECT TERM

0 4 9 6

SUBJECT CODE

U·M·I

Subject Categories

THE HUMANITIES AND SOCIAL SCIENCES

COMMUNICATIONS AND THE ARTS

Architecture	0729
Art History	0377
Cinema	0900
Dance	0378
Fine Arts	0357
Information Science	0723
Journalism	0391
Library Science	0399
Mass Communications	0708
Music	0413
Speech Communication	0459
Theater	0465

EDUCATION

General	0515
Administration	0514
Adult and Continuing	0516
Agricultural	0517
Art	0273
Bilingual and Multicultural	0282
Business	0688
Community College	0275
Curriculum and Instruction	0727
Early Childhood	0518
Elementary	0524
Finance	0277
Guidance and Counseling	0519
Health	0680
Higher	0745
History of	0520
Home Economics	0278
Industrial	0521
Language and Literature	0279
Mathematics	0280
Music	0522
Philosophy of	0998
Physical	0523

Psychology	0525
Reading	0535
Religious	0527
Sciences	0714
Secondary	0533
Social Sciences	0534
Sociology of	0340
Special	0529
Teacher Training	0530
Technology	0710
Tests and Measurements	0288
Vocational	0747

LANGUAGE, LITERATURE AND LINGUISTICS

Language

General	0679
Ancient	0289
Linguistics	0290
Modern	0291

Literature

General	0401
Classical	0294
Comparative	0295
Medieval	0297
Modern	0298
African	0316
American	0591
Asian	0305
Canadian (English)	0352
Canadian (French)	0355
English	0593
Germanic	0311
Latin American	0312
Middle Eastern	0315
Romance	0313
Slavic and East European	0314

PHILOSOPHY, RELIGION AND THEOLOGY

Philosophy	0422
Religion	
General	0318
Biblical Studies	0321
Clergy	0319
History of	0320
Philosophy of	0322
Theology	0469

SOCIAL SCIENCES

American Studies	0323
Anthropology	
Archaeology	0324
Cultural	0326
Physical	0327
Business Administration	
General	0310
Accounting	0272
Banking	0770
Management	0454
Marketing	0338
Canadian Studies	0385
Economics	
General	0501
Agricultural	0503
Commerce-Business	0505
Finance	0508
History	0509
Labor	0510
Theory	0511
Folklore	0358
Geography	0366
Gerontology	0351
History	
General	0578

Ancient	0579
Medieval	0581
Modern	0582
Black	0328
African	0331
Asia, Australia and Oceania	0332
Canadian	0334
European	0335
Latin American	0336
Middle Eastern	0333
United States	0337
History of Science	0585
Law	0398
Political Science	
General	0615
International Law and Relations	0616
Public Administration	0617
Recreation	0814
Social Work	0452
Sociology	
General	0626
Criminology and Penology	0627
Demography	0938
Ethnic and Racial Studies	0631
Individual and Family Studies	0628
Industrial and Labor Relations	0629
Public and Social Welfare	0630
Social Structure and Development	0700
Theory and Methods	0344
Transportation	0709
Urban and Regional Planning	0999
Women's Studies	0453

THE SCIENCES AND ENGINEERING

BIOLOGICAL SCIENCES

Agriculture	
General	0473
Agronomy	0285
Animal Culture and Nutrition	0475
Animal Pathology	0476
Food Science and Technology	0359
Forestry and Wildlife	0478
Plant Culture	0479
Plant Pathology	0480
Plant Physiology	0817
Range Management	0777
Wood Technology	0746
Biology	
General	0306
Anatomy	0287
Biostatistics	0308
Botany	0309
Cell	0379
Ecology	0329
Entomology	0353
Genetics	0369
Limnology	0793
Microbiology	0410
Molecular	0307
Neuroscience	0317
Oceanography	0416
Physiology	0433
Radiation	0821
Veterinary Science	0778
Zoology	0472
Biophysics	
General	0786
Medical	0760

EARTH SCIENCES

Biogeochemistry	0425
Geochemistry	0996

Geodesy	0370
Geology	0372
Geophysics	0373
Hydrology	0388
Mineralogy	0411
Paleobotany	0345
Paleoecology	0426
Paleontology	0418
Paleozoology	0985
Palynology	0427
Physical Geography	0368
Physical Oceanography	0415

HEALTH AND ENVIRONMENTAL SCIENCES

Environmental Sciences	0768
Health Sciences	
General	0566
Audiology	0300
Chemotherapy	0992
Dentistry	0567
Education	0350
Hospital Management	0769
Human Development	0758
Immunology	0982
Medicine and Surgery	0564
Mental Health	0347
Nursing	0569
Nutrition	0570
Obstetrics and Gynecology	0380
Occupational Health and Therapy	0354
Ophthalmology	0381
Pathology	0571
Pharmacology	0419
Pharmacy	0572
Physical Therapy	0382
Public Health	0573
Radiology	0574
Recreation	0575

Speech Pathology	0460
Toxicology	0383
Home Economics	0386

PHYSICAL SCIENCES

Pure Sciences

Chemistry

General	0485
Agricultural	0749
Analytical	0486
Biochemistry	0487
Inorganic	0488
Nuclear	0738
Organic	0490
Pharmaceutical	0491
Physical	0494
Polymer	0495
Radiation	0754
Mathematics	0405

Physics

General	0605
Acoustics	0986
Astronomy and Astrophysics	0606
Atmospheric Science	0608
Atomic	0748
Electronics and Electricity	0607
Elementary Particles and High Energy	0798
Fluid and Plasma	0759
Molecular	0609
Nuclear	0610
Optics	0752
Radiation	0756
Solid State	0611
Statistics	0463

Applied Sciences

Applied Mechanics	0346
Computer Science	0984

Engineering

General	0537
Aerospace	0538
Agricultural	0539
Automotive	0540
Biomedical	0541
Chemical	0542
Civil	0543
Electronics and Electrical	0544
Heat and Thermodynamics	0348
Hydraulic	0545
Industrial	0546
Marine	0547
Materials Science	0794
Mechanical	0548
Metallurgy	0743
Mining	0551
Nuclear	0552
Packaging	0549
Petroleum	0765
Sanitary and Municipal	0554
System Science	0790
Geotechnology	0428
Operations Research	0796
Plastics Technology	0795
Textile Technology	0994

PSYCHOLOGY

General	0621
Behavioral	0384
Clinical	0622
Developmental	0620
Experimental	0623
Industrial	0624
Personality	0625
Physiological	0989
Psychobiology	0349
Psychometrics	0632
Social	0451



2000-01-10

© Weining Liu 1992
All Rights Reserved

ABSTRACT

Two types of primary, aqueous fluid inclusions are present in monticellite, apatite and calcite from the Oka carbonatite: 1) liquid-vapour (LV) inclusions, and 2) liquid-vapour-halite (LVH) inclusions. LV inclusions have salinities of 4.3 to 24.7 wt. % and densities of 0.75 to 1.04 g/cm³, and homogenize to the liquid phase between 95 and 435°C. LVH inclusions homogenize to the liquid phase by halite dissolution between 248 to 360°C, and have salinities of 34.5 to 43.3 equiv. wt. % NaCl and densities of 1.04 to 1.25 g/cm³. The observed crystallization sequence of the host minerals was monticellite-apatite-calcite. Systematic variation in homogenization temperatures, salinities and densities of LV inclusions, combined with the crystallization sequence, suggests that type 1 fluids evolved from high to low salinity and probably from high to low temperature. The minimum pressure at which monticellite, apatite and calcite crystallized is estimated to have been about 7 to 10 kb.

The nature of the trapped minerals in the inclusions and data from leachate and decrepitate analyses indicate that the fluids in the inclusions are principally composed of Na, Cl and S (sulphate?), and contain Ca, Mg, K, Fe, Si (silicate?) in subordinate amounts. LV fluid have high Ca/Na, K/Na, and Mg/Na ratios and lower Fe/Na ratios than LVH fluid.

REE concentrations and La/Lu ratios of apatite increase with decreasing inclusion abundance in apatite and LV inclusion-rich apatites have higher REE concentrations but lower La/Lu ratios than LVH inclusion-rich apatites. This suggests that hydrothermal fluids may have removed LREE from the magma, and that the chemistry of fluids may have had an influence on REE distribution in the magma. The rare earth elements substitute for Ca in the apatite structure through the coupled substitution: $REE^{3+} + Si^{4+} \rightarrow Ca^{2+} + P^{5+}$.

Saline, aqueous, hydrothermal fluids were present during crystallization of monticellite, apatite and calcite from some of the carbonatite magmas. These fluids were principally composed of Na, Cl, sulphate and carbonate, and may have had high LREE concentrations and become a source of the late LREE mineralization in Oka.

ACKNOWLEDGEMENTS

I would like to express my gratitude to all of the people who have given assistance to me over the past three years.

In particular, I would like to thank my supervisor, Dr. Iain M. Samson of the Department of Geology, University of Windsor, for his guidance during the preparation of this thesis.

I would also like to give my thanks to Dr. Anthony E. Williams-Jones of the Department of Geological Sciences, McGill University, for his assistance during the field work in Oka and lab work at McGill University and for his advice on this thesis.

Finally, I would like to thank Mr. Antun Knitl for his instruction in the preparation of doubly-polished fluid inclusion wafers.

This work was supported by NSERC operating grants to Dr. I.M. Samson and Dr. A.E. Williams-Jones.

TABLE OF CONTENTS

	Page
ABSTRACT.....	iv
ACKNOWLEDGEMENTS.....	v
LIST OF TABLES.....	ix
LIST OF FIGURES.....	x
LIST OF ABBREVIATIONS.....	xii
LIST OF ACRONYMS.....	xiii
COMPOSITIONS OF SOME UNUSUAL MINERALS.....	xiv
 CHAPTER	
I INTRODUCTION	1
1.1 Introduction.....	1
1.2 Previous Research.....	1
1.2.1 Nature of hydrothermal fluids in carbonatites.....	1
1.2.2 REE distribution in carbonatites.....	4
1.3 Objectives.....	5
1.4 Methods.....	6
 II GEOLOGIC SETTING	 8
2.1 General Geology.....	8
2.2 Rock Types.....	8
2.3 Sequence of Events.....	10
2.4 Economic Geology.....	11
 III PETROGRAPHY.....	 12
3.1 Sampling	12
3.2 Classification of Samples.....	12
3.3 Crystallization Sequence of Primary, Fluid Inclusion- Bearing Minerals in Carbonatites.....	14

	Page
IV FLUID INCLUSION CHARACTERISTICS.....	17
4.1 Introduction.....	17
4.2 Analytical Methods.....	17
4.3 Fluid Inclusion Types.....	18
4.4 Identification of Solid Phases	19
4.5 Distribution and Origin of Fluid Inclusions.....	27
4.5.1 Primary fluid inclusions	27
4.5.2 Pseudosecondary Fluid Inclusions.....	31
4.5.3 Secondary Fluid Inclusions.....	31
V MICROTHERMOMETRY OF FLUID INCLUSIONS.....	32
5.1 Analytical Methods.....	32
5.2 Results.....	32
5.2.1 LV inclusions.....	37
5.2.2 LVH inclusions.....	39
5.3 Discussion.....	41
5.3.1 Composition and salinity of inclusions.....	41
5.3.2 Fluid evolution.....	41
5.3.3 Estimation of crystallization conditions of inclusion-bearing minerals.....	48
VI COMPOSITION OF FLUID INCLUSIONS.....	51
6.1 Introduction.....	51
6.2 Leachate Analyses.....	51
6.2.1 Experimental procedure.....	51
6.2.2 Results and discussion.....	53
6.3 Decrepitate Analyses.....	55
6.3.1 Decrepitate formation.....	55
6.3.2 Analytical procedure.....	55
6.3.3 Calculation of decrepitate composition.....	56
6.3.4 Results.....	57

	Page
6.3.5 Discussion	63
6.4 Gas Chemistry.....	66
6.4.1 Analytical methods.....	66
6.4.2 Results and discussion.....	66
VII REE GEOCHEMISTRY OF THE OKA CARBONATITE	69
7.1 Introduction.....	69
7.2 Analytical Method.....	69
7.2.1 Instrumental neutron activation analyses.....	69
7.2.2 Electron microprobe analyses.....	69
7.3 Results.....	71
7.3.1 Instrumental neutron activation analyses.....	71
7.3.2 Electron microprobe analyses.....	81
7.4 Discussion.....	82
7.4.1 Substitutions involving REE in apatite.....	82
7.4.2 Origin of LREE-rich hydrothermal fluids.....	82
7.4.3 Mineralizing potential of the Oka magmatic fluids.....	88
VIII CONCLUSIONS.....	89
REFERENCES.....	92
APPENDICES	
I SUMMARY OF THE MINERALOGY OF THE MAIN ROCK TYPES IN THE OKA CARBONATITE	98
II MICROTHEMOMETRY DATA.....	101
III RAW DATA FOR DECREPITATE ANALYSES.....	107
VITA AUCTORIS.....	109

LIST OF TABLES

	Page
1.1 Summary of solid phases in fluid inclusions in carbonatites.....	3
3.1 Summary of mineralogy of main rock types of samples.....	13
4.1 SEM instrument parameters and analysis conditions	18
4.2 Summary of solid phases in primary inclusions.....	20
4.3 Compositions of two unidentified trapped minerals.....	24
4.4 Summary of primary fluid inclusion types.....	26
5.1 Coefficients of Equation 5.1.....	32
5.2 Summary of microthermometric data for LV fluid inclusions.....	34
5.3 Summary of microthermometric data for LVH fluid inclusions.....	36
5.4 Eutectic temperatures of aqueous solutions	42
6.1 Summary of leachate analysis data.....	53
6.2 Materials used as standards for EM analysis.....	56
6.3 Chemistry of decrepitates in apatite.....	58
6.4 Summary of decrepitate analysis data from calcite.....	62
6.5 Comparison of leachate analyses and decrepitate analyses.....	65
6.6 Chemistry of fluid inclusions in apatite.....	65
7.1 Modal mineralogy and inclusion abundances in apatite.....	70
7.2 Detection limits of INAA	70
7.3 Result of apatite-standard analysis	71
7.4 INAA data of REE concentrations in whole rocks.....	72
7.5 INAA data of REE concentrations in apatites.....	72
7.6 Summary of EM data of apatites.	76

LIST OF FIGURES

	Page
2.1 Geological map of the Oka complex	9
3.1 Monticellite cut and replaced by apatite and calcite.....	14
3.2 Monticellite embayed and replaced by calcite.....	15
3.3 Apatite aggregates with interstitial calcite.....	15
3.4 Apatite as inclusions in calcite.....	16
4.1 A group of LVH inclusions with consistent phase rati.....	19
4.2 SEM view of strontianite in an opened inclusion in calcite	21
4.3 EDA spectra of strontianite in an inclusion in calcite.....	21
4.4 Raman spectra of calcite in an inclusion in apatite	22
4.5 SEM view of minerals in inclusions in apatite.....	22
4.6 Raman spectra of nahcolite in an inclusion in apatite.....	24
4.7 Raman spectra of mirabilite in an inclusion in apatite	25
4.8 Raman spectrum of mirabilite.	25
4.9 EDA spectra of V-rich amphibole in an inclusion in apatite	26
4.10 An isolated LV (S) inclusion in calcite.....	28
4.11 Elongate inclusions aligned parallel to the c-axis of the host apatite.....	29
4.12 Spheroidal LV inclusions in apatite.	29
4.13 An spheroidal LV inclusion with a "tail" in apatite.....	30
4.14 An isolated LV inclusion in monticellite.....	30
4.15 An isolated LVH inclusion in monticellite.....	31
5.1 Salinity-Th plot of LV inclusions in calcite.....	38
5.2 Salinity-Th plot of LV inclusions in apatite.....	38
5.3 Salinity-Th plot of LV inclusions in monticellite.....	38
5.4 Salinity-TdV/TdH plot of the LVH inclusions in apatite.....	39
5.5 Salinity-TdV/TdH plot of the LVH inclusions in monticellite.....	41
5.6 Phase diagram for part of the NaCl-Na ₂ CO ₃ -H ₂ O system.	41
5.7 Phase diagram for part of the NaCl-Na ₂ SO ₄ -H ₂ O system.....	43
5.8 Isotherms of the ice liquidus in the system NaCl-CaCl ₂ -H ₂ O	44
5.9 Salinity-density plot of all inclusions from the Oka carbonatite.....	45
5.10 Salinity-density plot of the LV inclusions from the Manny Zone.....	46
5.11 Salinity-density plot of the LV inclusions from the Bond Zone.	46

	Page
5.12 Salinity-density plot of the LV inclusions from the Mine.	47
5.13 Isochores for the LV inclusions.....	49
6.1 Apatite separates.....	52
6.2 SEM view of a discrete decrepitate mount in apatite.....	54
6.3 SEM view of a linear decrepitate along a fracture in apatite.....	54
6.4 EDA spectra of a decrepitate and its host apatite.....	60
6.5 Ca-K-Na plots of decrepitates from apatite.....	60
6.6 EDA spectra of a decrepitate and its host calcite.....	62
6.6 Anion deficiency-Cl plots of decrepitates from apatite.....	63
6.8 Relationship between CO ₂ concentration and Th of fluid inclusions.....	67
7.1 Chondrite-normalized curves of whole rocks.....	73
7.2 Chondrite-normalized curves of apatite.....	74
7.3 Total REE contents of whole rocks and apatites.....	75
7.4 La/Lu ratios of whole rocks and apatites.....	75
7.5 Comparison of LREE contents in two types of apatites.....	78
7.6 La-Ce-Nd plot of LV inclusion-bearing and LVH inclusion-bearing apatites.....	80
7.7 Chondrite-normalize curves of apatites containing LV-inclusions.....	80
7.8 Chondrite-normalize curves of apatites containing LVH-inclusions.....	81
7.9 REE-Si plots of apatites.....	83
7.10 REE-P plots of apatites.....	83
7.11 REE+Si - Ca+P plots of apatites.....	84
7.12 REE-Sr plots of apatites.....	84
7.13 Sr-REE/Ca plots of apatites.....	85
7.14 Chondrite-normalized curves of niocalites and apatites.....	85

LIST OF ABBREVIATIONS

Abbreviations for Minerals

Agt:	aegerine augite
Ap:	apatite
Bast*:	bastnaesite
Bt:	biotite
Cal:	calcite
Hem:	hematite
Mag:	magnetite
Ms:	muscovite
Mtc:	monticellite
Mtn*:	melanite
Nio*:	niocalite
Po:	pyrrhotite
Prv:	perovskite
Py:	pyrite
Pyr*:	pyrochlore
Ric:	richterite

Abbreviations (except *) are from Kretz (1983).

Abbreviation for Inclusion Phases

H:	halite
L:	liquid
V:	vapour
S:	trapped solid

Abbreviations for Microthermometry

Te:	eutectic temperature
TmI:	ice melting temperature
TdHh:	hydrohalite dissolution temperature

TdH: halite dissolution temperature
TdV: vapour disappearance temperature
Th: homogenization temperature
TD: decrepitate temperature

LIST OF ACRONYMS

EDA: energy dispersive analyzer
EDS: energy dispersive spectrometer
EM: electron microprobe
INAA: instrumental neutron activation analysis
LRS: laser raman spectroscopy
SEM: scanning electron microscopy
WDS: wavelength dispersive spectrometer
QMS: quadrupole mass spectrometry
REE: rare earth element
LREE: light rare earth elements (La, Ce, Nd, Pm and Sm; Henderson, 1984)
MREE: middle rare earth elements (Pm, Sm, Eu, Gd, Tb, Dy and Ho; Henderson, 1984)
HREE: heavy rare earth elements (Gd, Tb, Dy, Ho, Er, Tm, Yb and Lu; Henderson, 1984)

COMPOSITIONS OF SOME UNUSUAL MINERALS

Ancylite	$\text{SrCe}(\text{CO}_3)_2(\text{OH}) \cdot \text{H}_2\text{O}$
Bastnaesite	$(\text{Ce}, \text{La})\text{CO}_3\text{F}$
Briotholite	$(\text{Ce}, \text{La})_3(\text{SiO}_4, \text{PO}_4)_3(\text{OH}, \text{F})$
Monticellite	$\text{Ca}(\text{Mg}, \text{Fe})\text{SiO}_4$
Melanite	$\text{Ca}_3(\text{Fe}, \text{Ti})_2(\text{SiO}_4)_3$
Melilite	$\text{Ca}_2\text{MgSi}_2\text{O}_7$
Mirabilite	$\text{NaSO}_4 \cdot 10\text{H}_2\text{O}$
Nahcolite	NaHCO_3
Niocalite	$\text{Ca}_4\text{NbSi}_2\text{O}_{10}(\text{O}, \text{F})$
Parisite	$\text{Ca}(\text{Ce}, \text{La})_2(\text{CO}_3)_2\text{F}_2$
Perovskite	$\text{Ca}_2\text{Ti}_2\text{O}_6$
Pyrochlore	$(\text{Na}, \text{Ca})_2(\text{Nb}, \text{Ta})_2\text{O}_6(\text{OH}, \text{F})$
Richterite	$\text{Na}_2\text{Ca}(\text{Mg}, \text{Ti}, \text{Al})_5\text{Si}_8\text{O}_{22}(\text{OH})_2$
Synchisite	$\text{CaCe}(\text{CO}_3)_2\text{F}$

CHAPTER I

INTRODUCTION

1.1 Introduction

Several lines of evidence indicate that hydrothermal activity is associated with the emplacement of carbonatite-alkalic complexes. Petrological experiments with carbonate-silicate-water systems reveal that an aqueous vapour phase coexists with both the carbonate liquid phase and the silicate liquid phase (Koster van Groos and Wyllie, 1973; Freestone and Hamilton, 1980). Country rocks around some carbonatite-alkalic complexes have been altered to fenite by fluids that originated in either carbonatite or alkalic-silicate magma (Heinrich, 1966; Gold, 1963, 1967, 1972; Anderson, 1986). Primary fluid inclusions have been found in apatite, calcite, monticellite and fluorite from many carbonatite-alkalic complexes (Girault, 1966; Roedder, 1973; Rankin and Le Bas, 1974; Rankin, 1975 and 1977; Nesbitt and Kelly, 1977; Aspden, 1980; Haapala, 1980; Andersen, 1986).

Hydrothermal fluids have been responsible for a variety of types of mineralization in carbonatite-alkalic complexes, including REE, Nb, Th-U, Ti, fluorite, barite and apatite (Semenov, 1974; Mariano, 1989). REE-rich minerals, such as ancylite, bastnaesite, britholite, parisite and synchysite, in most carbonatites are precipitated from hydrothermal solutions (Mariano, 1989). The REE-rich minerals occur in veins, as interstitial fillings, or as fine-grained polycrystalline clusters, and are commonly associated with barite, fluorite, hematite, quartz, strontianite, and Fe-sulphides (Mariano, 1989).

In order to understand and model the genesis of hydrothermal REE mineralization, it is necessary to quantify the composition, temperatures, pressures and the evolution of the hydrothermal fluids in equilibrium with carbonatite magmas. It is also important that the relationship between the distribution of REE and the nature of the hydrothermal fluids associated with carbonatite magmas be established.

1.2 Previous Research

1.2.1 Nature of hydrothermal fluids in carbonatites

Koster van Groos and Wyllie (1973) studied the joins $Ab_{80}An_{20}-Na_2CO_3$ and

$\text{Ab}_{50}\text{An}_{50}\text{-Na}_2\text{CO}_3$ in the system $\text{NaAlSi}_3\text{O}_8\text{-CaAl}_2\text{Si}_2\text{O}_8\text{-Na}_2\text{CO}_3\text{-H}_2\text{O}$ between 650 and 950°C at 1 kb pressure. They found that an aqueous vapour phase coexisted with carbonate and silicate liquid phases, and that the vapour was rich in sodium silicate and CO_2 . Treiman and Essene (1984) calculated the composition of the fluids in equilibrium with a carbonatite magma from the Oka complex assuming that the rock they used was a eutectic assemblage. Their calculated composition is 88.2% H_2O , 11% CO_2 , 0.46% H_2 , 0.27% H_2S , 0.05% CO and 0.01% CH_4 . However, Gittins et al. (1990) argued on the basis of experimental work that the rock Treiman and Essene used was not a eutectic assemblage and that the fluids in equilibrium with the magma were not dominated by H_2O .

Four types of fluid inclusions have been found in carbonatites: gaseous inclusions, liquid-vapour aqueous inclusions, liquid-vapour-halite aqueous inclusions and CO_2 liquid- CO_2 vapour-aqueous liquid inclusions. In addition to halite, a variety of other solid phases are present in the inclusions. Some of these solids have been identified using microscopy, laser Raman spectroscopy, scanning electron microscopy (energy dispersive analysis) and are dominated by carbonates and sulphates (Table 1.1).

A minor amount of microthermometric data has been obtained from inclusions in apatite. Eutectic temperatures of aqueous inclusions range from -22 to -20°C, which suggests that NaCl and possibly KCl are the dominant ionic species in solution (Andersen, 1986). Salinities of the solutions range from 1 to 35 eq. wt% NaCl (Haapala, 1980; Andersen, 1986). Liquid-vapour inclusions homogenized to the liquid phase at temperatures between 168 and 439°C (Rankin, 1977; Aspden, 1980; Haapala, 1980; Williams-Jones, 1990), although inclusions from carbonatites in the Wasaki area of western Kenya homogenized to the liquid phase, gas phase or by critical behaviour at temperatures from 425 to 460°C (Rankin, 1975). CO_2 in CO_2 -rich inclusions melts at the triple point of pure CO_2 (-56°C), which implies that no CH_4 , N_2 , CO , H_2S or SO_2 are dissolved in the CO_2 in detectable quantities (Andersen, 1986).

The amount of data available on the ionic compositions of hydrothermal fluids associated with carbonatite and alkalic complexes is very sparse. The variety of solid phases in the inclusions suggests that the composition of the fluids is complicated and that the important ionic species are chloride, carbonate, sulphate, phosphate, sodium, potassium, and calcium. Analysis of leachates from crushed apatite samples from

Table 1.1: Summary of solid phases in fluid inclusions in carbonatites

Mineral	Composition	1	2	3	4	5	5	5
		Ap WVS	Ap WVS	Ap WVS	Ap WVS	Ap WV/CS	Mtc WV/CS	Cal WCS
Ce-La carbonate								x
Fe-Cu sulphate								x
alkali sulphates				x				
amphibole		?						
apatite	Ca ₅ (PO ₄) ₃ (OH,F)						x	x
arcanite	K ₂ SO ₄							x
barite	BaSO ₄							x
calcite	CaCO ₃						x	
carbonate		x			x			
celestite	SrSO ₄							x
chlorocalcite	KCaCl ₃							x
diopside	CaMg(SiO ₃) ₂						x?	
fluorite	CaF ₂	?						
glauberite	Na ₂ Ca(SO ₄) ₂ .H ₂ O							x
gypsum	CaSO ₄							x
halite	NaCl		x	x	x?			x
hydrophyllite	CaCl ₂							x
kalicinite	KHCO ₃		x	x				
larnite	Ca ₂ SiO ₄						x	
magnetite	Fe ₃ O ₄		?				x	
merwinite	Ca ₃ Mg(SiO ₄) ₂						x?	
nahcolite	NaHCO ₃	x	x	x				?
phlogopite	K(Mg,Fe) ₃ (Al,Si) ₃							x
pyrrhotite	FeS		x					
strontianite	SrCO ₃							x
sylvite	KCl	?		x				x
syngenite	K ₂ Ca(SO ₄) ₂ .2H ₂ O							x
thenardite	Na ₂ SO ₄							x
trona	Na ₃ H(CO ₃) ₂ .2H ₂ O							x?
zeolites								x?

1: Fen (Andersen, 1986); 2: Wasaki (Rankin, 1975); 3: Alno (Aspden, 1980); 4: Oka (Girault, 1966); 5: Magnet Cove (Nesbitt and Kelly, 1977); Ap: apatite; Cal: calcite; Mtc: monticellite; W: water; V: vapour; S: solid; C: CO₂

some East African carbonatites and ijolites shows that Na^+/K^+ ratios range from 3.1:1 to 16.0:1 for carbonatites and 1.3:1 to 3.8:1 for ijolite (Rankin and Le Bas, 1974).

Girault (1966) and Girault & Chaigneau (1967) measured the gaseous compositions of the fluid inclusions in the apatite in the Oka carbonatite. The gases were released from the apatite mostly at 600 to 800°C, and were composed of CO_2 (74-97 volume %), CO , H_2 and N_2 . H_2O was detected only in one sample and made up 0.3% of the volume of the gases.

Melt inclusions have also been reported from calcite, apatite, nepheline, pyroxene, melilite, wollastonite, sanidine, nyererite, and monticellite from carbonatites and alkalic rocks. The inclusions homogenized to the melt phase from 550 to 880°C in carbonatites and from 700 to 1260°C in alkalic rocks (Romanchev, 1972; Kogarko and Romanchev, 1977; Romanchev and Sokolov, 1979). The bulk composition of the melt trapped in monticellite from the Magnet Cove complex has been estimated from the volumetric proportions of phases present in primary melt inclusions, which were determined using scanning electron microscopy (Nesbitt and Kelly, 1977).

1.2.2 REE distribution in carbonatites

Carbonatites have the highest REE contents ($\Sigma\text{REE}=72\text{-}15515$ ppm) and the highest LREE/HREE ratios ($\text{La}/\text{Lu}=7.1\text{-}1240$) of any rock type (Schofield and Haskin, 1964; Kapustin, 1966; Loubet et al., 1972; Barber, 1974; Eby 1975; Mitchell and Brunfelt, 1975; Cullers and Medaris, 1977; Armbrustmacher, 1979). In a complex, REE are distributed among minerals in early-stage carbonatites such as calcite, apatite, and pyrochlore, but are concentrated in late-stage carbonatites in hydrothermal REE-rich minerals such as ancylite, bastnaesite, britholite, parisite and synchysite (Cullers and Graf, 1984; Mariano, 1989). Alkalic silicate rocks associated with carbonatites have lower REE concentrations than the associated carbonatites. REE abundances in carbonatite complexes increase in the order urtite < ijolite < sovite (Eby, 1975; Mitchell & Brunfelt, 1975).

Hydrothermal REE-minerals may have been formed from REE-rich magmatic hydrothermal fluids or from hydrothermal fluids of other origins which have

remobilized REE from primary phases. A high temperature, magmatic origin for REE-Th-U mineralization has been proposed by Lira & Ripley (1990) and Phillips et al. (1990). This might be expected as the REE are incompatible elements relative to main rock-forming minerals and have a tendency to concentrate in residual fluids (Haskin, 1984). A variety of other models involving low temperature external fluids have been suggested by Andersen (1984, 1986), Salvi & Williams-Jones (1990) and Williams-Jones (1992). Andersen explains the relative enrichment in middle rare earth elements (MREE) in the formation of late-stage, metasomatic, hematite-rich carbonatite at Fen by preferential leaching of light rare earth elements (LREE) by a F-rich fluid. Salvi and Williams believe that REE are mobile in low temperature (<200°C) fluids, as indicated by the presence of REE minerals in low temperature fluid inclusions (<200°C) at the Strange Lake REE-Zr-Y deposits. Williams-Jones (1992) believes that REE have been leached from the St Honore carbonatite by a mixture of magmatic and meteoric fluids.

Theoretical considerations and experimental data indicate that the trivalent REE form the strongest complexes with fluoride, sulphate, carbonate, phosphate and hydroxide ligands (Wood, 1990a), and that the stabilities of all trivalent REE complexes with fluoride, sulphate, chloride hydroxide increase relatively rapidly with increasing temperature (Wood, 1990b). REE could be deposited by diluting the ligand or decreasing temperature (Williams-Jones, 1990).

1.3 Objectives

In summary, most REE mineralization associated with carbonatites is hydrothermal in origin. The fluids responsible for such mineralization could have been exsolved from the carbonatite or alkali-silicate magmas (orthomagmatic)(Lira and Ripley, 1990; Phillips et al., 1990), or they could have been externally derived (meteoric or formation) water (Andersen, 1984 and 1986; Salvi and Williams-Jones, 1990; Williams-Jones, 1992). In the former case, the REE may have been partitioned into the hydrothermal fluid when it was exsolved, and in the latter case, the REE may have been leached from primary igneous phases.

In order to test these models, it is important that we know the chemical composition and densities of the orthomagmatic fluids evolved from carbonatite and

alkali-silicate magmas. This could be achieved either through petrological experiments and or through fluid inclusion studies. Only one petrological experiment has qualified the composition of hydrothermal fluids coexisting with carbonatite melt and silicate melt, and there is relatively little fluid inclusion data available from carbonatites. Only two studies have attempted low temperature fluid inclusion microthermometry, and four provide some heating data. The volatile composition of fluid inclusions have been quantified in only one study, and the characterization of electrolyte chemistry is restricted to Na/K ratios in one study.

The major objective of this research was to obtain better data on the compositions and densities of orthomagmatic fluids in carbonatite-alkali-silicate intrusions. This was achieved by studying fluid inclusions in primary phases from the Oka carbonatite complex, Quebec.

In addition, the possible role of orthomagmatic hydrothermal fluids in controlling the distribution of REE in carbonatites may be assessed by studying the REE chemistry of primary magmatic minerals and the correlation of this chemistry with the inclusion assemblages in the minerals.

1.4 Methods

Seventy five samples were collected from the Oka carbonatite complex and were supplemented by samples from the Redpath museum and the Department of Geological Sciences of McGill University. Thin sections were prepared for almost all of the samples. About 35 samples were selected for the preparation of doubly polished wafers for microthomometric measurements of fluid inclusions.

A microscope was used to study the mineralogy of all samples and the petrography of the fluid inclusions. Laser Raman spectroscopy was used to identify the solid phases in fluid inclusions and the host minerals. A heating-freezing stage was used to obtain microthermometric data from fluid inclusions. Scanning electron microscopy and electron microprobe spectrometry were used to analyze the compositions of decrepitates (salt precipitates) from individual fluid inclusion and the compositions of solid phases in inclusions. Leachates from apatite separates were analyzed by atomic absorption spectrophotometry and ion chromatography. Quadrupole mass spectrometry was utilized for analyzing the gas compositions of fluid inclusions. Electron microprobe spectrometry was also used to analyze major

elements and REE in apatite. Instrumental neutron activation analysis was used to obtain the REE compositions of whole rocks and apatite.

CHAPTER II GEOLOGIC SETTING

The geology of the Oka Complex has been discussed by Stansfield (1923), Rowe (1955, 1958), Maurice (1956) and more recently by Gold (1963, 1967, 1972). The following summary of the geology of the complex is based mainly on Gold's work.

2.1 General Geology

The Oka complex is located about 20 miles west of Montreal, Quebec, on the north shore of Lac de Deux Montagnes. The complex is hosted by Precambrian rocks of the Morin Series, which is composed of anorthosites, gabbros, diorites, monzonites, granulites, and quartz-feldspar gneisses, with lesser amounts of garnet gneiss and quartzite. The Morin Series was intruded during the Early Cretaceous by a series of carbonatite-alkalic rocks which collectively make up the Oka complex. Isotopic data on biotite from the complex yielded K-Ar ages of 95 ± 5 and 117 m.y., and a Rb-Sr age of 114 ± 7 m.y. (Fairbairn et al., 1963; Shafiqullah et al., 1970).

The Oka complex is four and a half miles long by one and a half miles wide, and trends northwest-southeast (Figure 2.1). The complex is composed of two rings of ultramafic-alkaline-silicate rocks and carbonatites. The silicate rocks occur as ring dikes within carbonatite masses, and in the outer zones of the complex. The carbonatites mainly occur in the cores of the two rings, but also as ring dikes in the outer zones of the complex.

2.2 Rock Types

The intrusive rocks in the Oka Complex have been classified into five main groups. In addition, the local country rocks have been fenitized. The proportions of common minerals in these rocks are summarized in Appendix I.

Carbonatites

The Oka carbonatites have been subdivided into twelve types based on their modal mineralogy. Most types are coarse-grained sovites, composed mainly of calcite and minor or accessory aegerine-augite, biotite, apatite, nepheline,

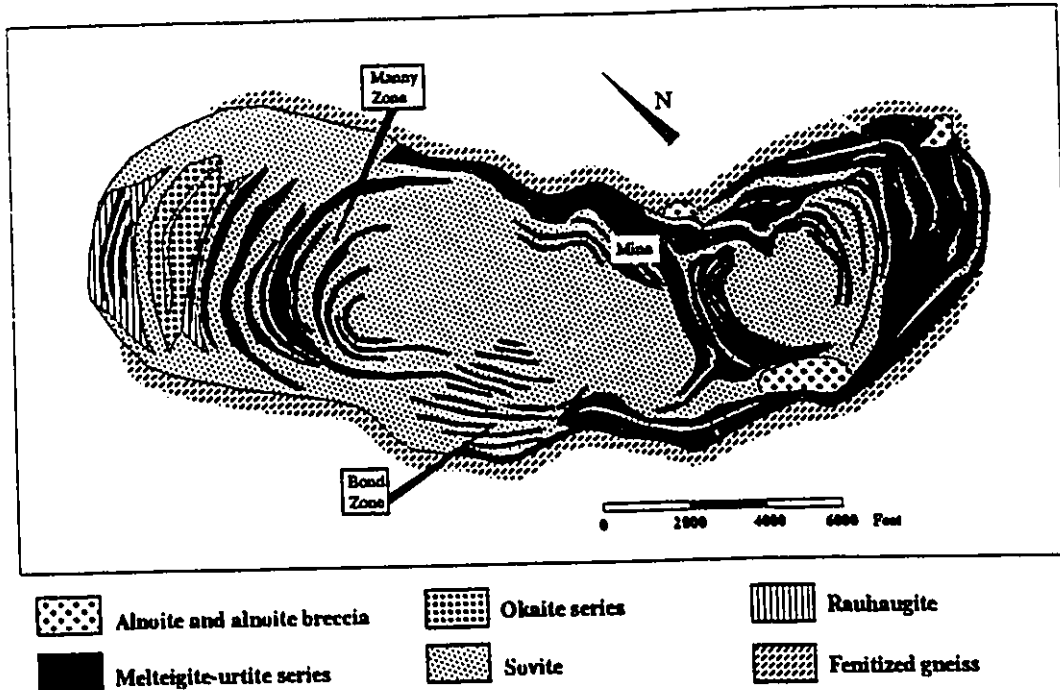


Figure 2.1. Geological map of the Oka complex (modified from Gold, 1972).

monticellite, melilite, pyrochlore, perovskite, niocalite, richterite, pyrite and pyrrhotite. Rauhaugite, in which dolomite is major carbonate mineral, is common in the northern part of the complex around Husereau Hill. The carbonatites are layered, and a foliation is defined by concentrations of mafic minerals such as magnetite, sodian augite, biotite, hornblende, and olivine. The layers of mafic minerals are usually 0.5 to 3 cm thick, and spaced 2 to 20 cm apart. Hydrothermal veins of calcite, biotite, pyrite, and rare-earth-rich minerals such as bastnaesite, britholite and parisite occur in most parts of the complex. They are obviously late features and appear to be emplaced along joint planes that are associated with minor faults. They cut layers in carbonatite and the boundary zones between silicate rocks and carbonatites.

Okaite-Jacupirangite Series

Rocks of the okaite-jacupirangite series occur only in the northern ring, and mainly consist of melilite and titanaugite with minor or accessory amounts of nepheline, hauyne, perovskite, apatite, biotite, magnetite and calcite.

Ijolite-Urtite Series

Rocks of the ijolite-urtite series are common, and are chiefly composed of aegerine-augite and nepheline with minor or accessory amounts of calcite, melanite, biotite, wollastonite and magnetite.

Glimmerites

Glimmerites occur as zones within ijolite in the St. Lawrence Columbian and Metals Corporation mine (Mine), the Manny zone and the Bond zone, and are made up chiefly of biotite and calcite with minor zeolites and rare-earth carbonates. They are interpreted to have been formed by reaction between late hydrothermal fluids and silicate rocks (Gold, 1972).

Lamprophyres and intrusive breccias

Lamprophyres and intrusive breccias occur as dykes or in irregular pipelike bodies. They are made up of either: 1) polymict breccia comprising country rock fragments in a matrix of either alnoite or comminuted country rock with calcite, chlorite and rare phlogopite; or 2) massive alnoite with phenocrysts of olivine, augite, phlogopite and hornblende in a calcite-rich matrix comprising melilite, apatite, perovskite, magnetite, phlogopite, titanaugite, olivine and nepheline.

Fenite

Metasomatic alteration of the country rocks occurs around the complex as an irregular fenite aureole. Near the pluton, the gneissic structure in the Morin Series was either destroyed or reorientated and replaced by structures concordant to the margin of the pluton. The alteration is characterized by replacement of alkali-feldspar, plagioclase and quartz by aegerine and nepheline. The alteration was controlled by fracture systems.

2.3 Sequence of Events

The sequence of events in the complex is as follows (Gold, 1972):

1. Fenitization of gneissic country rocks occurred, followed by emplacement of early carbonatites as dikes and ring dikes with accompanying ijolitization of the enclosed country rock.

2. Okaite-jacupirangite series rocks were intruded as crescent-shaped masses and arcuate dikes.
3. Intrusion of the main pyrochlore-bearing carbonatite, followed by intrusion of the monticellite-carbonatite.
4. Intrusion of ijolite and micro-ijolite dikes.
5. Hydrothermal activity along fractures causing biotitization forming glimmerites and deposition of thorian pyrochlore.
6. Emplacement of late, white carbonatite dikes.
7. Emplacement of alnoite and alnoite breccia pipes and dikes.

2.4 Economic Geology

The Oka carbonatite contains abundant niobium-bearing minerals including pyrochlore, perovskite and niocalite. Exploration on the complex started in 1953. Pyrochlore was mined for Nb₂O₅ at the St. Lawrence Columbian and Metals Corporation mine up until the early 1970s.

CHAPTER III PETROGRAPHY

3.1 Sampling

75 samples were collected from the Oka carbonatite complex by the author, Dr. I.M. Samson and Dr A.E. Williams-Jones. Of these samples, 43 were collected from the two open pits at the St. Lawrence Columbian and Metals Corporation mine (the Mine) and dumps around the pits; 7 from several outcrops and a trench in the Manny zone; and 25 from six trenches in the Bond zone (Figure 2.1). We also obtained 10 samples from the Redpath Museum and the Department of Geological Sciences at McGill University.

3.2 Classification of Samples

Using the classification of Gold (1972), the samples have been classified into the following types (Table 3.1):

Sovites

Samples of sovite have been collected from the Mine, the Manny zone and the Bond zone. They are composed of 60 to 100% calcite and a variety of minor and accessory minerals including apatite, magnetite, biotite, aegerine-augite, monticellite, richterite, niocalite, melanite, dolomite, pyrite, pyrrhotite, hematite, pyrochlore, perovskite and bastnaesite. The sovite samples have been subdivided, according to mineralogy, into eight subtypes (Table 3.1). Except for aegerine augite-apatite-niocalite sovite, all the sovite types are present in the Mine. The samples from the Manny zone comprise monticellite-apatite sovite and apatite sovite. The samples from the Bond zone consist of aegerine augite-apatite-niocalite sovite, apatite sovite, calcite sovite, monticellite sovite and aegerine augite-magnetite-biotite sovite.

Ijolite-urtite series

Samples of ijolite-urtite series rocks have been collected from the Mine and from the Bond zone. These rocks are essentially composed of aegerine augite

and nepheline and minor or accessory calcite, magnetite, apatite and pyrochlore.

Table 3.1: Summary of mineralogy of main rock types of samples

Type	Subtype	Main minerals	Accessory minerals
Sovite	Ap sovite	Cal, Ap	Agt, Mag, Bt, Pyr, Prv
	Cal sovite	Cal	Ap, Mag, Bt,
	Mtc-Ap sovite	Cal, Ap, Mtc	Bt, Mag, Agt, Mln, Prv, Pyr
	Nio-Agt-Ap sovite	Cal, Ap, Agt, Nio	Mag, Bt, Mtc, Mln, Prv, Pyr
	Sulphide sovite	Cal, Py, Po	Bt, Ms, Ap, Hem, Bast,
	Ric-Ap sovite	Cal, Ap, Ric	Mag, Bt, Prv, Pyr
	Agt-Mag-Bt sovite	Cal, Bt, Mag, Agt	Ap, Mln, Pyr, Prv, Ric
	Hem sovite	Cal, Hem	Bast
Ijolite-Urtite	Melteigite	65% Agt, 35% Ne	
	Cal Melteigite	65% Agt, 35% Cal	Ne
	Ijolite	50% Agt, 50% Ne	
Glimmerite	Glimmerite	Bt, Cal	Mag, Mln, Ap, Agt, Prv, Pyr

They have been subdivided, according to the proportions of aegerine-augite, nepheline and calcite, into three subtypes (Table 3.1). Some of these rocks have been subjected to biotitization and contain 10 to 30% biotite.

Glimmerites

Glimmerites are present in the Mine, the Manny zone and the Bond zone. Glimmerites are composed of 50 to 90% biotite and contain minor or accessory calcite, apatite, magnetite, aegerine augite, melanite, perovskite and pyrochlore. Biotites in glimmerites normally occur as small, dark-green, subhedral crystals.

3.3 Crystallization Sequence of Primary-Fluid-Inclusion-Bearing

Minerals in Carbonatites

Primary fluid inclusions were only found in calcite, apatite and monticellite in the carbonatites. In order to model the evolution of the hydrothermal fluids in equilibrium with the carbonatite magma during crystallization, it is necessary to establish a crystallization sequence for these minerals.

Monticellite occurs as large, subhedral to euhedral prismatic crystals in monticellite-apatite carbonatite. In general, monticellite crystallized earlier than apatite and calcite. Apatite is distributed along edges of monticellite crystals, and monticellite is cut by apatite and calcite (Figure 3.1). In places, monticellite is embayed and replaced by calcite (Figure 3.2). However, the presence of apatite inclusions in monticellite indicates that some apatites crystallized before monticellite.

Apatite is present in most types of carbonatites. Apatite crystals are small (~ 0.1 mm in length), euhedral to subhedral, and prismatic. They occur as polycrystalline aggregates with interstitial calcite (Figure 3.3) or as single crystals at the boundary between calcite crystals. Some apatites occur as inclusions in calcite (Figure 3.4). It

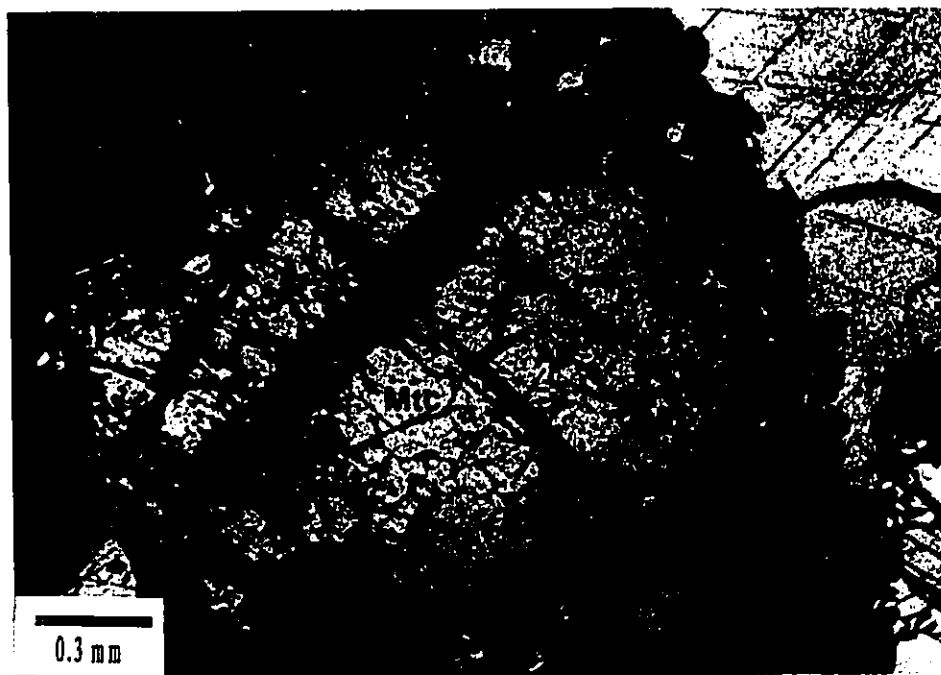


Figure 3.1. Monticellite cut and replaced by apatite and calcite, and surrounded by apatite.

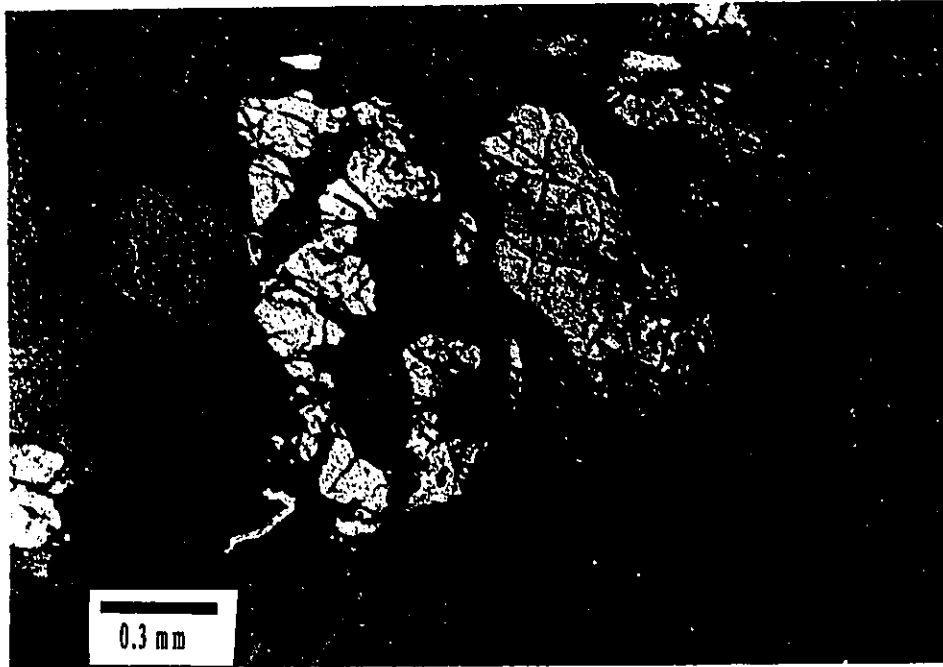


Figure 3.2. Monticellite embayed and replaced by calcite.



Figure 3.3. Apatite aggregates with interstitial calcite.

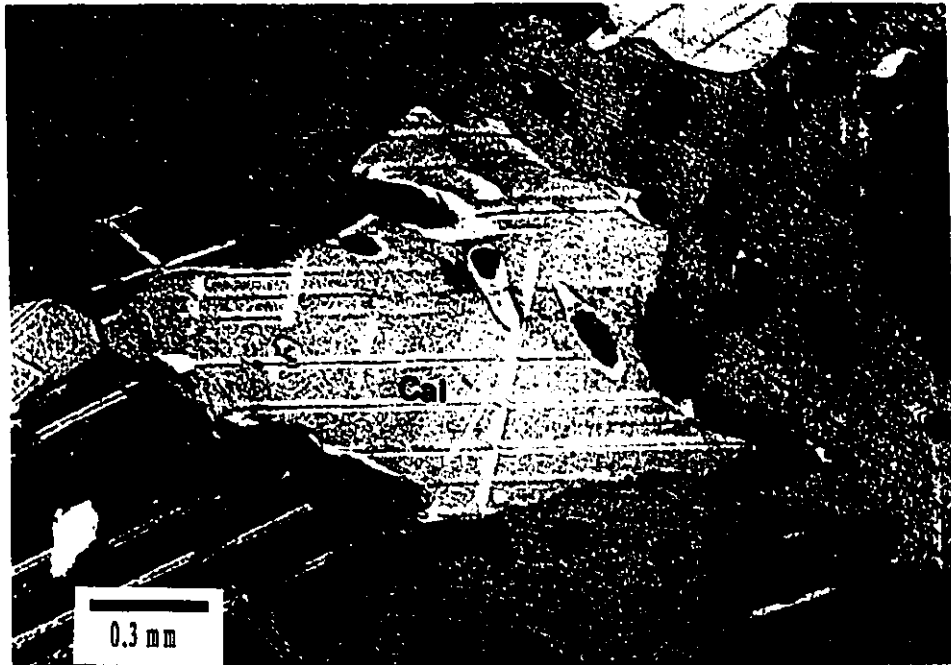


Figure 3.4. Apatite as inclusions in calcite.

is evident that apatite crystallized earlier than calcite. However, the presence of small spheroidal calcite inclusions in apatite indicates that some calcite predated or accompanied apatite crystallization.

In summary, the general crystallization sequence of the primary fluid inclusion-bearing minerals is monticellite-apatite-calcite. In the Magnet Cove carbonatite complex, primary fluid inclusions are present in these three minerals, and the crystallization sequence of the minerals is same as that in Oka (Nesbitt and Kelly, 1977).

CHAPTER IV

FLUID INCLUSION PETROGRAPHY

4.1 Introduction

All thin sections and doubly-polished wafers were examined with a transmitted light microscope in order to determine the types of fluid inclusions present. Aqueous fluid inclusions are present in calcite, apatite, monticellite and aegerine-augite in the sovites. Inclusion-bearing calcite crystals are present in 50 samples of all subtypes of sovites. Inclusion-bearing apatites are present in 31 samples of all subtypes of sovites, excluding sulphide sovite and hematite sovite. Inclusion-bearing monticellites are present in 7 samples of monticellite-apatite sovite. Inclusion-bearing aegerine-augite are present in 8 samples of aegerine augite-magnetite-biotite sovite and niocalite-aegerine augite-apatite sovite. The inclusions include primary, secondary and pseudosecondary types.

4.2 Analytical Methods

In addition to microscopy, laser Raman spectroscopy (LRS) and scanning electron microscopy (SEM) have been used to study the fluid inclusions.

LRS was used to identify solid phases in fluid inclusions and to analyze for gases in the inclusions. LRS was performed at the University of Windsor on doubly-polished wafers using a Ramanor U-1000 spectrometer, fitted with a Spectra Physics Ar ion laser (514.5nm green line). Spectra were collected with a x80 objective, using monochromator slit widths of 400 μm . A laser power of 300 mW, a stepping interval of 1 cm^{-1} , and a counting time of 1 second were used for the solid analysis. A laser power of 500 mW, a stepping intervals of 0.5 cm^{-1} and a counting time of 10 seconds were used during gas analysis.

SEM was principally utilized for analyzing the compositions of decrepitates from the fluid inclusions, which will be discussed in Chapter VI. It was also used to identify solid phases present in fluid inclusion cavities opened by decrepitation or fracturing. Decrepitation of fluid inclusions was achieved by heating doubly-polished wafers in a Linkam THM 600 heating-freezing stage to temperatures of between 400 and 500°C, which is about 130°C above the homogenization temperatures of the inclusions. On decrepitation, water from the inclusions evaporated, leaving behind any

daughter or trapped minerals along with minerals precipitated during evaporation. Fracturing was achieved by crushing frozen rock chips into several pieces in order to avoid plucking solids from inclusion cavities. A JSM-U3 scanning electron microscope, located at McGill University, and fitted with an energy dispersive analyzer (EDA) was used for the analyses. The analysis parameters are listed in Table 4.1.

Table 4.1: SEM instrument parameters and analysis conditions

Bean energy:	15 kV
Beam current:	0.3 nA
Raster area:	10-300 μm
Time of raster scan:	1 sec
Beam current density:	0.03 nA/ μm^2
Count time:	60 sec

4.3 Fluid Inclusion Types

Fluid inclusions were classified according to the types and proportions of phases present at room temperature. Inclusions which were interpreted to have undergone necking were not included in the classification. Trapped minerals were ignored in classifying the inclusions as they do not reflect the bulk composition of the inclusions. Fluid inclusions have been classified into two types:

1. LV inclusions are aqueous, liquid-rich, liquid-vapour inclusions that homogenize to the liquid phase. Some of the inclusions contain from one to nine trapped solid phases.
2. LVH inclusions are aqueous liquid-vapour-halite inclusions which homogenize to the liquid phase either by halite disappearance or by vapour disappearance. The halite was classified as a daughter mineral because the ratios of halite to liquid and to vapour are consistent between inclusions in a group or plane (Figure 4.1). The halite usually occupies 20% to 30% of an inclusion. In addition to halite, between one and three other trapped solid phases are present in some of the inclusions.

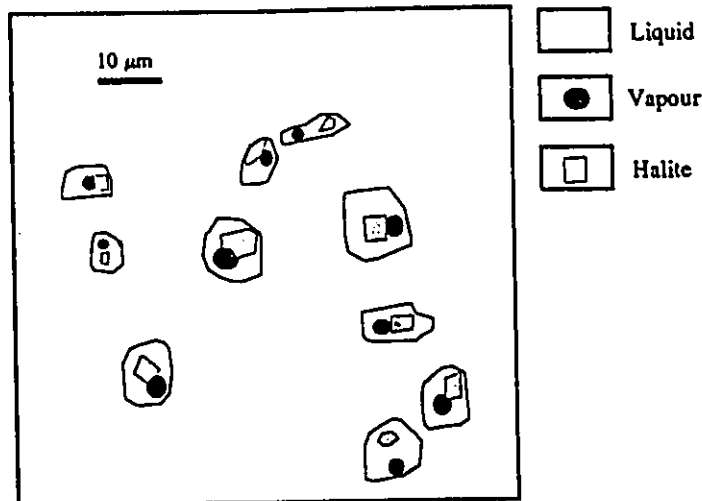


Figure 4.1. A group of LVH inclusions with consistent phase ratios

4.4 Identification of Solid Phases

A variety of solid phases are present in fluid inclusions in calcite, apatite, monticellite and aegerine-augite. They are irregularly distributed, which suggests that they were either trapped during inclusion formation or crystallized in the inclusions prior to necking. However, as it is difficult to discriminate between these two models, these minerals will be referred to as trapped phases for convenience. The minerals have been identified using microscopy, LRS and SEM (Table 4.2).

Halite

Isotropic minerals with square form and low relief are present either as daughter minerals in the LVH inclusions in apatite and monticellite or as trapped minerals in the LV inclusions in calcite, apatite and monticellite. They have been identified as halite by microthermometry (see Chapter V) and their presence is consistent with the dominance of NaCl in the decrepitates (see Chapter VI).

Table 4.2: Summary of solid phases in primary inclusions.

Solid Phase	Characteristics	Host and inclusion type				
		Cal	Ap	Ap	Mtc	Mtc
		LV	LV	LVH	LV	LVH
Halite	cubic, isotropic, low relief	x	x	x	x	x
Apatite	prismatic, colourless, moderate relief, first-order grey, parallel extinction, length-slow	x				
Calcite	anhedral, colourless, low relief, high-order creamy, dissolved		x	x		
Nahcolite	anhedral, colourless, low relief, high-order creamy, dissolved		x			
Mirabilite	colourless, moderate relief, first-order grey		x	x		
Na-Mg-V silicate	anhedral		x			
Ce silicate	anhedral		x			
Strontianite	subhedral	x				
Magnetite	cubic, opaque				?	?

Apatite

Colourless minerals with moderate relief and first-order yellow interference colours are present in inclusions in calcite and occur as short prisms with rounded ends. They have parallel extinction and are length-fast and are probably apatite.

Strontianite

A euhedral mineral present in an inclusion cavity in calcite, which was observed under SEM (Figure 4.2), gives a strong Sr peak in the EDA spectrum in addition to two Ca peaks contributed by the host calcite (Figure 4.3). The lack of peaks of other elements such as S, P and Cl suggests that the mineral is a Sr carbonate or oxide,

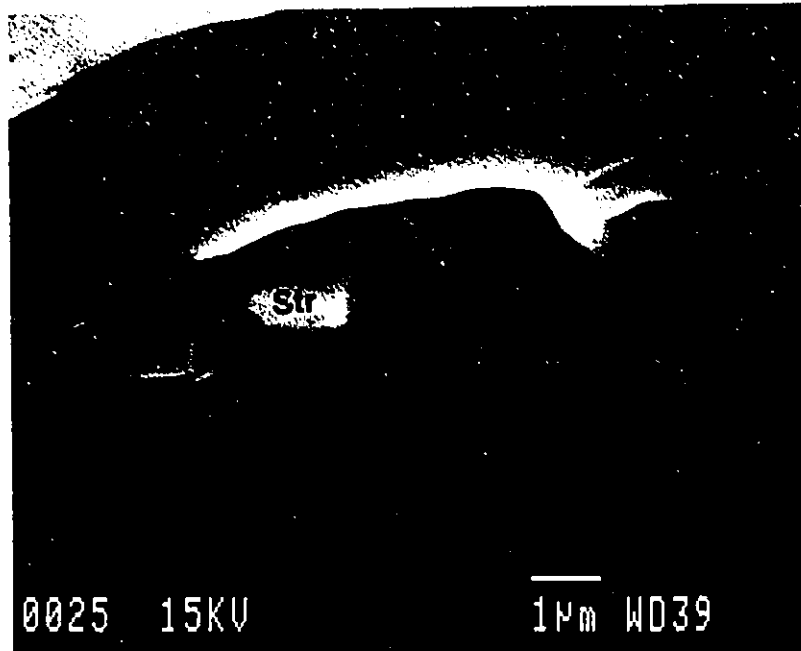


Figure 4.2: SEM view of an opened inclusion in calcite containing a crystal of strontianite.

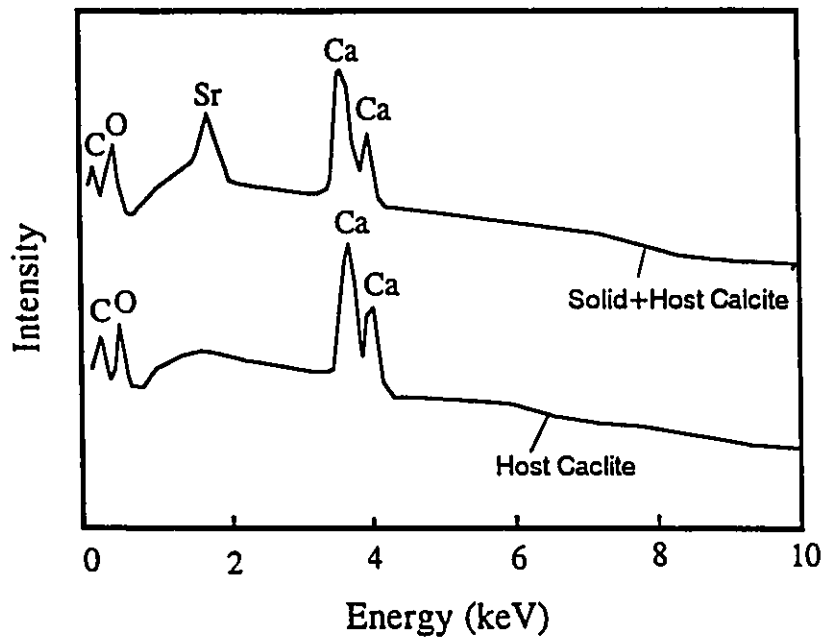


Figure 4.3: EDA spectra of strontianite in an inclusion in calcite and of host calcite.

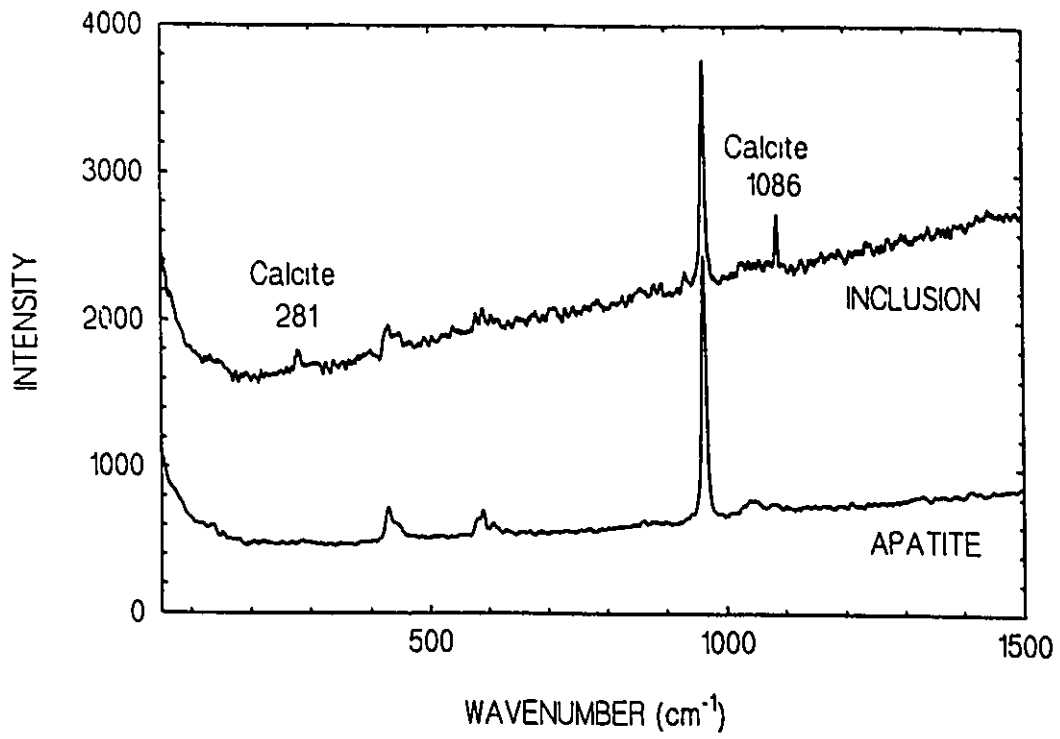


Figure 4.4. Raman spectra of calcite in an inclusion in apatite and the host apatite.

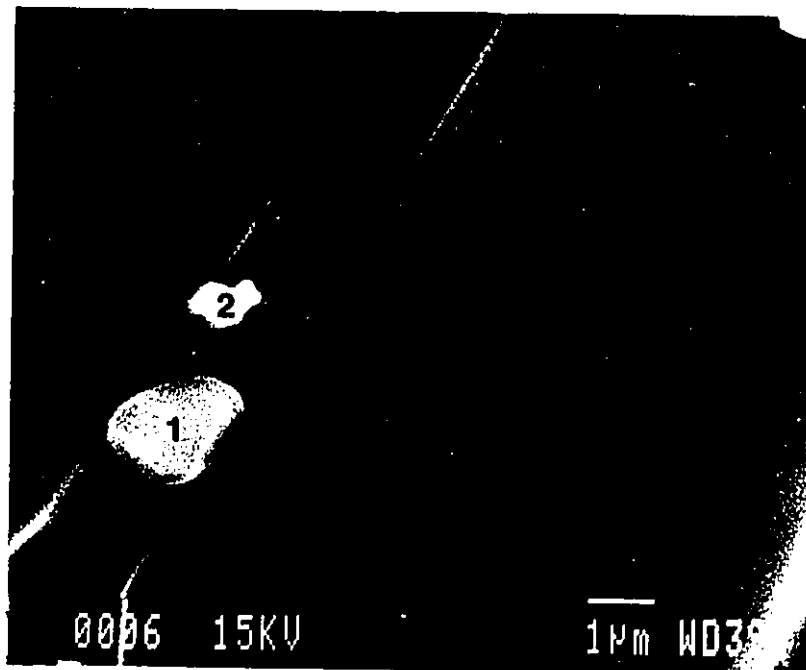


Figure 4.5: SEM view of calcite (1), V-rich amphibole (2), mirabilite (3) and S-rich Ce-Ca silicate (4) in inclusions in apatite

most likely Strontianite.

Calcite

Highly birefringent, anhedral minerals, which showed no change on heating to 400°C, are abundant in the inclusions in apatite. Raman spectra of these minerals contain bands at 281 and 1086 cm⁻¹ (Figure 4.4), which corresponds to the strongest bands of calcite (White, 1974).

A rounded mineral in an opened inclusion cavity in apatite (Figure 4.5) gave a strong Ca peak in its EDA spectrum. There are no peaks for other elements, which indicates that the mineral is a Ca carbonate or oxide, calcite being the most likely.

Nahcolite

Highly birefringent, anhedral minerals, which dissolved at about 180°C, are present in the inclusions in apatite. One of the minerals shows a peak at 1048 cm⁻¹ in its Raman spectrum (Figure 4.6), which corresponds to the strongest peak of nahcolite (White, 1974; Dhamelincourt et al, 1979).

Mirabilite

Colourless, euhedral square minerals with low to moderate relief and first-order grey interference colours are present in the inclusions in apatite. One of the minerals exhibits a peak at 993 cm⁻¹ in its Raman spectrum (Figure 4.7), which corresponds to the strongest peak of mirabilite (Figure 4.8).

A mineral present in an opened inclusion cavity in apatite (Figure 4.5) gave strong Na and S peaks in addition to P and Ca peaks contributed by the host apatite, which indicates that the mineral is either a Na sulphate or Na sulphide. Mirabilite is most likely as mirabilite has been identified using LRS and thenardite is not stable at room temperature.

Unidentified silicate

Two anhedral minerals in two opened inclusion cavities in apatite (Figure 4.5) were analyzed using EDA. The composition of one mineral (Figure 4.9; Table 4.3, mineral 1) is similar to the composition of sodium amphibole. Its calculated structural formula is approximately Na₂(NaCa)₂(Mg,Fe,V)₄Si₈O₂₂. The other mineral is rich in

Ca, Ce, Si and S (Table 4.3, mineral 2) and is probably a S-rich Ce-Ca silicate.

Table 4.3: Compositions (wt %) of two unidentified trapped minerals

Min.	SiO ₂	CaO	MgO	MnO	FeO	Na ₂ O	V ₂ O ₅	Ce ₂ O ₃	SO ₃
1	54.4	12.9	9.3	3.0	2.6	11.4	5.4		
2	12.4	46.1				3.7		22.9	11.7

Magnetite

Opaque, square solid phases are present in some inclusions in monticellite. They showed no change before homogenization of the inclusions, and are tentatively identified as magnetite as the monticellite contains abundant magnetite inclusions.

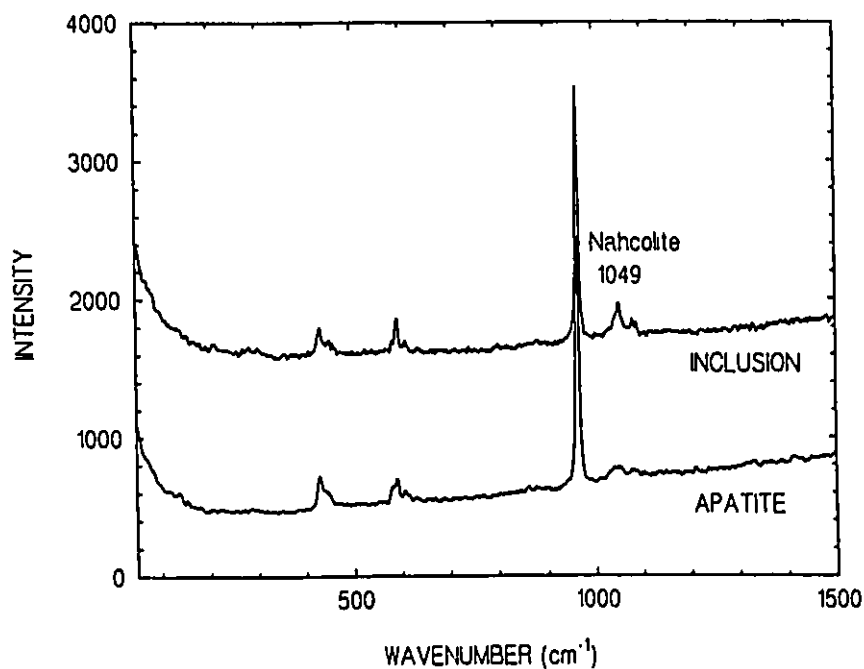


Figure 4.6. Raman spectra of nahcolite in an inclusion in apatite and the host apatite.

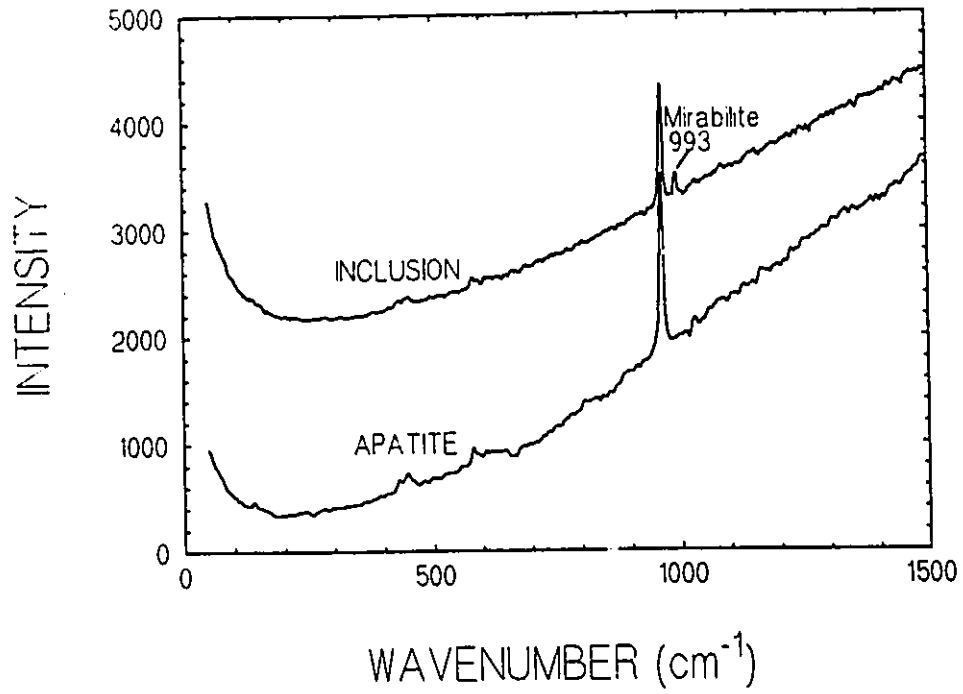


Figure 4.7. Raman spectra of mirabilite in an inclusion in apatite and the host apatite.

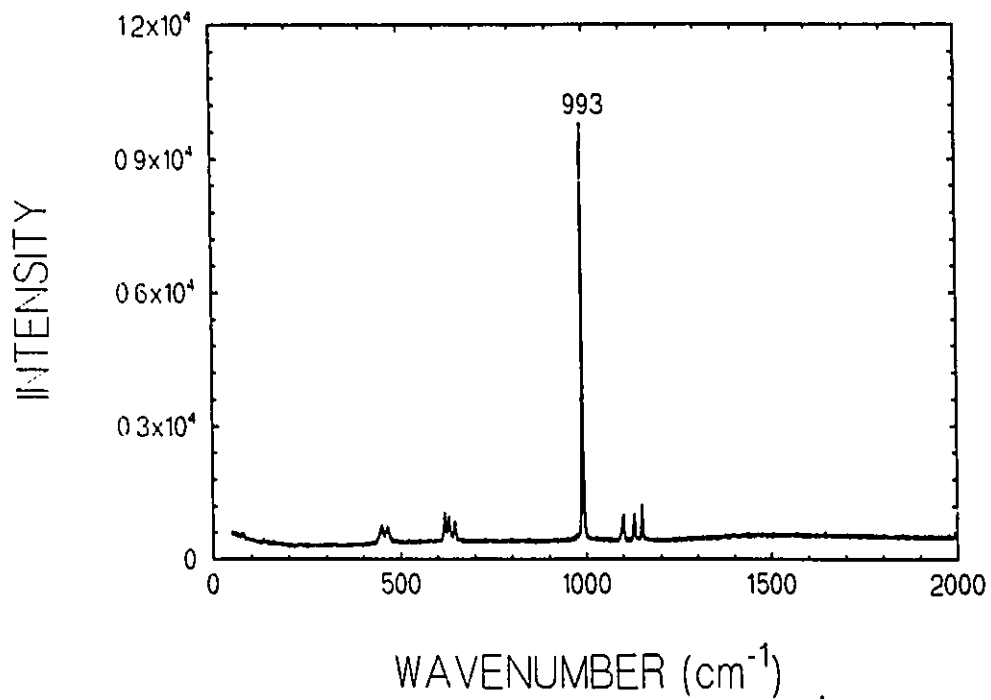


Figure 4.8. Raman spectrum of mirabilite.

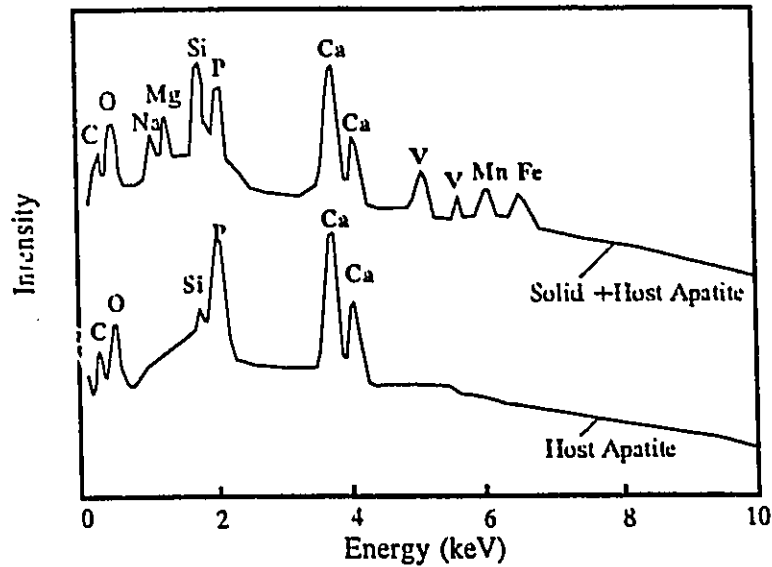


Figure 4.9. EDA spectra of V-rich amphibole in an inclusion in apatite and the host apatite

Table 4.4: Summary of primary fluid inclusion types

Host Minerals	Inclusion Types		
Calcite	LV (S)		
	LVH (S)		
Apatite	LV (S)		
	LVH (S)		
Monticellite	LV (S)		
	LVH (S)		

4.5 Distribution and Origin of Fluid Inclusions

4.5.1 Primary fluid inclusions

The origins of the fluid inclusions from the Oka carbonatite were identified based on the criteria of Rodder (1984). Primary fluid inclusions are present in calcite, apatite and monticellite. The types of primary fluid inclusions are summarized in Table 4.4.

Inclusions in calcite

More than 50% of the calcite crystals contains fluid inclusions. Some calcite crystals are very rich in fluid inclusions, giving the crystals a murky appearance. More than 80% of the inclusions are secondary, but some inclusions away from planes of secondary inclusions are interpreted as primary inclusions. These primary inclusions occur as isolated inclusions or in three dimensional arrays. They are usually small (5-10 μm) and irregular (Figure 4.10), and make up less than 1% of the volume of the host calcite. They are all LV inclusions. About 10% of the inclusions contain one or two solid phases including halite, apatite and strontianite.

Inclusions in apatite

Primary fluid inclusions are very abundant in apatite. Usually, 10 to 20% of the apatite crystals contain fluid inclusions, although inclusion-bearing crystals make up 40% of the apatites in four of the samples. The inclusions generally occupy 5 to 10% of the volume of a host apatite, but in some crystals, make up 30 to 40% of the volume. In most crystals, the inclusions occur as slender tubes which are aligned parallel to the c-axis of the host crystal (Figure 4.11). The inclusions are normally between 10 and 20 μm in length (up to 130 μm), and between 1 and 10 μm in width. The length/width ratios of the inclusions range from 1:1 to 20:1. The inclusions in most of the samples are LV inclusions, however LVH inclusions are present in two monticellite-apatite sovite samples and one richterite-apatite sovite sample, all of which came from the mine. About 20% of the LV inclusions contain 1 to 5 trapped minerals including halite, calcite, nahcolite, mirabilite, S-rich Ce-Ca silicate (?) and V-rich sodium amphibole (?). Trapped solid phases are present in 10% of the LVH inclusions and include calcite, nahcolite and mirabilite. Spheroidal inclusions (Figure

4.12) have been found in one apatite sovite sample from the mine. The inclusions are usually between 5 and 15 μm in diameter and have wide, dark edges. Some of them have a "tail" (Figure 4.13). They are LV inclusions with highly variable vapour/liquid ratios. 50% of them contain 1 to 9 trapped solid phases including halite, calcite and mirabillite.

Inclusions in monticellite

Most monticellite crystals contain fluid inclusions. The inclusions normally make up 5 to 20% of the volume of a host crystal. Most (more than 80%) of the inclusions are secondary or pseudosecondary, however inclusions that do not appear to be related to planes have been interpreted as primary inclusions. These primary inclusions occur either as isolated inclusions or in three-dimensional arrays. They are large (10-20 μm) and irregular (Figure 4.14), but are rare and only make up about 1% of the volume of a host crystal. Approximately 95% of the inclusions are LV inclusions and 5% are LVH inclusions (Figure 4.15). These two types of inclusions are present in the same samples. About 10% of the inclusions contain one or two solid phases including halite, magnetite and some unidentified non-birefringent minerals.

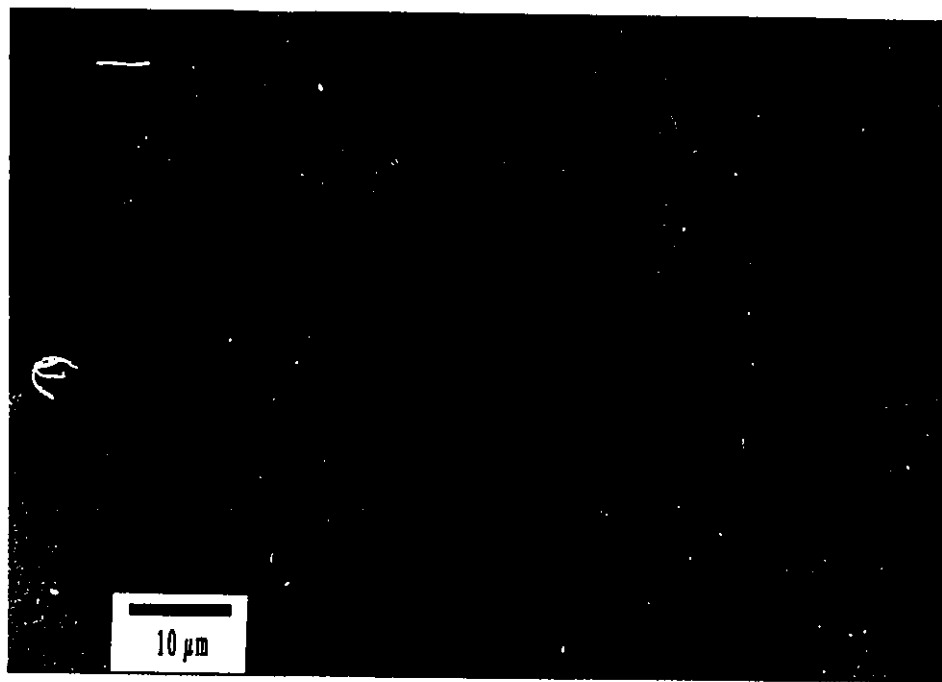


Figure 4.10. An isolated LV (S) inclusion in calcite.

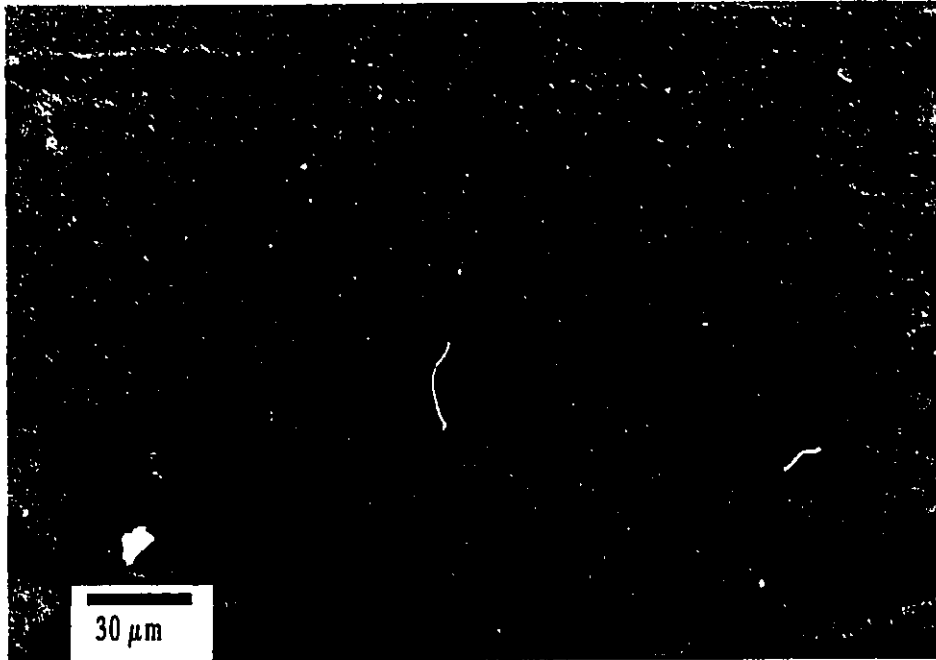


Figure 4.11. Elongate inclusions aligned parallel to the c-axis of the host apatite

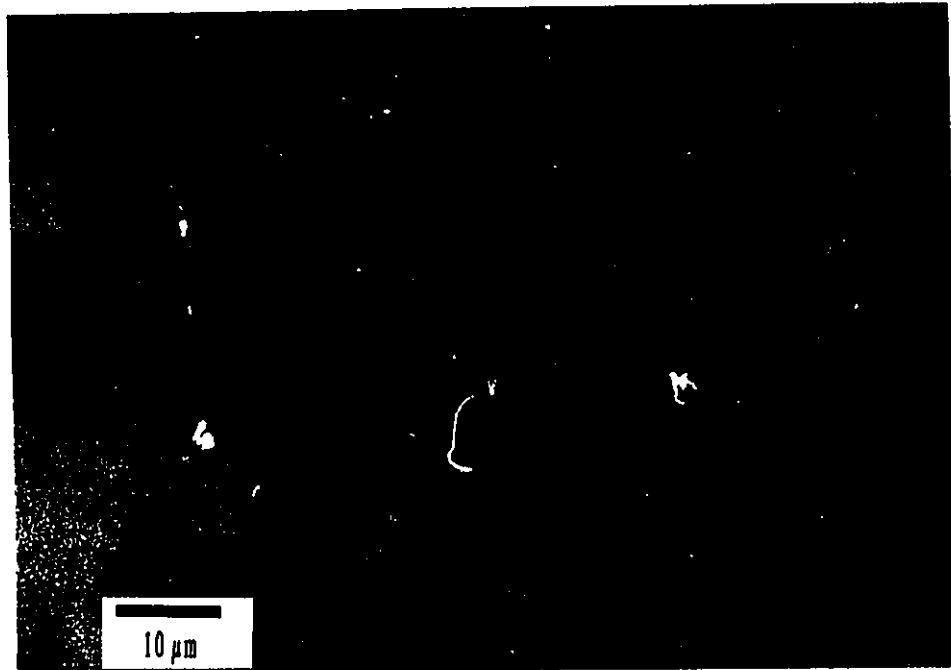


Figure 4.12. Spheroidal LV inclusions in apatite.

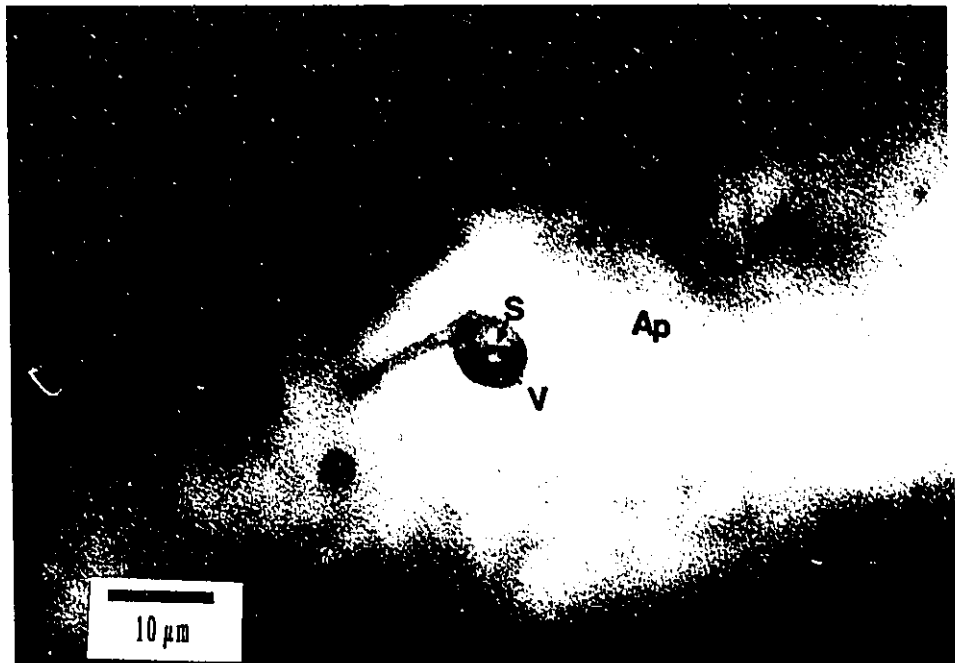


Figure 4.13. An spheroidal LV inclusion with a "tail" in apatite.

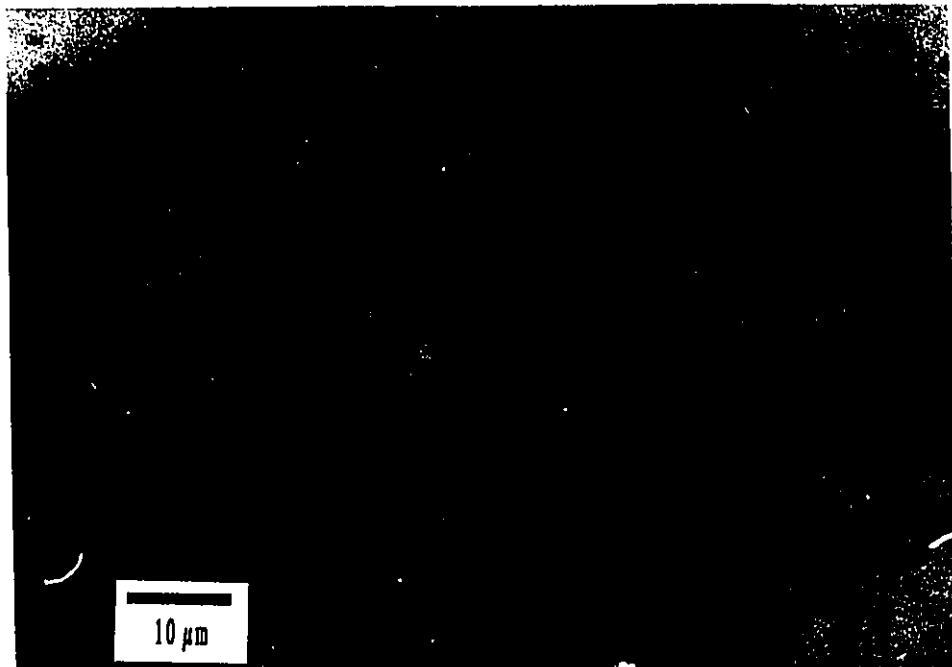


Figure 4.14. An isolated LV inclusion in monticellite.

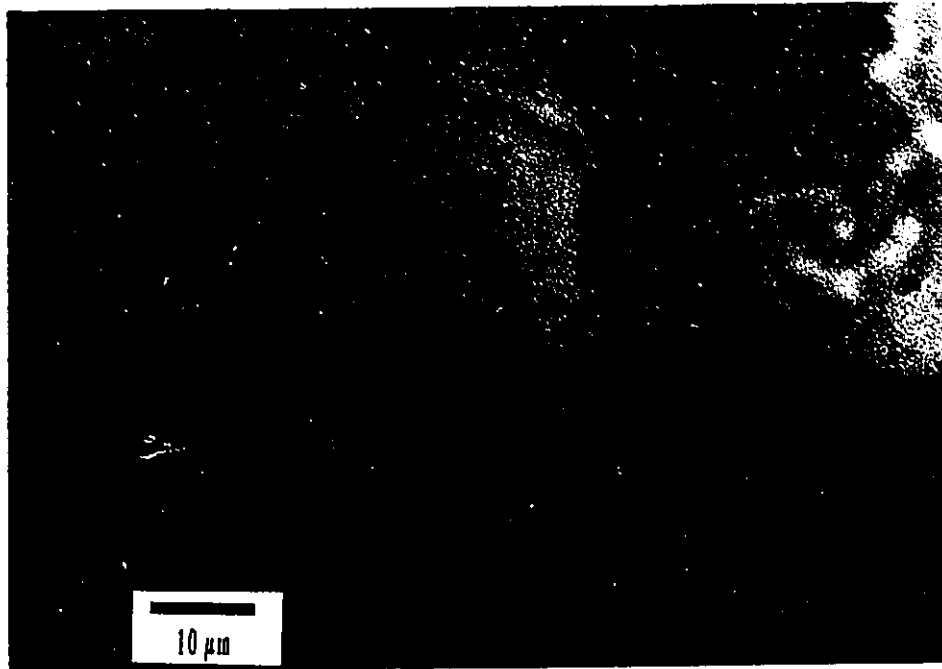


Figure 4.15. An isolated LVH inclusion in monticellite.

4.5.2 Pseudosecondary Fluid Inclusions

There are a few pseudosecondary fluid inclusions in monticellite. They are large (10-20 μm) and irregular, and occur in short planes which never cross grain boundaries. They comprise LV and LVH inclusions, both of which occur in the same sample.

4.5.3 Secondary Fluid Inclusions

Secondary fluid inclusions are present in calcite, monticellite and aegerine-augite. They occur along extensive healed fractures which cross-cut grain boundaries in places. Most of the inclusions in calcite and all of the inclusions in monticellite and aegerine-augite are LV inclusions. LVH inclusions are present in some calcite crystals.

CHAPTER V
MICROTHERMOMETRY OF FLUID INCLUSIONS

5.1 Analytical Method

The phase behaviour of fluid inclusions was studied in the temperature interval -100 to +500°C, using a Linkam THM 600 heating-freezing stage. The stage was repeatedly calibrated using a variety of organic and inorganic liquids and solids. The accuracy of measured temperatures range from < ±0.3°C below 0°C to ±1.5°C at 300°C. Heating rates were normally lower than 10°C/min and were 0.1 to 0.5°C/min during phase changes. The precision of measurements depends on the nature of the phase transition: < ±0.3°C for ice melting temperatures and < ±2°C for vapour or solid disappearance temperatures.

Final ice melting temperatures were used to calculate the salinities of the LV inclusions in terms of the NaCl-CaCl₂-H₂O system. Salinities reported as weight % were calculated using the following equation (Oakes et al. 1990):

$$W = \sum_{i=0}^6 a_i T^i + \sum_{j=1}^4 b_j T^j X_{NaCl} + \sum_{k=2}^6 c_k T^k X_{NaCl}^2 \dots \dots \dots (5.1)$$

- where: W = salinity of solution in wt %
- T = final ice melting temperature in °C/10
- X_{NaCl} = weight fractions of NaCl
- a_i, b_j, c_k = regression coefficients

Values of the regression coefficients for Equation 5.1 are listed in Table 5.1. An X_{NaCl}

Table 5.1: Coefficients of Equation 5.1.

a ₀ =0.00079300	a ₄ =-1.63493939	b ₂ =8.52707977	c ₃ =1.42997903
a ₁ =-23.60559803	a ₅ =-0.22344814	b ₃ =3.58341351	c ₄ =0.00000000
a ₂ =-14.28248382	a ₆ =-0.01233080	b ₄ =0.50474224	c ₅ =-0.34061248
a ₃ =-6.28485097	b ₁ =5.93722121	c ₂ =1.46447853	c ₆ =-0.08075286

value of 0.9 was used for the inclusions in apatite based on the result of decrepitate analysis (see Chapter VI). The same X_{NaCl} value was used for the inclusions in calcite and monticellite as no decrepitate data were available for the inclusions in these minerals.

Halite disappearance temperatures were used to calculate the salinities of the LVH inclusions in terms of the NaCl-H₂O system. Salinities reported as "equivalent weight % NaCl" were calculated using the following equation (Sterner et al, 1988):

$$W = 26.242 + (0.4928T) + (1.42T^2)(0.223T^3) + (0.04129T^4) + (0.006295T^5) - (0.00196T^6) + (0.0001112T^7) \dots\dots\dots (5.2)$$

where: W = salinity of solution in eq. wt % NaCl
 T = halite disappearance temperature in °C/100

The densities of the LV inclusions were calculated from homogenization temperatures and salinities using the following equation (Bodnar, 1983):

$$D = 0.9923 - 3.0512 \times 10^{-2} T^2 - 2.1977 \times 10^{-4} T^4 + 8.6241 \times 10^{-2} S - 4.1768 \times 10^{-2} TS + 1.4825 \times 10^{-2} T^2 S + 1.4460 \times 10^{-3} T^3 S - 3.0852 \times 10^{-9} T^8 S + 1.3051 \times 10^{-2} TS^2 - 6.1402 \times 10^{-3} T^2 S^2 - 1.2843 \times 10^{-3} TS^3 + 3.7604 \times 10^{-4} T^2 S^3 - 9.9594 \times 10^{-9} T^2 S^7 \dots\dots\dots (5.3)$$

where: D = density in g/cm³,
 T = homogenization temperature in °C/100,
 S = salinity in wt%/10.

The densities of the LVH inclusions were calculated from vapour disappearance temperatures and salinities using the equation of state of Brown and Lamb (1989) in the computer program FLINCOR (Brown, 1989).

5.2 Results

152 primary LV inclusions and 43 primary LVH inclusions were measured. All these inclusions were either isolated or in a three dimensional arrays with consistent

Table 5.2: Summary of microthermometric data for LV fluid inclusions.

Sample	Min	Set	No	Type	Orig	T _e		T _{mI}		Salinity		TdV(Th)		Density	
						(°C)	std	(°C)	std	(wt%)	std	(°C)	std	(g/cm ³)	std
The Bond Zone															
B12-1	Ap	1	5	LV	p	-44	1	-21.5	2.1	23.2	1.4	359	35	0.84	0.04
B12-1	Ap	2	3	LV	p							320	19		
B12-1	Cal	1	1	LV	p	-30	0	-10.6	0.0	14.6	0.0	129	0	1.04	0.00
B12-1	Cal	2	1	LV	p	-28	0	-6.9	0.0	10.4	0.0	102	0	1.03	0.00
B12-1	Cal	3	1	LV	p	-30	0	-9.2	0.0	13.1	0.0	114	0	1.04	0.00
B12-1	Cal	4	1	LV	p	-38	0	-7.1	0.0	10.6	0.0	91	0	1.04	0.00
B12-1	Cal	5	1	LV	p			-2.5	0.0	4.3	0.0	107	0	0.98	0.00
B12-1	Cal	6	1	LVS	p	-28	0	-3.0	0.0	5.0	0.0	126	0	0.98	0.00
B12-1	Cal	7	1	LV	p	-30	0	-8.0	0.0	11.7	0.0	117	0	1.03	0.00
B4-2	Ap	1	3	LV	p	-50	0	-18.0	1.6	20.9	1.3	335	39	0.86	0.04
B4-2	Ap	2	7	LV	p	-35	0	-23.1	1.7	24.2	1.1	309	63	0.91	0.07
B4-2	Ap	3	3	LV	p	-35	0	-19.8	0.6	22.1	0.4	363	34	0.83	0.04
B4-8	Cal	1	1	LV	p	-51	0	-21.7	0.0	23.3	0.0	261	0	0.96	0.00
B4-8	Cal	2	1	LV	p							295	0		
B4-9	Cal	1	1	LV	p	-25	0	-14.0	0.0	17.8	0.0	274	0	0.92	0.00
B4-9	Cal	2	1	LV	p	-26	0	-14.9	0.0	18.5	0.0	231	0	0.97	0.00
The Mine															
IS90-68	Ap	1	1	LV	p							271	0		
IS90-68	Ap	2	1	LV	p							310	0		
IS90-68	Ap	3	1	LV	p	-32	0	-7.7	0.0	11.4	0.0	341	0	0.77	0.00
IS90-72	Cal	1	5	LV	p	-30	2	-8.7	0.8	12.5	1.0	224	7	0.93	0.00
IS90-72	Cal	2	2	LV	p			-10.4	0.2	14.4	0.2	240	2	0.93	0.00
IS90-79	Ap	1	3	LV	p	-24	1	-9.4	0.7	13.4	0.8	257	8	0.90	0.01
IS90-79	Cal	2	7	LV	p							233	36		
IS90-79	Cal	3	4	LV	p							229	10		
L91-1	Cal	1	3	LV	p			-10.7	1.5	14.7	1.6	155	39	1.02	0.02
L91-6	Cal	2	2	LV	p			-10.3	0.0	14.3	0.0	181	8	0.99	0.00
L91-6	Cal	3	1	LV	p			-9.1	0.0	13.0	0.0	101	0	1.05	0.00
The Manny Zone															
MA-1	Ap	1	2	LV	p	-53	0	-20.9	2.6	22.8	1.8	257	4	0.97	0.01
MA-1	Ap	2	3	LV	p			-13.0	0.0	16.9	0.0	315	11	0.86	0.01
MA-1	Ap	3	4	LV	p	-54	3	-20.6	1.3	22.6	0.9	269	2	0.95	0.00
MA-1	Ap	4	1	LV	p	-58	0	-23.4	0.0	24.4	0.0	310	0	0.91	0.00
MA-1	Ap	5	2	LV	p	-55	0	-17.3	1.8	20.3	1.4	339	3	0.85	0.00
MA-1	Ap	6	5	LV	p	-48	2	-15.8	1.5	19.2	1.2	276	13	0.92	0.01

Table 5.2 (Continued)

Sample	Min	Set	No	Type	Orig	Te		TmI		Salinity		TdV(Th)		Density	
						(°C)	ave	(°C)	ave	(wt%)	ave	(°C)	ave	(g/cm ³)	ave
The Monny Zone															
MA-1	Ap	7	5	LV	p	-51	0	-21.7	1.8	23.3	1.2	261	7	0.96	0.00
MA-1	Ap	8	1	LV	p	-31	0	-21.0	0.0	22.9	0.0	330	0	0.88	0.00
MA-1	Ap	9	3	LV	p	-52	1	-10.7	1.3	14.7	1.4	301	9	0.86	0.00
MA-1	Mtc	1	1	LVS	p	-59	0	-12.3	0.0	16.3	0.0	373	0	0.77	0.00
MA-1	Mtc	2	3	LV	ps	-39	0	-23.1	0.6	24.2	0.4	393	21	0.80	0.03
MA-1	Mtc	3	2	LV	ps	-31	0	-23.2	0.5	24.2	0.3	435	42	0.75	0.06
MA-1	Mtc	4	2	LV	ps							394	1		
MA-1	Mtc	5	1	LVS	p	-32	0	-24.0	0.0	24.7	0.0	378	0	0.82	0.00
MA-3	Ap	1	1	LV	p							348	0		
MA-3	Ap	2	4	LV	p	-35	0	-21.9	1.7	23.5	1.2	389	17	0.80	0.02
MA-3	Ap	3	5	LV	p	-29	0	-21.5	2.3	23.2	1.6	384	4	0.81	0.00
MA-4	Ap	1	2	LV	p			-9.9	1.5	13.9	1.6	219	25	0.95	0.01
MA-4	Ap	2	3	LV	p	-37	1	-12.6	3.3	16.5	3.3	279	8	0.90	0.02
MA-4	Ap	3	3	LV	p	-25	0	-15.5	2.7	18.9	2.3	263	4	0.94	0.01
MA-4	Ap	4	5	LV	p	-29	0	-14.3	3.5	18.0	2.9	255	32	0.94	0.02
MA-4	Ap	5	1	LV	p			-17.3	0.0	20.3	0.0	270	0	0.94	0.00
MA-4	Ap	6	2	LV	p	-25	0	-9.4	0.5	13.4	0.5	261	4	0.90	0.00
MA-4	Ap	7	2	LV	p	-51	0	-16.2	2.0	19.5	1.6	285	2	0.91	0.01
MA-4	Cal	1	1	LV	p							149	0		
MA-4	Cal	2	1	LV	p							179	0		
MA-4	Cal	3	1	LV	p							162	0		
MA-4	Cal	4	1	LV	p							177	0		
MA-4	Cal	5	2	LV	p			-11.1	0.0	15.1	0.0	185	11	0.99	0.01
MA-4	Cal	6	1	LVS	p							172	0		
MA-4	Cal	7	3	LV	p			-4.7	0.0	7.6	0.0	199	48	0.92	0.05
MA-4	Cal	8	1	LV	p							216	0		
MA-4	Cal	9	1	LV	p	-28	0	-10.1	0.0	14.1	0.0	209	0	0.96	0.00
MA-4	Cal	10	1	LV	p	-25	0	-12.5	0.0	16.5	0.0	205	0	0.98	0.00
MA-4	Cal	11	1	LV	p	-28	0	-7.5	0.0	11.1	0.0	208	0	0.94	0.00
MA-4	Mtc	1	2	LV	p			-17.2	0.0	20.2	0.0	382	6	0.79	0.00
MA-4	Mtc	2	4	LV	p	-27	0	-18.5	0.8	21.2	0.6	339	8	0.86	0.01
MA-4	Mtc	3	1	LV	p	-30	0	-21.9	0.0	23.5	0.0	350	0	0.85	0.00
MA-4	Mtc	4	1	LV	p							379	0		
MA-4	Mtc	5	2	LVS	p							367	8		
MA-5	Ap	1	2	LV	p							423	5		

Orig=origin of inclusion; Min=host mineral; Set=cogenetic group of inclusion
 Ap=apatite; Cal=calcite; Mtc=monticellite; No=number of inclusions measured
 in a cogenetic group; Ave: average; Std: standard deviation

Table 5.3: Summary of microthermometric data for LVH fluid inclusions.

Sample no.	Min	Set	No	Orig	Te (°C)			TdHh (°C)			Tdh (°C)			Salinity (wt% NaCl)			TdV (°C)			Th (°C)			Density (g/cm ³)			TD (°C)		
					ave	std	ave	std	ave	std	ave	std	ave	std	ave	std	ave	std	ave	std	ave	std	ave	std	ave	std	ave	std
The Mine																												
IS90-68	Ap	1	2	P	-48	3	1.9	0.4	284	7	37.0	0.5	334	37	334	37	334	37	334	37	334	37	1.04	0.04				
IS90-68	Ap	2	2	P	-41	0	-0.1	0.0	329	85	40.5	7.4	262	47	329	85	329	85	329	85	329	85	1.15	0.12				
IS90-69	Ap	1	1	P	-35	0	0.3	0.0	340	0	41.5	0.0	214	0	340	0	340	0	340	0	340	0	1.20	0.00	399	0		
IS90-69	Ap	2	1	P	-39	0	0.2	0.0					211	0														
IS90-69	Ap	3	2	P	-39	0	1.1	0.6	331	12	40.7	1.0	158	4	331	12	331	12	331	12	331	12	1.23	0.01				
IS90-69	Ap	4	1	P	-50	0	4.6	0.0																				
IS90-69	Ap	5	1	P			3.0	0.0	360	0	43.3	0.0	182	0	360	0	360	0	360	0	360	0	1.24	0.00				
IS90-69	Ap	6	1	P	-35	0							172	0														
IS90-69	Ap	7	1	P	-45	5	3.1	0.0	335	0	41.1	0.0	157	0	335	0	335	0	335	0	335	0	1.24	0.00				
IS90-69	Ap	8	1	P	-47	1	-0.5	0.0	291	0	37.5	0.0	146	0	291	0	291	0	291	0	291	0	1.21	0.00				
IS90-69	Ap	9	1	P	-50	2	2.1	0.0	285	0	37.0	0.0	99	0	285	0	285	0	285	0	285	0	1.24	0.00				
IS90-69	Ap	10	1	P	-35	8	-2.1	0.0	341	0	41.6	0.0	178	0	341	0	341	0	341	0	341	0	1.23	0.00				
IS90-69	Ap	11	2	P					339	14	41.4	1.3	158	20	339	14	339	14	339	14	339	14	1.24	0.02				
IS90-69	Ap	12	6	P	-48	2	2.2	1.6	319	23	39.7	1.9	196	12	319	23	319	23	319	23	319	23	1.20	0.02				
IS90-69	Ap	13	4	P	-40	0	0.7	0.8	342	9	41.7	0.8	147	9	342	9	342	9	342	9	342	9	1.25	0.01				
IS90-69	Ap	14	5	P	-40	0	0.1	0.0	334	15	40.9	1.3	200	44	334	15	334	15	334	15	334	15	1.21	0.04				
IS90-69	Ap	15	1	P	-35	0	2.1	0.0	343	0	41.7	0.0	265	0	343	0	343	0	343	0	343	0	1.16	0.00				
L91-5	Ap	1	5	P	-38	3	1.7	1.5	283	26	36.9	1.9	173	21	283	26	283	26	283	26	283	26	1.19	0.03				
L91-5	Ap	2	1	P					248	0	34.5	0.0	128	0	248	0	248	0	248	0	248	0	1.20	0.00				
L91-5	Ap	3	2	P					269	16	35.9	1.0	140	9	269	16	269	16	269	16	269	16	1.21	0.02				
The Manny Zone																												
MA-1	Mtc	1	1	P					175	0	30.7	0.0	460	0	460	0	460	0	460	0	460	0	0.85	0.00				
MA-1	Mtc	2	1	P	-26.3	0	0.5	0.0	146	0	29.5	0.0	468	0	468	0	468	0	468	0	468	0	0.83	0.00				

Origin of inclusion; Min-host mineral; Set-cogenetic group of inclusions; Ap=apatite;
 No-number of inclusions measured in a co-genetic group

phase ratios, and are therefore not considered to have undergone necking. No phase changes were observed that might indicate the presence of CO₂, such as clathrate melting (Rodder, 1984).

Temperatures of the eutectic point (Te), final ice melting (TmI), hydrohalite dissolution (TdHh), vapour disappearance (TdV), halite dissolution (TdH), inclusion homogenization (Th), and inclusion decrepitation (TD), salinities and densities are summarized in Tables 5.2 and 5.3, and Figures 5.1, 5.2, 5.3, 5.4 and 5.5. All of these values are presented as averages for a co-genetic group of inclusions, along with the standard deviation for each group.

5.2.1 LV inclusions

Inclusions in calcite

Te values for LV inclusions in calcite range from -25 to -51°C. TmI values lie in the range -2.5 to -20.9°C, which translate into salinities of 4.3 to 23.3 wt. % (Figure 5.1). The inclusions homogenized to the liquid phase between 95 and 295°C (Figure 5.1). The densities of the inclusions range from 0.92 to 1.04 g/cm³. The inclusions from the Mine have relatively consistent salinities but variable Th values. The inclusions from the Manny Zone have variable salinities and consistent Th values. The data from the Bond Zone are divided into two groups: 1) high Th and salinities which are from the inclusions in niocalite-bearing sovites; and 2) low Th and salinities which are from the inclusions in niocalite-free sovites.

Inclusions in apatite

Te values for LV inclusions in apatite lie in a range -24 to -58°C. TmI values range from -7.4 to -23.4°C, which translate into salinities of 11.1 to 24.4 wt. % (Figure 5.2). The inclusions homogenized to the liquid phase between 219 and 423°C (Figure 5.2). The densities of the inclusions lie in the range 0.77 to 0.97 g/cm³.

All of the LV inclusions in apatite from the Mine are spheroidal. They have low Th values and salinities relatively to the elongate LV inclusions from the Manny Zone and the Bond Zone. The Th values and salinities of the inclusions from the Bond Zone are relatively high and consistent. In contrast, the Th values and salinities of the inclusions from the Manny Zone are very variable.

Two of the spheroidal LV inclusions showed unusual behaviour. In most LV

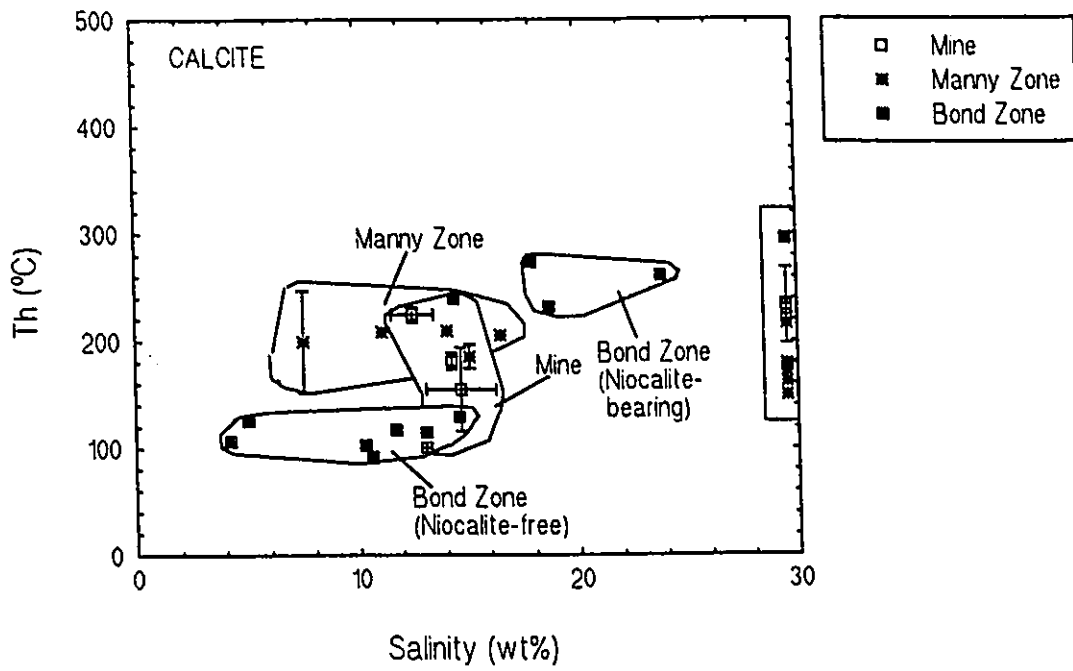


Figure 5.1. Salinity-Th plot of LV inclusions in calcite.

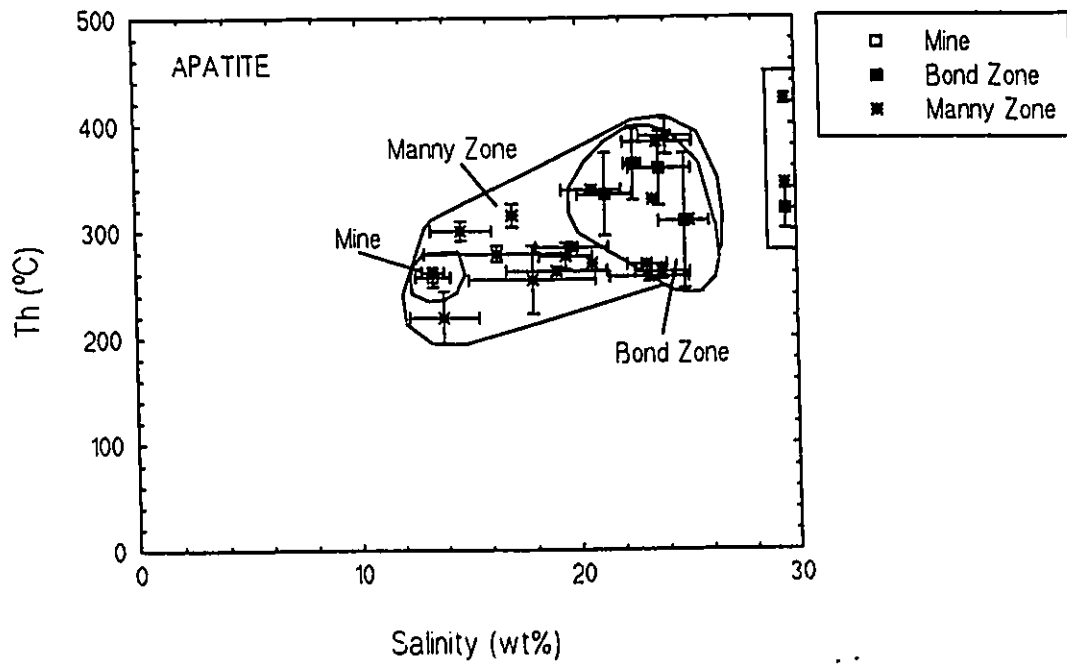


Figure 5.2. Salinity-Th plot of LV inclusions in apatite.

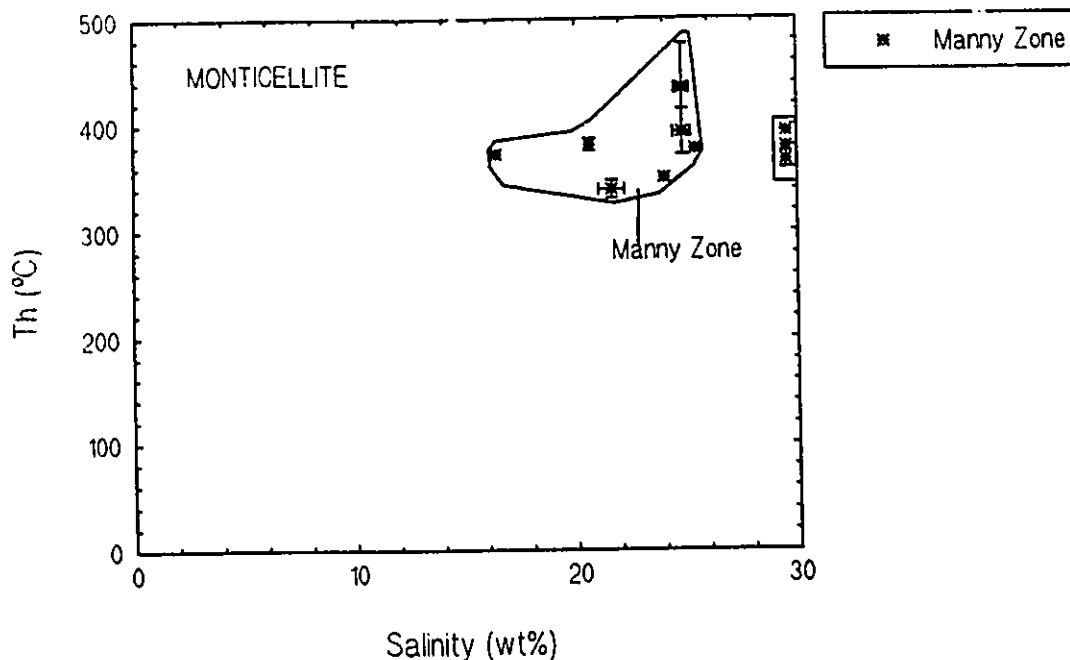


Figure 5.3. Salinity-Th plot of LV inclusions in monticellite.

inclusions, including both elongate and spheroidal types, ice was the last phase to melt and they homogenized to the liquid phase between 219 and 423°C. However, the ice in the two spheroidal inclusions melted at -7.5°C in the presence of crystals with high interference colours. Their high birefringence and the fact that they did not dissolve until 27°C suggest that they may be natron. The two inclusions decrepitated at 92 and 121°C.

Inclusions in monticellite

The values for LV inclusions in the monticellite from the Manny Zone lie between -27 and -59°C. TmI values lie in the range -12.3 to -24.0°C, which gives salinities ranging from 16.3 to 24.7 wt. % (Figure 5.3). The inclusions homogenized to the liquid phase between 339 and 435°C (Figure 5.3). Their densities range from 0.75 to 0.86 g/cm³.

5.2.2 LVH inclusions

On cooling the LVH inclusions, the cubic mineral normally does not change, and freezing is accompanied by shrinkage and disappearance of the vapour bubble. On

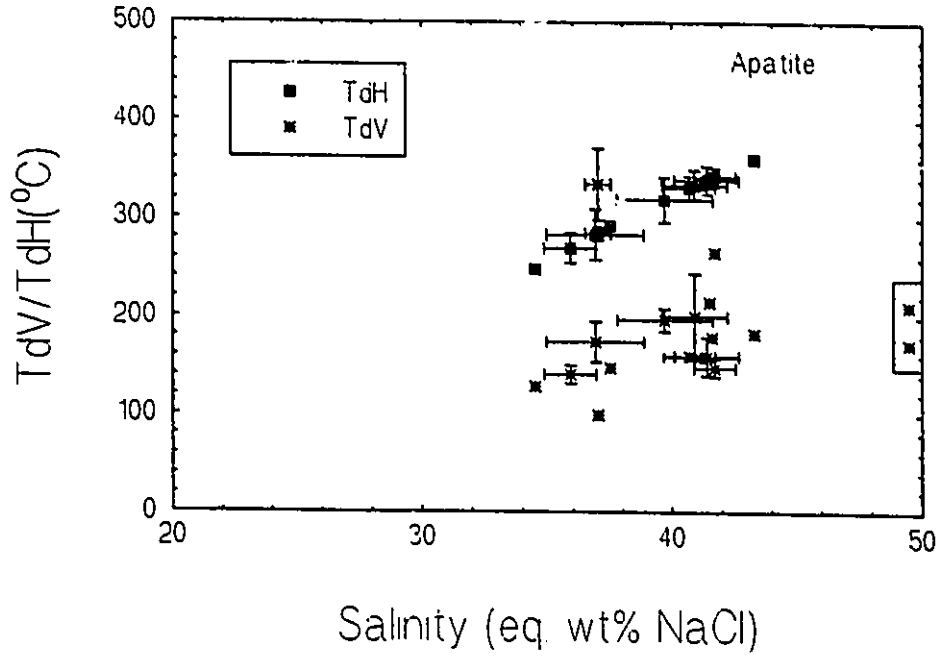


Figure 5.4. Salinity-TdV/TdH plot of the LVH inclusions in apatite

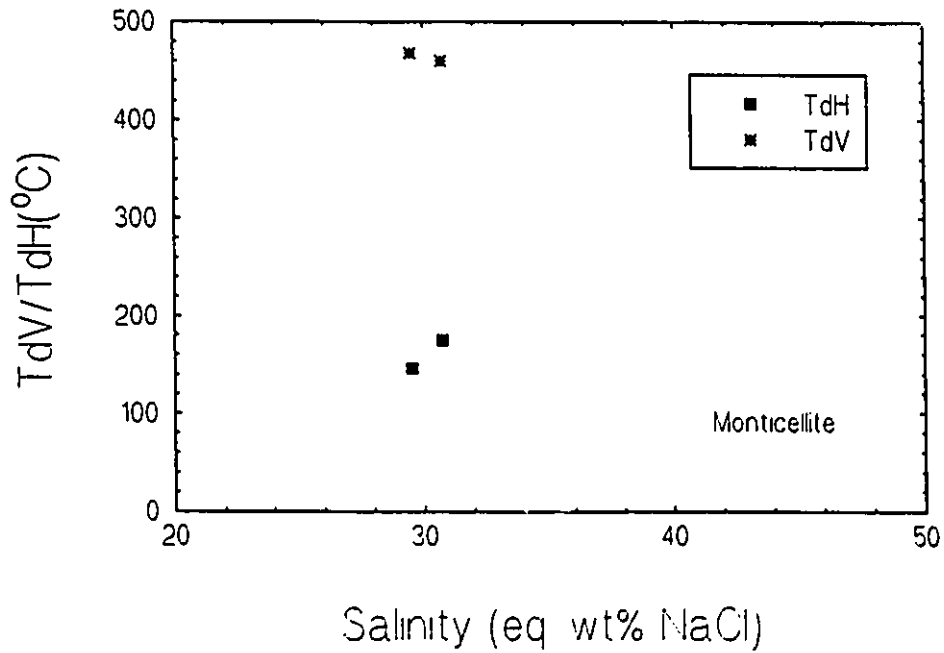


Figure 5.5. Salinity-TdV/TdH plot of the LVH inclusions in monticellite.

heating, the inclusions started to melt at temperatures of -26 to -50°C. At about -10 to -20°C, the cubic mineral reacted with the liquid and diminished in size with formation of abundant, small birefringent crystals around the cubic mineral. The birefringent crystals have a higher refractive index than the liquid and are probably hydrohalite. This reaction suggests that the cubic mineral is halite. On further heating, the halite reappeared on dissolution of the hydrohalite at temperatures ranging from -2.1 to 4.6°C. Although hydrohalite can not exist in equilibrium with halite at temperatures above 0°C, it is often present as a metastable phase (Roedder, 1984).

Inclusions in apatite

Te values for LVH inclusions in apatite from the Mine range from -35 to -50°C. Final ice melting was not observed because of the small size of the inclusions. TdHh varied from -2.1 to 4.6°C. The inclusions normally homogenized to the liquid phase by halite dissolution between 248 and 360°C, with TdV in the range 99 to 265°C (Figure 5.4). TdH shows a positive correlation with TdV. Only one of the inclusions homogenized to the liquid phase by vapour disappearance at 334°C (TdH=284°C) (Figure 5.4). The salinities of all inclusions lie in the range 34.5 to 43.3 equiv. wt. % NaCl (Figure 5.4). The densities of the inclusions vary from 1.04 to 1.25 g/cm³.

Inclusions in monticellite

Two LVH inclusions in monticellite from the Manny Zone were measured. One of the inclusions gave a Te value of -26°C and a TdHh value of 0.5°C. These inclusions homogenized to the liquid phase by vapour disappearance at 460 and 468°C, with TdH of 175 and 146°C (Figure 5.5). The salinities of the inclusions are 30.7 and 29.5 equiv. wt. % NaCl (Figure 5.5). The densities of the inclusions are 0.85 and 0.83 g/cm³.

5.3 Discussion

5.3.1 Composition and salinity of inclusions

Te values provide qualitative information about the components dissolved in the aqueous portion of inclusions (Table 5.4). Te values for the inclusions from the Oka carbonatite lie in the range -24 to -59°C. The presence of halite in the LVH

inclusions indicates they are rich in NaCl, and it is likely that the LV inclusions also contain significant NaCl. However, the low Te values require the presence of several other chloride species, presumably including Ca chloride as Ca is a major component of host calcite and apatite, which also occur as trapped minerals in the inclusions.

Table 5.4: Eutectic temperatures (Te) of aqueous solutions (Crawford, 1981).

Solution	Te (°C)	Solution	Te (°C)
NaCl-H ₂ O	-20.8	NaCl-CaCl ₂ -H ₂ O	-52.0
KCl-H ₂ O	-10.6	NaCl-MgCl ₂ -H ₂ O	-35
CaCl ₂ -H ₂ O	-49.8	Na ₂ CO ₃ -H ₂ O	-2.1
MgCl ₂ -H ₂ O	-33.6	NaHCO ₃ -H ₂ O	-2.3
NaCl-KCl-H ₂ O	-22.9	Na ₂ SO ₄ -H ₂ O	-1.2

The presence of calcite, nahcolite and mirabilite in the inclusions in apatite suggest that, in addition to Cl⁻, CO₃²⁻, HCO₃⁻ and SO₄²⁻ are present in significant amounts in the inclusions. The contents of CO₃²⁻ and SO₄²⁻ can be estimated by considering phase equilibria in the NaCl-Na₂CO₃-H₂O and NaCl-Na₂SO₄-H₂O systems. In the LV inclusions in apatite, ice is the last phase to melt (between -7.4 and -23.4°C), which suggests that Na₂CO₃ and Na₂SO₄ concentrations in the inclusions are less than 2.5 % and 2 % respectively (Figure 5.6 and 5.7). If Na₂CO₃ and Na₂SO₄ concentrations were any higher, mirabilite or natron would be the last phases to melt. The ice melting temperature of -7.5°C and the natron melting temperature of 27°C of two spheroidal inclusions indicates that the inclusions contain about 70% H₂O, 24 % Na₂CO₃ and 6% NaCl (Figure 5.6).

Minor errors are inherent in calculating the salinities of the LV inclusions by using the NaCl-CaCl₂-H₂O system and assuming an X_{NaCl} value of 0.9. The X_{NaCl} value is an average for all inclusions in apatite. The results of the decrepitate analyses indicate that the X_{NaCl} values of the inclusions in apatite vary from 0.4 to 1 (see Chapter 6). However, the resultant errors in salinities are small as the TmI values of most

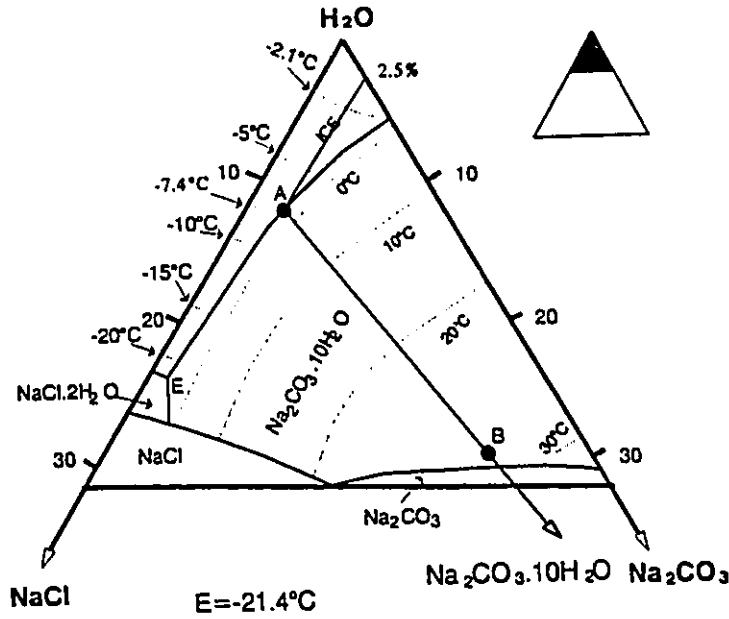


Figure 5.6. Phase diagram for part of the NaCl-Na₂CO₃-H₂O system. The melting path for the two spheroidal inclusions proceeded from E (eutectic point at -21.4°C), through A (ice melting at -7.5°C), to B (natron dissolution at 27°C). Data from Linke (1965).

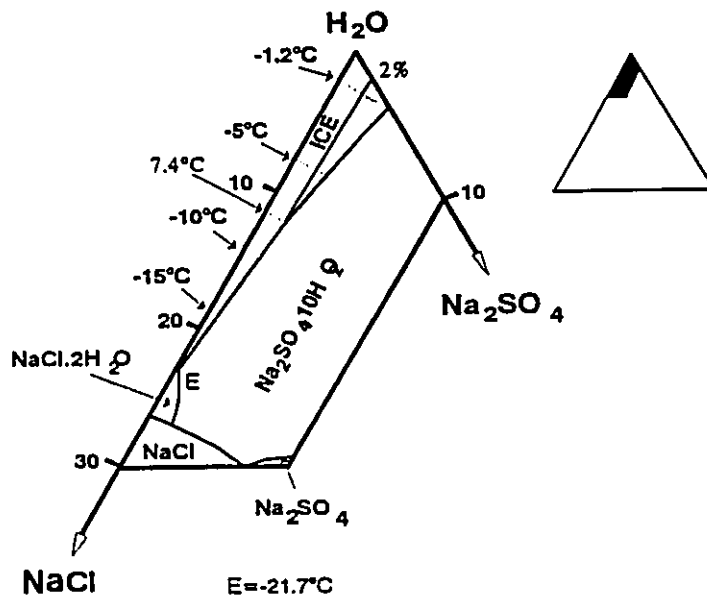


Figure 5.7. Phase diagram for part of the NaCl-Na₂SO₄-H₂O system. Data from Linke (1965).

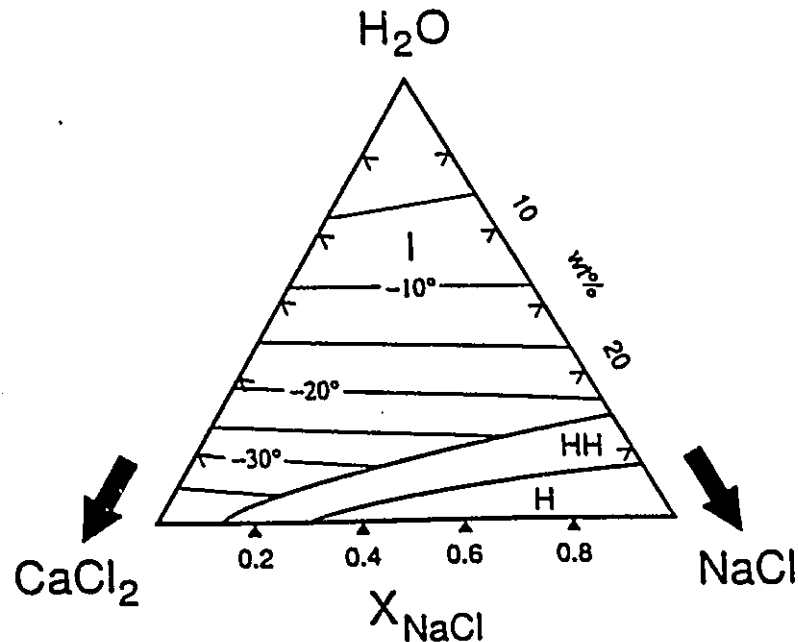


Figure 5.8. Isotherms of the ice liquidus at 1 atm total pressure in the system NaCl-CaCl₂-H₂O as calculated from Equation 5.1 (Oakes et al. 1990).

inclusions in apatite range from -10 to -22°C and the X_{NaCl} value does not affect the calculated salinity much (Figure 5.7). The maximum error is about 0.14 wt. %. It is difficult to estimate the errors of salinities for the inclusions in calcite and monticellite as no data on NaCl/CaCl₂ ratios are available for these inclusions. The effect of X_{NaCl} on salinities will be less for inclusions in monticellite than for inclusions in calcite as X_{NaCl} has a greater effect on T_{mI} at low salinities compared to high salinities (Figure 5.8). The magnitude of the error will vary depending on the NaCl/CaCl₂ ratios in the inclusions.

The presence of Na₂SO₄ and Na₂CO₃ slightly decreases ice melting temperatures (Figure 5.6 and 5.7), which may affect the calculated salinity. However, this error will be small for most inclusions because the concentration of these components in the inclusions is low.

5.3.2 Fluid evolution

Abundant primary fluid inclusions in calcite, apatite and monticellite in the Oka carbonatite suggest that hydrothermal fluids existed in the carbonatite magma during

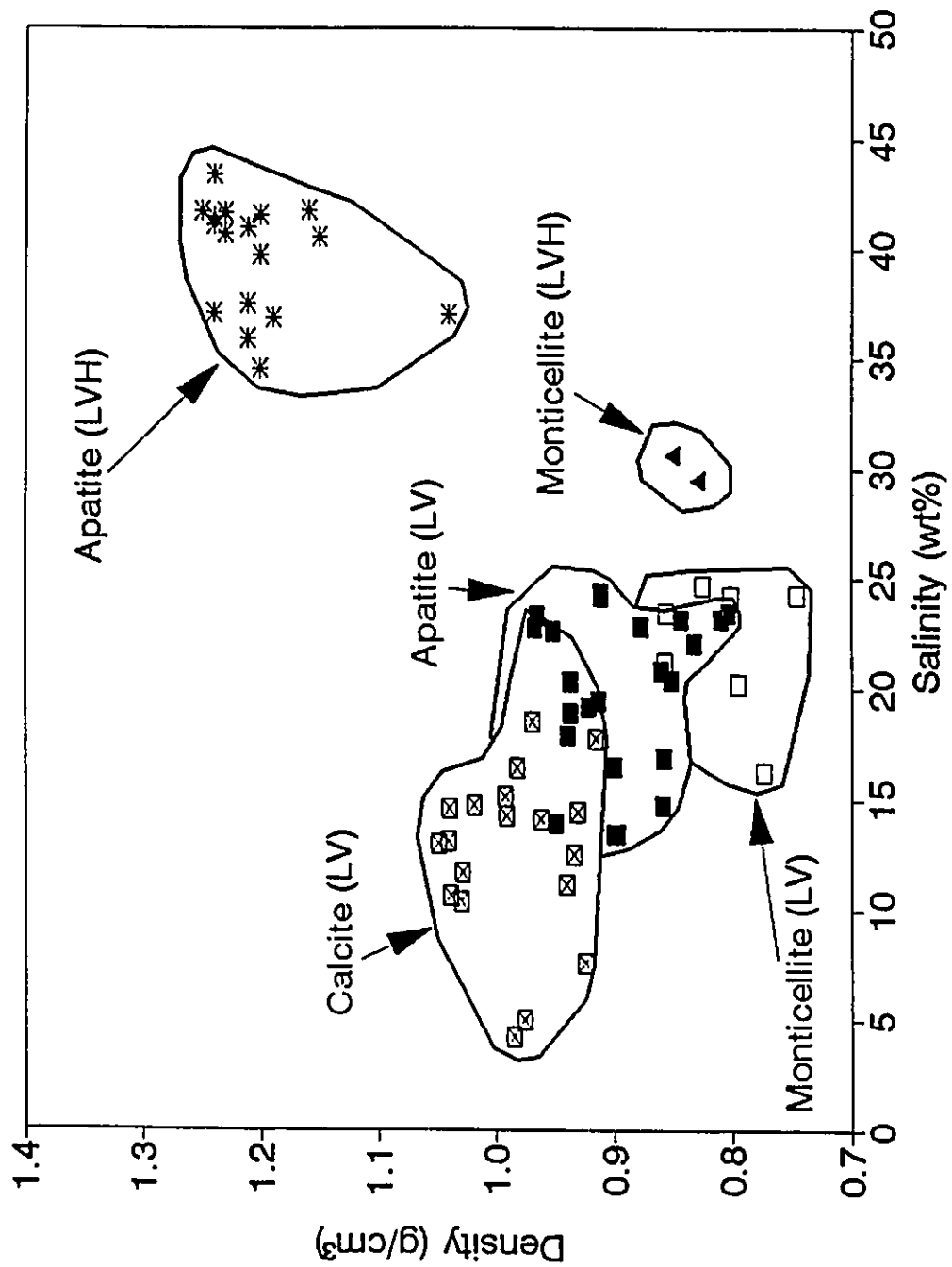


Figure 5.9. Salinity-density plot of all inclusions from the Oka carbonatite.

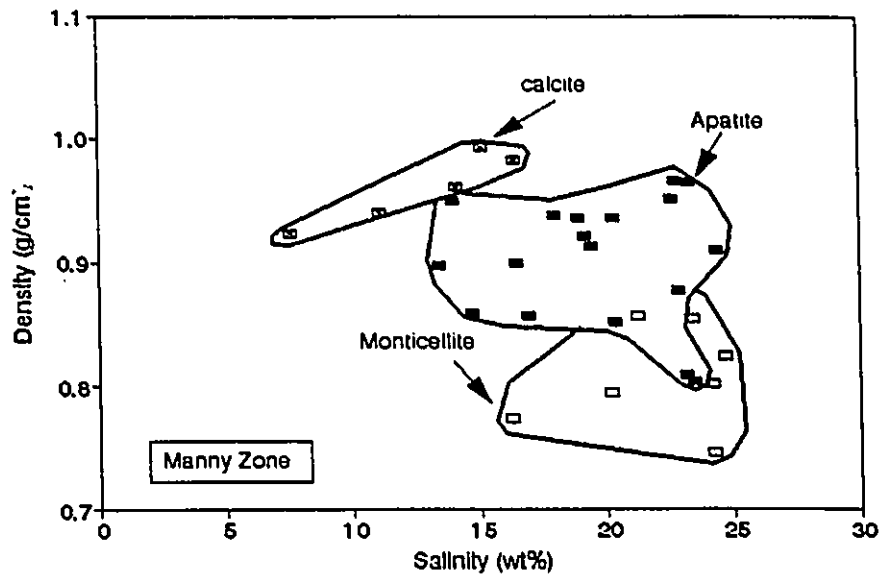


Figure 5.10. Salinity-density plot of the LV inclusions from the Manny Zone.

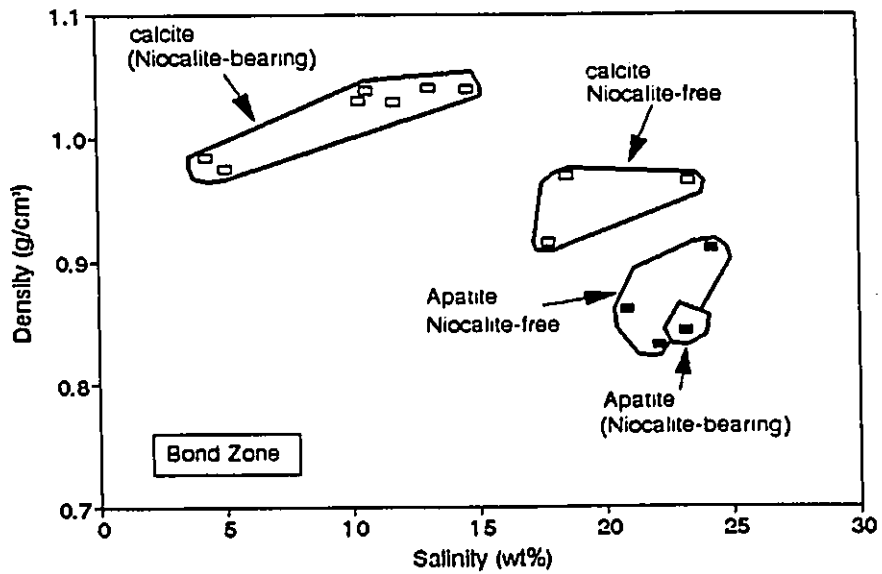


Figure 5.11. Salinity-density plot of the LV inclusions from the Bond Zone.

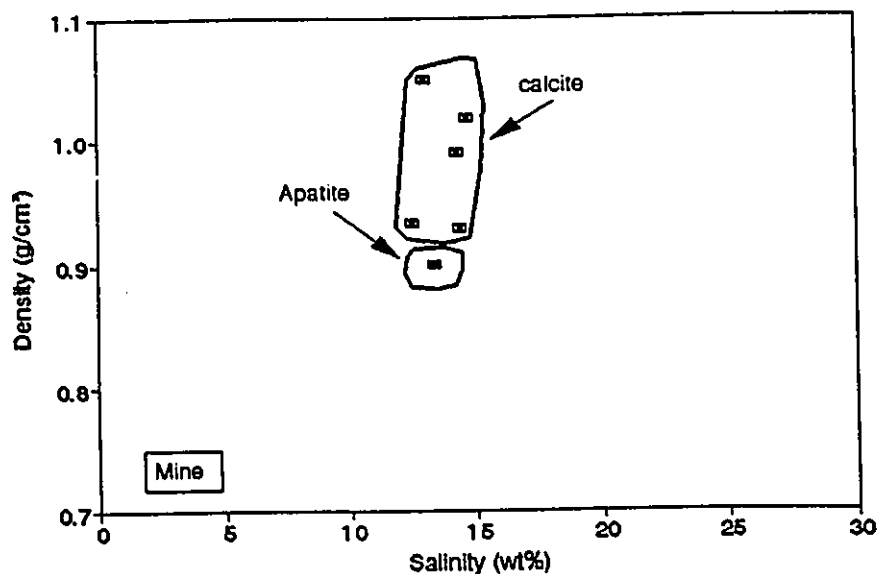


Figure 5.12. Salinity-density plot of the LV inclusions from the Mine.

the crystallization of these minerals. There are two types of fluids: low-salinity fluids which are represented by the LV inclusions and high-salinity fluids which are represented by the LVH inclusions.

As discussed in Chapter III, the inclusion-bearing minerals crystallized in the sequence monticellite-apatite-calcite. The microthermometric results of the LV inclusions indicate that the salinities decrease and the densities increase from monticellite, through apatite, to calcite (Figure 5.9). An increase in density can be caused by an increase in pressure or fluid salinity, or by a decrease in temperature. Pressure is usually constant or decreases during crystallization as the magma ascends and the fluid salinities show a decrease from monticellite, through apatite, to calcite, which implies that the increase in fluid density resulted from decreasing temperature. Therefore, the hydrothermal fluid trapped in the LV inclusions evolved from high to low salinity and from high to low temperature during crystallization. This evolution trend is evident in the Manny Zone and the Bond Zone (Figure 5.10 and 5.11). In the Mine, LV inclusions in apatite have almost the same salinities as the inclusions in calcite (Figure 5.12). In the Bond Zone, the difference in salinity and density between

the inclusions in calcite and the inclusions in apatite is much larger in the niocalite-bearing sovite than in niocalite-free sovite (Figure 5.11), which suggest that crystallization conditions for apatite and calcite had changed much more in niocalite-bearing sovite than in niocalite-free sovite.

In monticellite, most inclusions are LV inclusions and a few are LVH inclusions. These two types of inclusions occur in the same crystals and have the same densities and similar salinities (Figure 5.9), which suggests that the inclusions were formed from the same fluids under similar conditions. It is likely that the LVH inclusions were formed by necking after the inclusions were trapped. Most of the primary inclusions in apatite from the mine are LVH, whereas those in calcite are LV. Again this indicates evolution from high to low salinity, although clearly the early fluids in the Mine were of much higher salinity than in the other zone (Figure 5.9). The decrease in density signifies decrease in salinity, rather than a pressure or temperature variation.

5.3.3 Estimation of crystallization conditions of inclusion-bearing minerals

Wyllie & Tuttle (1960) determined that the eutectic temperature in carbonatite melts at 1 kb is as low as 625°C, which is considered a minimum crystallization temperature for calcite. Isochores were calculated (Figure 5.13) using the computer program FLINCOR (Brown, 1989) and the equation of state of Brown and Lamb (1989). The isochores were drawn beyond the pressure range (0 to 3 kb) over which of the equation of state is valid by simple straight line extrapolation. Assuming a minimum crystallization temperature for calcite of approximately 625°C, the minimum pressure at which calcite can have crystallized is estimated to be about 7 to 10 kb (Figure 5.13, range A). Assuming that calcite, apatite and monticellite crystallized at the same pressure, or that pressure decreased during crystallization (magma ascent), the minimum crystallization temperatures for apatite and monticellite are estimated to be about 625 to 850 and 800 to 1180°C respectively (Figure 5.13, range B and C).

Conway & Taylor (1969) measured $^{18}\text{O}/^{16}\text{O}$ ratios of coexisting calcite and magnetite, which were in isotopic equilibrium, in two aegerine augite-biotite-magnetite-apatite carbonatite samples from the Mine and one niocalite-biotite-magnetite-apatite carbonatite sample from the Bond Zone. They calculated

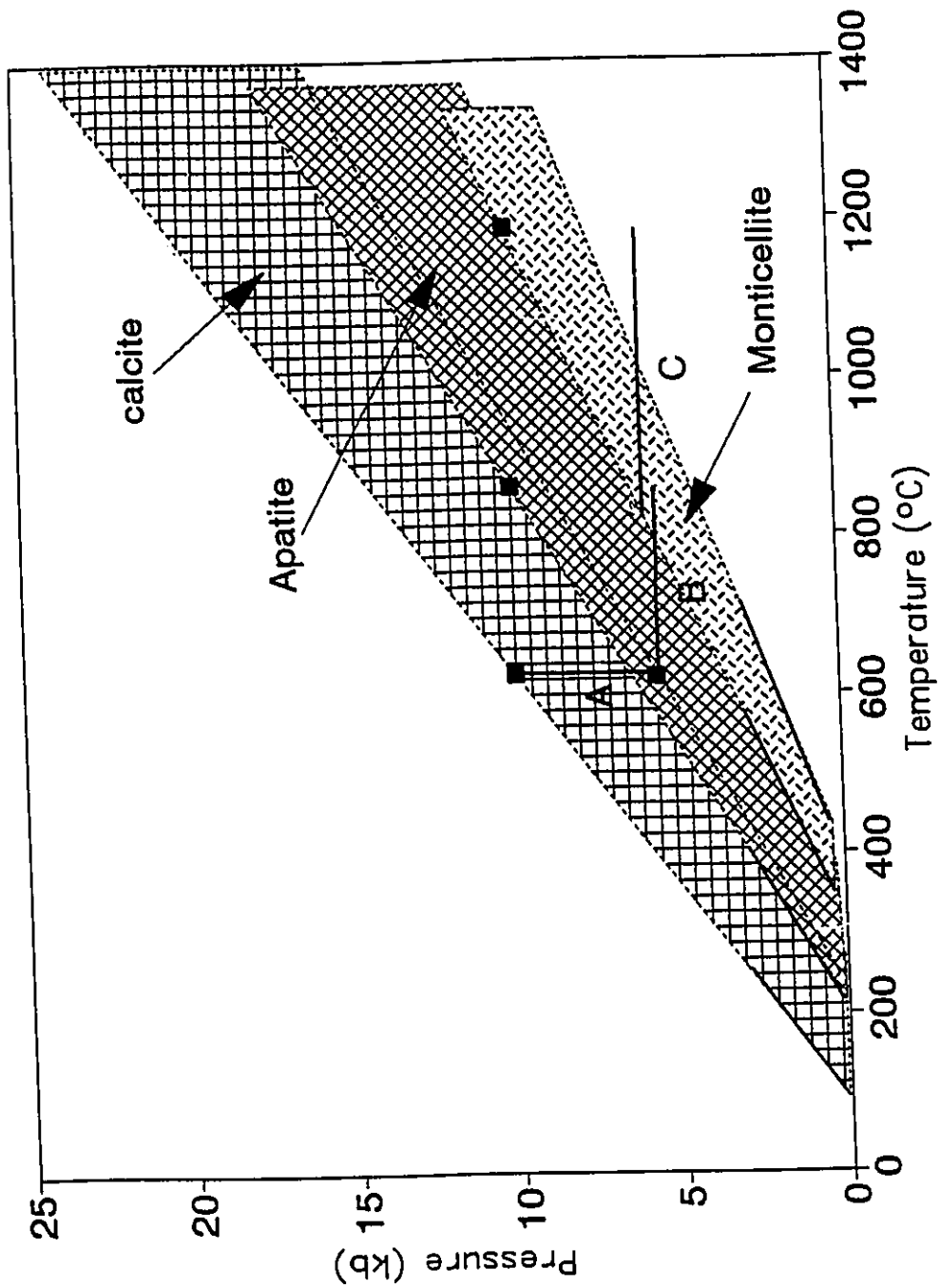


Figure 5.13. Isochores for the LV inclusions.

crystallization temperatures for the rocks from the fractionation of ^{18}O and ^{16}O between calcite and magnetite, and found that they ranged from 720 to 730°C, which are consistent with the estimates made from the fluid inclusion data.

CHAPTER VI COMPOSITION OF FLUID INCLUSIONS

6.1 Introduction

Microthermometric data and the nature of the daughter minerals in fluid inclusions from Oka indicate that the fluids are CO₂-poor and chemically complex. In addition to Na⁺ and Cl⁻, the commonest components in fluid inclusions, the inclusions contain Ca²⁺, CO₃²⁻, HCO₃⁻ and SO₄²⁻ in significant amounts and probably Mg²⁺ and K⁺. In order to further characterize the fluid compositions, leachate analyses and decrepitate analyses were performed to obtain quantitative or semiquantitative data on electrolyte chemistry, and laser Raman spectroscopy and quadrupole mass spectrometry were used to determine the gas compositions of the inclusions.

6.2 Leachate Analyses

Apatite in the Oka carbonatite is suitable for leachate analysis as it contains only one generation of primary fluid inclusions. Apatite separates from four monticellite-apatite sovite samples were used for leachate analysis. The apatite from samples MA-1 and MA-4 from the Manny Zone contain abundant LV inclusions and the apatite from samples IS90-68 and IS90-69 from the Mine is rich in LVH inclusions. Inclusion-free apatite in sample B7-1 from the Bond Zone was used as a blank and went through the same cleaning, crushing-leaching and analytical procedures as the inclusion-rich samples.

6.2.1 Experimental procedure

Rocks were crushed into grains of 65 to 185 μm, the size of most apatite crystals, before mineral separation. Magnetite was picked out using a hand magnet. Apatite and calcite were separated from other minerals including monticellite, aegerine augite, biotite, pyrochlore and perovskite using an isodynamic magnetic separator. Apatite was separated from calcite using tetrabromoethane diluted to a density of 2.9 g/cm³ with acetone. Any remaining calcite was dissolved by washing the apatite separates in 10% acetic acid for 20 minutes. The visually estimated purity of the apatite separates was about 99% (Figure 6.1).

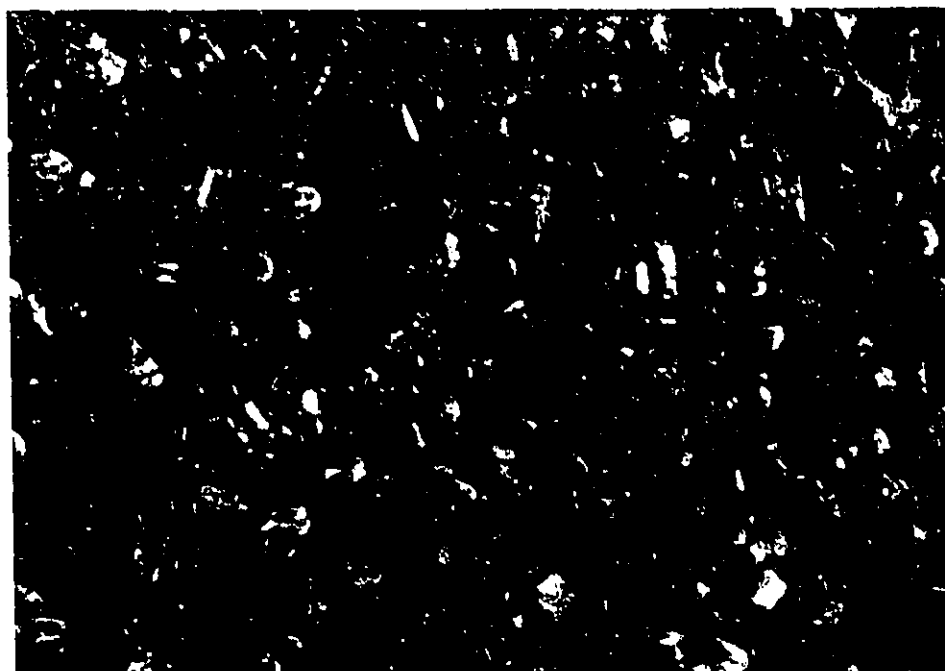


Figure 6.1. Apatite separates.

The apatite separates were soaked in 5% acetic acid for 2 hours, then cleaned in an ultrasonic cleaner with de-ionised water, which was changed every 30 minutes in first two hours, then every eight hours for the next two days. They were then washed in de-ionised water five times. The separates were dried in an oven at 120°C and crushed in a mortar and pestle which contained 5 ml of nanopure doubly distilled water to avoid evaporation of salt components. Leaching was carried out using nanopure doubly distilled water. The leachates were separated from the apatite powder by filtering and centrifuging. Ca, Fe, K, Mg, and Na were analyzed by graphite-furnace atomic absorption spectrophotometry at McGill University. Detection limits were 0.06, 0.1, 0.02, 0.01 and 0.01 ppm respectively. Cl was analyzed using a Dionex ion chromatograph at McGill University with a detection limit of 0.03 ppm. The remaining fluid was diluted with an equal amount of nanopure doubly distilled water in order to attempt HCO_3^- , CO_3^{2-} and SO_4^{2-} analyses (in order to provide enough fluid). However, the concentrations of the ions were below the detection limits of the ion-chromatograph.

6.2.2 Results and discussion

The results of the leachate analyses are summarized in Table 6.1. In comparison to sample values, blank values are high for Ca, Mg and Fe and relatively low for K, Na and Cl, which indicate that the errors of the Ca, Mg and Fe data are large (Table 6.1) and these data can not be used, and the data of K, Na and Cl are usable. The Ca contamination was possibly caused by dissolution of calcite inclusions in the apatite.

Atomic ratios of K and Cl to Na of the samples vary from 0.05 to 0.13 and from 0.21 to 0.4 respectively. There is not much difference in Cl/Na ratios between the two types of inclusions. The LV inclusions have higher K/Na ratios than the LVH inclusions.

As a check on the quality of the analyses, anion deficiency, which is the difference between total positive charge and total negative charge as a percentage of total positive charge, was calculated. Anion deficiencies for the samples are very large, ranging from 74 to 86%, which suggests either that a large amounts of Cl was absorbed onto apatite surfaces, or that other undetected anions, such as carbonate and/or sulphate were present in the fluids. The presence of calcite, nahcolite and

Table 6.1: Summary of leachate analysis data.

Sample #	Measured Concentrations (ppm)						Charge Anion			Atomic Ratios	
	Ca	Mg	Fe	K	Na	Cl	+	-	Def (%)	K/Na	Cl/Na
B7-1(Blank)	1.52	0.01	0.16	0.14	0.29	0.26	93	7	93	0.22	0.58
IS90-68	1.53	0.03	0.28	0.97	11.90	3.80	85	15	83	0.05	0.21
IS90-69	2.07	0.05	0.33	0.59	5.81	3.60	79	21	74	0.06	0.40
MA-1	1.72	0.05	0.15	0.79	3.69	1.40	87	13	86	0.13	0.25
MA-4	1.78	0.04	0.22	0.73	3.27	1.40	87	13	85	0.13	0.28
Ave of LVH	1.80	0.04	0.31	0.78	8.86	3.70	82	18	65	0.05	0.30
Ave of LV	1.75	0.05	0.19	0.76	3.48	1.40	87	13	74	0.13	0.26
Det Limit	0.06	0.01	0.10	0.02	0.01	0.03					
	Blank value/Sample value										
Sample #	Ca	Mg	Fe	K	Na	Cl					
IS90-68	0.99	0.67	0.57	0.14	0.02	0.07					
IS90-69	0.73	0.40	0.48	0.24	0.05	0.07					
MA-1	0.88	0.40	1.07	0.18	0.08	0.19					
MA-4	0.85	0.50	0.73	0.19	0.09	0.19					

Ave: average; Det: detection; Def: deficiency

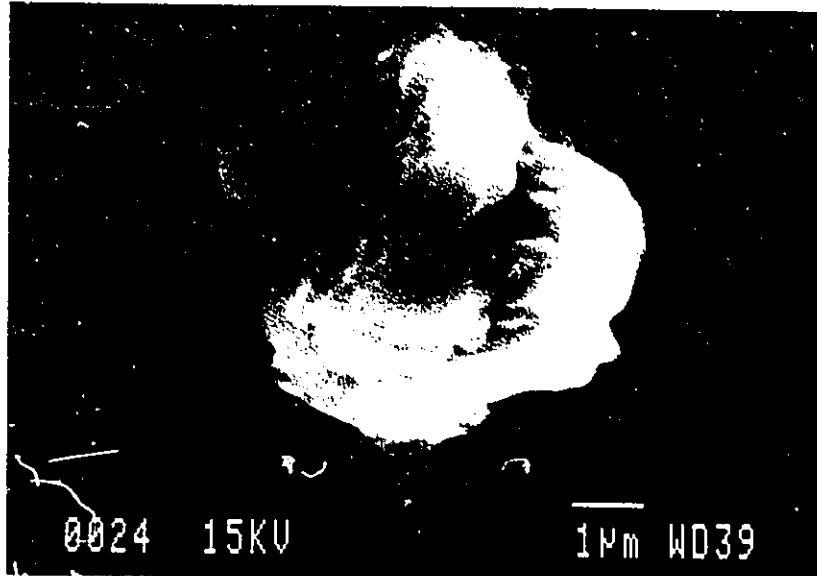


Figure 6.2. SEM view of a discrete decrepitate mount in apatite.

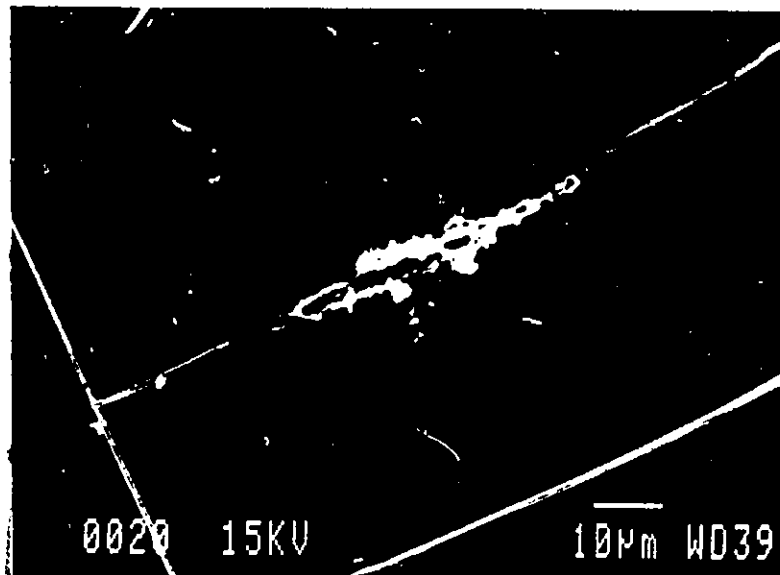


Figure 6.3. SEM view of a linear decrepitate along a fracture in apatite.

mirabilite in the inclusions suggests that carbonate and sulphate may be present in significant concentrations in the inclusions and may be the cause of the anion deficiencies.

6.3 Decrepitate Analyses

6.3.1 Decrepitate formation

Decrepitation of fluid inclusions was achieved by heating doubly-polished wafers of apatite and calcite to between 400 and 500°C, about 130 to 170°C above the homogenization temperatures of the inclusions. Fluids released upon decrepitation travelled to the wafer's surfaces from inclusion cavities or along fractures. The salt precipitates (decrepitates) were deposited either in discrete mounds (Figure 6.2) or in linear trails (Figure 6.3). The decrepitate mounds are 5 to 10 μm in diameter and the linear trails are 10 to 20 μm long and 1 to 3 μm wide.

6.3.2 Analytical procedure

After decrepitation, the samples were kept in a desiccator until they could be carbon-coated. They were analyzed using SEM or EM within 10 hours in order to reduce the loss of some components through evaporation and to avoid inhomogeneity produced either through CaCl_2 deliquescence, or NaCl or KCl creep, all of which occur when samples are left in a desiccator for a long time (Haynes et al., 1988).

SEM analyses were performed at McGill University on a JSM-U3 scanning electron microscope fitted with an energy dispersive analyzer (EDA). The analysis parameters are listed in Table 4.1. All analyses were conducted over rastered areas covering most of the decrepitate surface. Concentrations of elements were calculated using the instrument's computer software.

EM analyses were carried out at the University of Michigan, on a Cameca Camebax microprobe equipped with a wavelength dispersive spectrometer (WDS). Standard operating conditions use an accelerating voltage of 10 kV and a current of 10 μA . A 1 μm -diameter electron beam was used for all analyses. A variety of well-characterized natural and synthetic materials were used as standards for quantitative analysis (Table 6.2). Concentrations of elements were calculated using Cameca software.

Table 6.2 : Materials used as standards for EM analysis.

Element	Standard	Element	Standard
K	Adularia	P	Synthetic La phosphate
Na	Halite	S	Anhydrite
Ca	Anhydrite	F	Fluortopaz
Mg	Synthetic enstatite	Cl	Halite
Si	Synthetic enstatite	La	Synthetic La phosphate
Fe	Synthetic ferrosilite	Ce	Synthetic Ce phosphate
Sr	Celestite	Nd	Synthetic Nd phosphate

6.3.3 Calculation of decrepitate composition

The results of decrepitate analyses represent a mixture of the decrepitate and its substrate, therefore it is necessary to separate the contribution of the substrate from the decrepitate. The following relationship is established for the decrepitate analyses in apatite:

$$C_i^t = xC_i^{ap} + yC_i^d \dots\dots\dots(6.1)$$

$$C_p^t = xC_p^{ap} + yC_p^d \dots\dots\dots(6.2)$$

$$x + y = 1 \dots\dots\dots(6.3)$$

where:

- C_i^t = total concentration of element i;
- C_i^{ap} = concentration of element i in host apatite;
- C_i^d = concentration of element i in decrepitate;
- C_p^t = total phosphorus concentration;
- C_p^{ap} = phosphorus concentration in host apatite;
- C_p^d = phosphorus concentration in decrepitate;
- x = proportion of host apatite in the mixture;
- y = proportion of decrepitate in the mixture.

Solving Equations (6.1), (6.2) and (6.3) gives:

$$x = \frac{C_p^t - C_p^d}{C_p^{ap} - C_p^d} \dots \dots \dots (6.4)$$

$$C_i^d = \frac{C_i^t - xC_i^{ap}}{1-x} \dots \dots \dots (6.5)$$

In order to calculate C_i^d (Equation 6.5), x must be calculated. This may be achieved if there is an element in the mineral that is absent from the decrepitate or is present in low concentrations relative to the host mineral. The concentration of P in the inclusions in apatite will likely be limited by apatite solubility, which at low temperature is extremely low (Krauskopf, 1979). In addition, calcite-hosted inclusions, which, based on thermometry and daughter mineral assemblages, are similar to those in apatite, contain no P. A reasonable initial assumption is therefore that $C_p^d=0$. Analyses of host apatite immediately adjacent to decrepitates were performed to obtain C_i^{ap} and C_p^{ap} assuming that the compositions of the apatite do not change much in a small area. As $C_p^t < C_p^{ap}$ in all analyses, x is a maximum when $C_p^d=0$. If $C_i^t < xC_i^{ap}$, the calculated $C_i^d < 0$. In this case, a minimum C_p^d value was given to make all $C_i^d > 0$. Calculated Ca concentrations are greatly affected by the assumed C_p^d value because Ca is a major component in apatite. The assumed C_p^d value has a much smaller influence on the calculated concentrations of Na, K, Mg, Si, S and Cl in decrepitates as the concentrations of these ions in apatite are low.

An equivalent correction for calcite-hosted decrepitates could not be carried out as there is no element present in the calcite that is likely to be absent from the decrepitates.

6.3.4 Results

Decrepitates from apatite

The results of the decrepitate analyses for inclusions in apatite are given in Table 3. Figure 6.4 shows EDA spectra of a decrepitate analysis and its host apatite analysis. Cations in the decrepitates are dominated by Na. The decrepitates contain

Table 3: Chemistry of decrepitates in apatite.

Method	Sample	Dec	Calculated compositions of decrepitate (wt. %)								
			Ca	Mg	Fe	K	Na	Si	P	S	Cl
LV Inclusions											
SEM	MA4	1	32.1	0.0	n.a.	1.5	48.1	0.0	0.0	17.7	0.5
SEM	MA4	2	0.9	0.0	n.a.	4.2	61.4	0.3	3.4	29.8	0.0
SEM	MA4	3	0.5	0.0	n.a.	5.2	60.7	0.0	1.1	32.0	0.5
SEM	MA4	4	33.1	0.5	n.a.	0.5	43.3	3.0	0.0	19.7	0.0
SEM	MA4	5	2.4	0.0	n.a.	3.6	67.3	1.4	0.0	25.4	0.0
SEM	MA4	6	7.8	0.0	n.a.	3.3	61.7	3.5	0.0	23.7	0.0
SEM	MA4	7	1.3	0.0	n.a.	5.4	55.5	3.7	6.7	27.0	0.4
SEM	MA1	1	30.1	7.5	n.a.	8.0	26.6	19.5	0.0	3.1	5.2
SEM	MA1	3	0.4	0.0	n.a.	3.7	51.9	0.0	3.6	14.6	25.7
SEM	MA1	4	7.9	1.3	n.a.	7.0	47.0	2.8	0.0	17.1	17.0
SEM	MA1	5	29.1	0.0	n.a.	2.2	45.7	1.1	0.0	14.3	7.5
SEM	IS90-79	1	2.4	12.2	n.a.	23.3	16.6	0.4	0.0	1.7	43.5
SEM	IS90-79	2	0.2	0.0	n.a.	1.4	62.5	0.3	0.7	12.8	22.1
SEM	IS90-79	3	1.2	0.0	n.a.	7.6	50.5	0.5	1.4	15.7	23.0
EM	MA-4	1	2.3	0.0	0.0	11.9	55.1	0.4	0.0	5.0	25.4
EM	IS90-79	1	0.4	0.0	0.0	3.8	78.3	0.3	3.4	1.4	12.4
EM	IS90-79	2	0.3	0.0	0.2	3.2	79.5	1.1	2.0	3.3	10.5
EM	B12-1	1	0.5	0.0	0.0	23.8	50.9	0.5	5.9	15.3	3.1
EM	B12-1	2	33.9	0.0	0.0	10.5	39.3	0.1	0.0	10.5	5.6
	Average		9.8	1.1	0.0	6.9	52.7	2.0	1.5	15.3	10.6
	Std.		13.2	3.1	0.0	6.4	15.0	4.3	2.1	9.3	12.0
LVH Inclusions											
SEM	IS90-69	1	1.0	0.2	n.a.	1.2	50.7	0.5	1.3	7.8	37.2
SEM	IS90-69	2	0.9	0.0	n.a.	0.0	58.5	0.2	1.5	14.6	24.4
SEM	IS90-69	3	7.5	0.0	n.a.	0.9	58.8	0.0	0.0	18.8	14.0
SEM	IS90-69	4	1.3	0.0	n.a.	1.2	49.5	0.2	0.7	9.8	37.2
SEM	IS90-69	5	0.3	0.0	n.a.	0.0	58.2	0.1	3.1	5.6	32.7
SEM	IS90-69	6	1.4	0.0	n.a.	1.3	62.1	0.7	0.0	17.5	17.1
SEM	IS90-69	7	0.4	0.4	n.a.	0.9	60.2	1.2	0.0	8.2	28.7
SEM	IS90-69	8	1.1	0.0	n.a.	2.7	55.1	0.1	0.0	16.5	24.5
EM	LS1-5	1	0.7	0.1	0.0	1.5	85.7	2.1	2.7	6.9	0.4
EM	L91-5	2	0.1	0.1	0.4	2.2	86.8	1.7	0.5	7.9	0.2
EM	L91-5	3	9.3	0.6	0.8	3.0	66.3	5.6	0.0	14.0	0.3
EM	IS90-69	1	0.3	0.0	0.1	0.2	49.1	0.9	2.6	0.1	46.7
EM	IS90-69	2	0.4	0.0	0.1	2.8	87.7	1.0	5.1	2.5	0.3
EM	IS90-69	3	1.2	0.0	2.8	3.3	70.4	6.2	12.0	1.7	2.3
EM	IS90-68	1	0.7	0.1	0.8	6.9	63.6	9.8	8.6	9.0	0.6
EM	IS90-68	2	0.4	0.0	0.0	0.2	76.8	9.3	8.2	5.0	0.1
	Average		1.7	0.1	0.6	1.8	65.0	2.5	2.9	9.1	16.7
	Std.		2.6	0.2	0.7	1.7	12.6	3.2	3.6	5.5	16.0

Table 6.3 (continued)

Method	Sample	Dec	Charge		Anion Def(%)	Atomic ratios					
			+	-		Ca/Na	Mg/Na	Fe/Na	K/Na	Cl/S	Si/S
LV Inclusions											
SEM	MA4	1	77	23	70	0.38	0.00	n.a.	0.02	0.02	0.00
SEM	MA4	2	56	44	21	0.01	0.00	n.a.	0.04	0.00	0.01
SEM	MA4	3	57	43	24	0.00	0.00	n.a.	0.05	0.01	0.00
SEM	MA4	4	70	30	57	0.44	0.01	n.a.	0.01	0.00	0.19
SEM	MA4	5	64	36	45	0.02	0.00	n.a.	0.03	0.00	0.07
SEM	MA4	6	63	37	41	0.07	0.00	n.a.	0.03	0.00	0.19
SEM	MA4	7	49	51	-4	0.01	0.00	n.a.	0.06	0.01	0.17
SEM	MA1	1	59	41	30	0.65	0.27	n.a.	0.18	1.47	7.82
SEM	MA1	3	54	46	16	0.00	0.00	n.a.	0.04	1.56	0.00
SEM	MA1	4	60	40	32	0.10	0.03	n.a.	0.09	0.88	0.21
SEM	MA1	5	74	26	65	0.37	0.00	n.a.	0.03	0.47	0.10
SEM	IS90-79	1	64	36	44	0.08	0.69	n.a.	0.83	23.11	0.30
SEM	IS90-79	2	64	36	45	0.00	0.00	n.a.	0.01	1.53	0.03
SEM	IS90-79	3	57	43	26	0.01	0.00	n.a.	0.09	1.31	0.04
EM	MA-4	1	73	27	62	0.02	0.00	0.00	0.13	4.51	0.09
EM	IS90-79	1	82	18	78	0.00	0.00	0.00	0.03	7.79	0.22
EM	IS90-79	2	82	18	77	0.00	0.00	0.00	0.02	2.87	0.41
EM	B12-1	1	63	37	42	0.01	0.00	0.00	0.28	0.18	0.04
EM	B12-1	2	82	18	77	0.50	0.00	0.00	0.16	0.48	0.02
	Average		66	34	45	0.14	0.05	0.00	0.11	2.43	0.52
	Std.		10	10	23	0.20	0.16	0.00	0.18	5.24	1.72
LVH Inclusions											
SEM	IS90-69	1	57	43	25	0.01	0.00	n.a.	0.01	4.25	0.08
SEM	IS90-69	2	59	41	32	0.01	0.00	n.a.	0.00	1.49	0.02
SEM	IS90-69	3	65	35	47	0.07	0.00	n.a.	0.01	0.66	0.00
SEM	IS90-69	4	56	44	22	0.02	0.00	n.a.	0.01	3.37	0.03
SEM	IS90-69	5	62	38	38	0.00	0.00	n.a.	0.00	5.22	0.03
SEM	IS90-69	6	63	37	41	0.01	0.00	n.a.	0.01	0.87	0.05
SEM	IS90-69	7	65	35	46	0.00	0.01	n.a.	0.01	3.12	0.19
SEM	IS90-69	8	59	41	31	0.01	0.00	n.a.	0.03	1.32	0.01
EM	L91-5	1	81	19	76	0.00	0.00	0.00	0.01	0.05	0.37
EM	L91-5	2	84	16	81	0.00	0.00	0.00	0.02	0.03	0.26
EM	L91-5	3	70	30	58	0.08	0.01	0.01	0.03	0.02	0.50
EM	IS90-69	1	56	44	22	0.00	0.00	0.00	0.00	565	15.9
EM	IS90-69	2	84	16	80	0.00	0.00	0.00	0.02	0.10	0.49
EM	IS90-69	3	62	38	39	0.01	0.00	0.02	0.03	1.24	4.64
EM	IS90-68	1	55	45	18	0.01	0.00	0.01	0.06	0.06	1.37
EM	IS90-68	2	61	39	37	0.00	0.00	0.00	0.00	0.01	2.34
	Average		65	35	43	0.02	0.00	0.00	0.02	36.65	1.64
	Std.		9	9	20	0.02	0.00	0.00	0.02	136.3	3.86

Dec: decrepitate; Std: standard deviation; Defic: deficiency

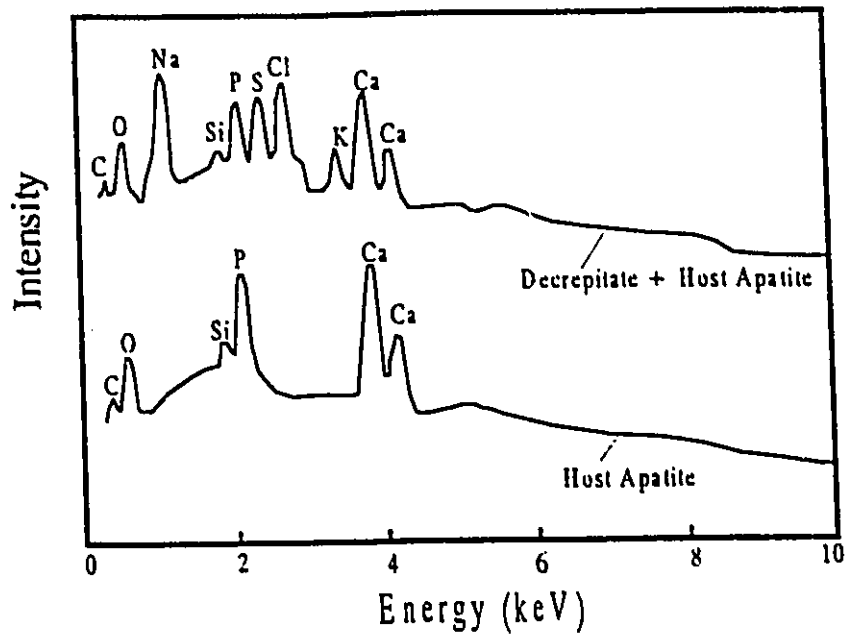


Figure 6.4. EDA spectra of a decrepitate and its host apatite.

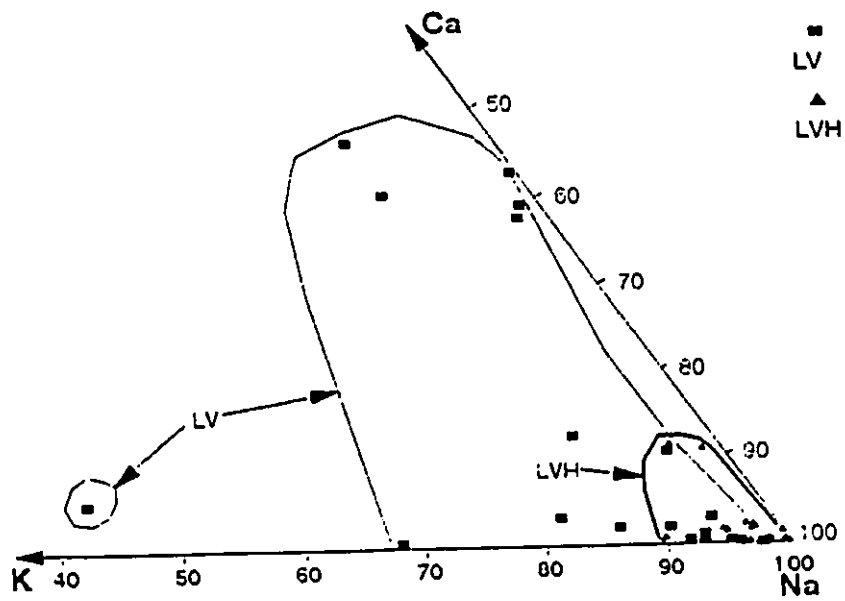


Figure 6.5. Ca-K-Na plots of decrepitates from apatite.

Ca and K in subordinate amounts and Mg and Fe in minor amounts. K/Na and Ca/Na ratios vary from 0 to 0.83 and from 0 to 0.85 (Table 3). Mg/Na and Fe/Na ratios range from 0 to 0.69 and from 0 to 0.02 (Table 6.3). The decrepitates from the LV inclusions have higher Ca/Na, K/Na and Mg/Na ratios and lower Fe/Na ratios than the decrepitates from the LVH inclusions (Table 6.3, Figure 6.5).

The presence of mirabilite in the inclusions indicates that the S was principally dissolved as sulphate. The results of an experiment on the system $\text{NaAlSi}_3\text{O}_8$ - $\text{CaAl}_2\text{Si}_2\text{O}_8$ - Na_2CO_3 - H_2O (Koster van Groos and Wyllie, 1973) reveal that an aqueous vapour phase, which coexisted with carbonate melt and silicate melt, is rich in sodium silicate and CO_2 , which suggests that Si is likely to occur as silicate in hydrothermal fluids in carbonatites. The results of the analyses (Table 3) indicate that anions in the decrepitates are dominated by Cl, and sulphate and silicate are present in subordinate amounts. Cl/S and Si/S ratios vary from 0 to 552 and from 0 to 18 respectively. It was found from the decrepitate calculations that P is present in at least some of the decrepitates as $C_p^d > 0$ was needed to make $C_i^d > 0$ in these decrepitates. Most of the analyses showed anion deficiency, although one analysis showed cation deficiency. The anion deficiencies range from 9 to 68%.

Decrepitates from calcite

SEM analyses were performed on the decrepitates from calcite in a monticellite-apatite carbonatite from the Manny Zone. The calcite contains abundant secondary LV inclusions in addition to primary LV inclusions. It was not possible to determine on SEM or EM whether these decrepitates came from primary or secondary inclusions. The results of the decrepitate analyses in calcite are given in Table 6.4. Figure 6.6 shows EDA spectra for a decrepitate and its calcite substrate. In comparison to concentrations in decrepitate-calcite mixtures, concentrations in calcite are low for Na, K, S and Cl and high for Ca, Mg, Si and P (Table 6.4), which suggests that the contributions of the host calcite to the decrepitate analyses are high for Ca, Mg, Si and P and relatively low for Na, K, S and Cl. Therefore, only the data for Na, K, S and Cl were considered. K/Na and Cl/S ratios range from 0 to 0.04 and from 0.26 to 13.5 (Table 6.4).

Table 6.4: Summary of decrepitate analysis data from calcite.

Sampl	Dec	Concentrations (wt. %)								Atomic Ratios	
		Ca	Mg	K	Na	Si	P	S	Cl	K/Na	Cl/S
Decrepitate+ Calcite											
MA4	1	38.2	0.3	0.4	20.3	0.2	0.0	3.8	7.1	0.01	1.65
MA4	2	44.5	0.0	0.2	15.5	0.1	0.1	3.9	5.5	0.01	1.24
MA4	3	43.9	0.2	0.1	16.4	0.0	0.0	0.7	11.1	0.00	13.50
MA4	4	56.6	0.6	0.4	5.6	0.0	0.1	3.4	1.0	0.04	0.27
MA4	5	41.3	0.5	0.0	18.6	0.0	0.0	2.7	7.6	0.00	2.51
Calcite											
		65.5	0.48	0.1	0.6	0.1	0.5	0.5	0.1		
Calcite/Decrepitate+ Calcite											
MA4	1	1.72	1.85	0.21	0.03	0.65		0.12	0.01		
MA4	2	1.47		0.53	0.04	0.92	4.64	0.12	0.01		
MA4	3	1.49	3.20	1.14	0.03			0.64	0.01		
MA4	4	1.16	0.84	0.22	0.10	2.75	6.38	0.14	0.06		
MA4	5	1.59	1.00	4.00	0.03	5.50		0.17	0.01		

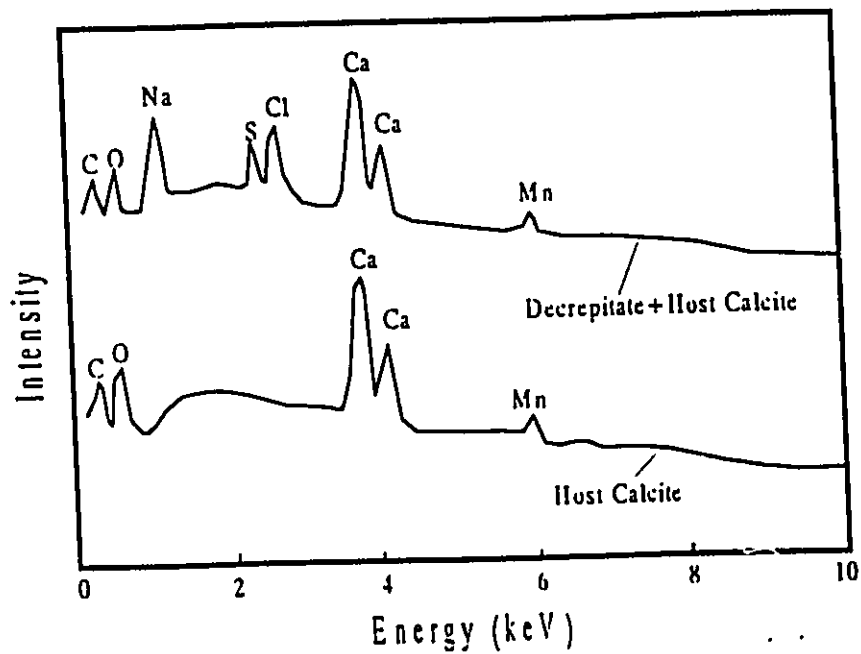


Figure 6.6. EDA spectra of a decrepitate and its host calcite.

6.3.5 Discussion

Precision and accuracy of decrepitate analyses

The precision and accuracy of decrepitate analyses have been studied by Haynes et al. (1988) using synthetic fluid inclusions in natural quartz. They found that the decrepitates analyzed were chemically representative of their precursor inclusions, but not all decrepitates analyzed provided accurate results. The main problems that cause analytical error are chemical inhomogeneity and Cl evaporation during decrepitation. The decrepitates from the Oka carbonatite were chemically inhomogeneous. It was found during EM analyses that the composition of a decrepitate varied from one point to another. Cl concentration in the decrepitates decreases with increasing anion deficiency (Figure 6.7), which suggest there was a significant Cl loss from the decrepitates because of high decrepitation temperatures (Haynes et al. 1988).

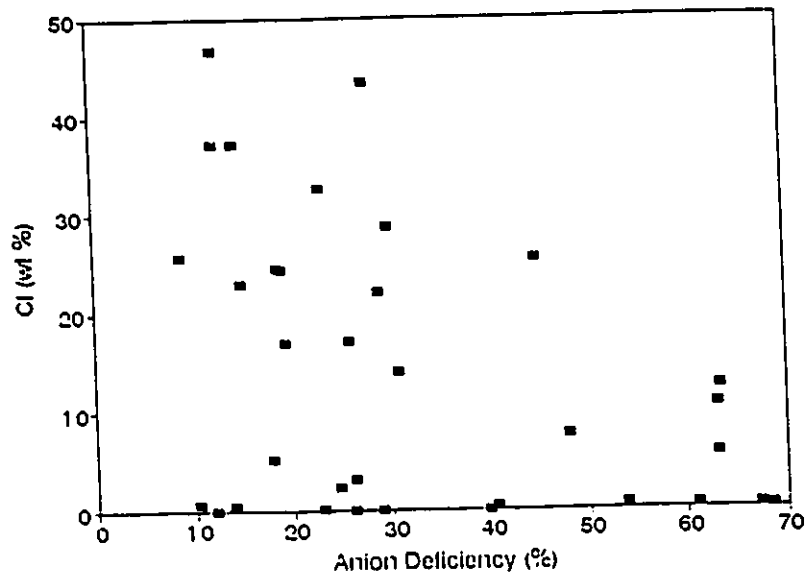


Figure 6.7. Anion deficiency-Cl plots of decrepitates from apatite.

Comparison of decrepitate analyses and leachate analyses

Leachate analysis and decrepitate analysis were performed on apatite from

samples IS90-68, IS90-69, MA-1 and MA-4. As discussed, the data for Ca, Mg and Fe from the leachate analyses could not be used. Therefore, a comparison was made on K/Na and Cl/Na ratios. Table 6.5 lists these two ratios from leachate analyses and from the decrepitate analyses (average values). These two ratios are lower in the decrepitate analyses than in the leachate analyses. The evidently low Cl/Na ratios in the decrepitate analyses of IS90-68 and MA-4 suggest that Cl evaporation occurred during decrepitation.

Table 6.5: Comparison of leachate analyses and decrepitate analyses.

Sample	Method	K/Na	Cl/Na
IS90-68	Leachate	0.05	0.21
	Decrepitate	0.04	0.01
IS90-69	Leachate	0.06	0.40
	Decrepitate	0.01	0.28
MA-1	Leachate	0.13	0.25
	Decrepitate	0.08	0.19
MA-4	Leachate	0.13	0.28
	Decrepitate	0.05	0.04

Estimation of chloride concentrations in fluid inclusions

Based on the average salinities of the LV inclusions (20 wt%) and the LVH inclusions (40 wt%) in apatite, approximate Ca, Mg, Fe, K and Na chloride concentrations in these the inclusions can be estimated from the concentrations of cations in the decrepitates. The method used to calculate molalities is as follows:

$$C_i^d = C_i + C_i V_i \frac{W_{Cl}}{W_i} \dots \dots \dots (6.6) \quad (3)$$

$$C_i^f = S \frac{C_i^d}{\sum C_i^f} \dots \dots \dots (6.7)$$

$$M_i = \frac{1000 C_i^f}{W_i^{Cl} (100 - \sum C_i^f)} \dots \dots \dots (6.8)$$

where

C_i^d : concentration (wt. %) of metal i chloride in decrepitate;

C_i^f : concentration (wt. %) of metal i chloride in fluid;

C_i : concentration (wt. %) of metal i in decrepitate;

V_i : valence of metal i ;

W_{Cl} : atomic weight of Cl;

W_i : atomic weight of metal i;

W_i^{Cl} : molecular weight of metal i chloride;

S : salinity of fluid;

M_i : molality of metal i chloride in fluid.

The calculated concentration of the chloride species in the fluids are listed in Table 6.6. These results are approximate because sulphate and carbonate are present in the fluids and may have influenced ice melting temperatures and therefore the calculated salinity of the fluids.

Table 6.6: Chemistry of fluid inclusions in apatite.

Type	Concentration of Cations in Decrepitates (wt. %)					Salinity (wt. %)
	Ca	Mg	Fe	K	Na	
LV	9.8	1.1	0.0	6.9	52.7	20
LVH	1.7	0.1	0.6	1.8	65.0	40
Type	Concentration of Chlorides in Fluids (Molalities)					
	CaCl ₂	MgCl ₂	FeCl ₂	KCl	NaCl	
LV	0.34	0.06	0.00	0.24	3.20	
LVH	0.16	0.02	0.04	0.17	10.75	

6.4 Gas Chemistry

6.4.1 Analytical methods

Laser Raman spectroscopy (LRS) and quadrupole mass spectrometer (QMS) were used in an attempt to characterize the gases present in the fluid inclusions from the Oka carbonatite. LRS instrumentation was described in Chapter III. QMS was carried out at the University of Michigan. The instrumentation and analytical procedures used are described in Jones and Kesler (1992). Gases were analyzed using a VG SXP 600 quadrupole mass spectrometer. Sixteen masses were monitored in order to analyze a variety of compounds including H₂O, CO₂, CO, CH₄, C₂H₆, C₃H₈, N₂, Ar, H₂S, and SO₂. Data were collected at a rate of approximately 100 cycles per minute. Gases were released from fluid inclusions by crushing or by decrepitation. Crushing was performed under vacuum with a modified Nupro valve. 5 to 25 mg of inclusion-bearing minerals was used for each analysis. In a decrepitation analysis, inclusion gases were liberated by heating small samples under vacuum in a Vycor tube until the inclusions decrepitated. Gases released in this way passed directly into the quadrupole source and produced episodic signal bursts that probably represent individual inclusions.

6.4.2 Results and discussion

Five inclusions with relatively large vapour bubbles from 3 samples were analyzed for CO₂, CO, CH₄, SO₂ and H₂S using LRS. None of these gases was detected. This indicates that these gases are absent in the inclusions or their concentrations are below detection limits. This result is consistent with the absence of any microthermometric phase changes that would indicate the presence of these gases (Chapter V).

Six apatite and three calcite samples were analyzed by QMS using the crushing method, however the amounts of the gases released were so low that the compositions of the gases could not be quantified. One apatite separate from MA-4, which contains abundant LV inclusions, was analyzed using the decrepitation method. H₂O and CO₂ released from an inclusion at about 500°C were measured and their mole fractions are 0.88 and 0.12 respectively. An X_{CO₂} value of 0.12 seemed high given the absence of CO₂-related phase changes in the inclusions. In order to test whether this is a reasonable X_{CO₂} value given the absence of phase changes and the nature of the

inclusions, mole fractions of CO_2 corresponding to different CO_2 homogenization temperatures were calculated based on the average salinity (20 wt. %) and the average vapour volume fraction (0.18) of the LV inclusions from sample MA-4. This was achieved using the FLINCOR program (Brown, 1989) and the equation of state of Brown and Lamb (1989), and assuming that the vapour phase is composed of CO_2 . The results of the calculations (Figure 6.8) indicate that a CO_2 phase change (homogenization) should be seen in inclusions if X_{CO_2} of the inclusions is between 0.0014 and 0.102. The absence of a CO_2 phase change in the inclusions from sample MA-4 suggests that X_{CO_2} in the inclusions is less than 0.0014, and that the result of QMS (0.12) is wrong. Some of the detected CO_2 may have been released from calcite inclusions in the apatite (decarbonation).

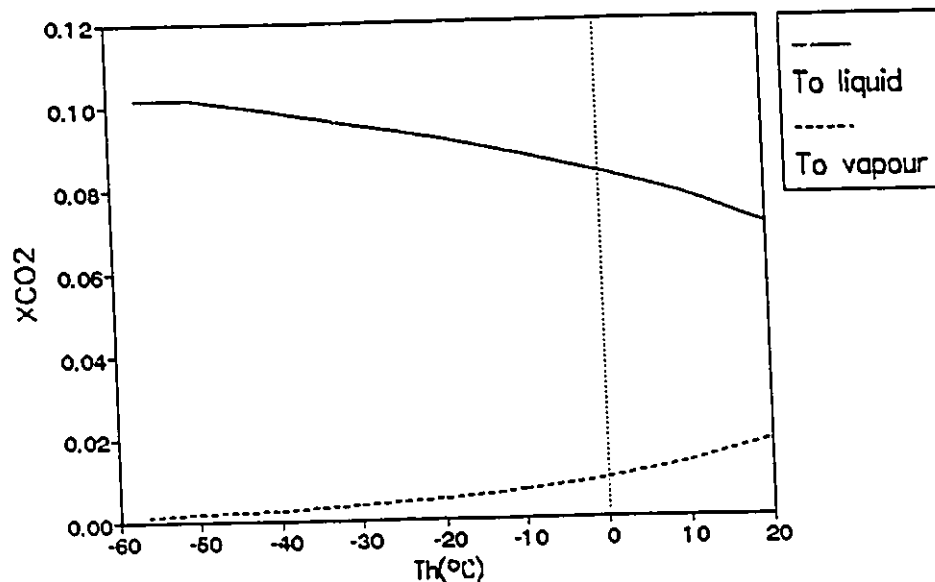


Figure 6.8. Relationship between CO_2 concentration and Th of fluid inclusions.

Girault (1966) and Girault & Chaigneau (1967) analyzed the gases released by decrepitation from the fluid inclusions in the apatite in a tremolite-apatite carbonatite

from the Mine, a monticellite-apatite carbonatite with perovskite from the Bone Zone and a britholite vein from Colline Dufresne. Their results indicated that CO₂ comprises 74 to 97% of the volume of the gases, and that the rest is CO, H₂ and N₂. H₂O was detected only in one sample and made up 0.3% of the volume of the gases. This result is contradictory to our microthermometric results, which show that these inclusions are H₂O-rich. The LV inclusions and LVH inclusions in apatite decrepitated at temperatures from 350°C to 450°C and from 400 to 500°C respectively. However, most of the gases measured by Girault and Girault & Chaigneau were released at temperatures from 600 to 800°C, which suggests that these gases did not come from the fluid inclusions, but from calcite inclusions in the apatite as a result of decarbonation.

CHAPTER VII

REE GEOCHEMISTRY OF THE OKA CARBONATITE

7.1 Introduction

It is known that many REE deposits in carbonatite-alkaline complexes have been formed from hydrothermal fluids. However, the origin of REE-rich hydrothermal fluids is still poorly understood. This part of the study was initiated to investigate any possible relationship between the REE chemistry of the carbonatites and the types of hydrothermal fluids involved.

7.2 Analytical Method

Instrumental neutron activation analysis (INAA) was used to determine REE compositions of whole rocks and apatite. The chemistry of individual apatite crystals was determined using an electron microprobe (EM). The modal mineralogy and the fluid inclusion petrography of the samples used in the REE study are given in Table 7.1. These samples come from early- or middle-stage carbonatites.

7.2.1 Instrumental neutron activation analyses

The rock samples were broken into chips, then pulverized. Apatite separates were obtained using an isodynamic magnetic separator and heavy liquids. The separation procedure was described in detail in Chapter VI. All neutron activation analyses were performed by Activation Laboratories Ltd and the detection limits of the analyses are listed in Table 2.

7.2.2 Electron microprobe analyses

Electron microprobe analyses were performed at McGill University and the University of Michigan on Cameca Camebax microprobes equipped with wavelength dispersive spectrometers (WDS) and energy dispersive spectrometers (EDS). The analyses at the University of Michigan were carried out using WDS and the analytical conditions and standards used were described in Chapter VI. WDS and EDS were used on the McGill microprobe. At McGill University, WDS analyses were

Table 7.1: Modal mineralogy and inclusion abundances in apatite.

Zone	Sample	Modal Mineralogy (%)	Inclusion in apatite
Mine	IS90-68	Cal(84), Ap(8), Mtc(5), Mag(2), Prv(1), Bt(minor)	Rich in LVH
	IS90-69	Cal(71), Ap(10), Mtc(5), Aug (5), Bt(5), Mag(3), Prv(1)	Rich in LVH
	IS90-79	Cal(90), Ap(10)	Bearing LV
	L91-5	Cal(60), Ric(20), Ap(10), Prv(5), Bt & Mag(minor)	Rich in LVH
Manny	MA-1	Cal(79), Ap(12), Mtc(8), Prv(1), Mag(minor)	Rich in LV
	MA-4	Cal(72), Ap(12), Mtc(10), Mag(5), Prv(1),	Rich in LV
Bond	B4-2	Cal(54), Aug(25), Ap(7), Nio(7), Bt(7), Pyr(minor)	Bearing LV
	B4-9	Cal(57), Aug(12), Mtc(10), Ap(7), Nio(7), Mag(7), Bt & Pyr(minor)	Inclusion-Free
	B7-1	Cal(54), Mtc(25), Ap(7), Mln(7), Bt(5), Mag(5), Prv(1), Aug(1), Nio(minor)	Inclusion-Free
	B12-1	Cal(55), Agt(30), Ap(10), Mag(5), Bt & Prv(minor)	Bearing LV

Table 7.2: Detection limits of INNA (ppm).

La	Ce	Nd	Sm	Eu	Gd	Tb	Dy	Yb	Lu
0.1	1	3	0.01	0.05	0.5	0.1	0.5	0.05	0.01

performed with an accelerating voltage of 15 kV and a current of 10 μA and an apatite sample of known composition was used as a standard. The results of the standard analysis show that the analytical accuracy is high for most of the elements analyzed (Table 7.3). EDS analyses were carried out with accelerating voltages of 15 or 20 kV and a current of 0.3 μA , and their detection limits were approximately 0.2 to 0.5% depending on element.

Table 7.3: Result of apatite-standard analysis (wt%)
using WDS at McGill University.

Element	True	Analyzed	Element	True	Analyzed
P	17.86	18.54	Sr	0.39	0.35
Ca	38.94	39.01	La	0.12	0.15
F	3.70	5.22	Ce	0.26	0.20
Si	0.06	0.09	Nd	0.15	0.05
Cl	0.05	0.02			

7.3 Results

7.3.1 Neutron activation analyses

Whole rock data

The results of the whole-rock analyses are listed in Table 7.4. All rocks are LREE-enriched (Figure 7.1). Σ REE ranges from 2630 to 6456 ppm, with La/Lu ratios varying from 763 to 1739. Σ REE and La/Lu ratios are highest in the carbonatites from the Bond Zone and lowest in the carbonatites from the Manny Zone. In the Bond Zone, the niocalite-rich carbonatites (B4-2 and B4-9) contain more REE than the niocalite-poor or -free carbonatites because of the high REE contents of niocalite (about 15000 ppm, Eby, 1975). Chondrite-normalized curves are similar to the whole-rock curves given by Eby (1975) (Figure 7.1). There is no difference in REE pattern between the niocalite-rich carbonatites and the niocalite-poor or -free carbonatites.

Table 7.4: INAA data of REE concentrations (ppm) in whole rocks.

Element	Manny Zone		Mine		Bond Zone			
	MA-1	MA-4	IS90-68	IS90-69	B12-1	B4-2	B4-9	B7-1
La	1000	667	1100	1000	1400	2400	2000	1400
Ce	1500	1050	2200	1500	1800	2000	3230	2030
Nd	456	821	600	480	551	1200	1010	569
Sm	48	36	64	56	55	110	98	59
Eu	15	9.7	18.7	15	15	31.3	26.1	16.2
Gd	26	20	36	36	28	62	48	28
Tb	4.3	3	5.6	4.6	4	9	6.1	4.2
Dy	16.7	15.6	30.7	24.5	17.6	33.8	27	16.7
Yb	8.23	6.77	9.27	8.94	6.56	10.6	10.1	8.65
Lu	1.19	0.86	1.13	1.31	1.04	2.01	1.15	1.28
REE	3075	2630	4065	3126	3878	5059	6456	4133
La/Lu	840	776	973	763	1346	1194	1739	1094

Table 7.5: INAA data of REE concentrations (ppm) in apatites.

Element	Manny Zone		Mine		Bond Zone			
	MA-1	MA-4	IS90-68	IS90-69	B12-1	B4-2	B4-9	B7-1
La	7000	6700	8300	9000	16000	11000	22000	15000
Ce	10000	10000	13000	13000	20000	10000	30000	19000
Nd	3100	3110	4500	4700	6600	5700	8000	5500
Sm	300	310	460	490	600	490	720	450
Eu	93	99	140	140	205	150	220	140
Gd	162	180	302	326	364	240	366	238
Tb	24	26	44	46	48	32	49	30
Dy	87.9	103	157	173	161	85.5	114	80.7
Yb	26.1	29.8	45.9	57	60.7	18	28.2	17.4
Lu	3.54	3.85	8.12	8.03	8.96	2.75	3.85	2.49
REE	20797	20562	26957	27940	44048	27718	61501	40459
La/Lu	1977	1740	1022	1121	1786	4000	5714	6024

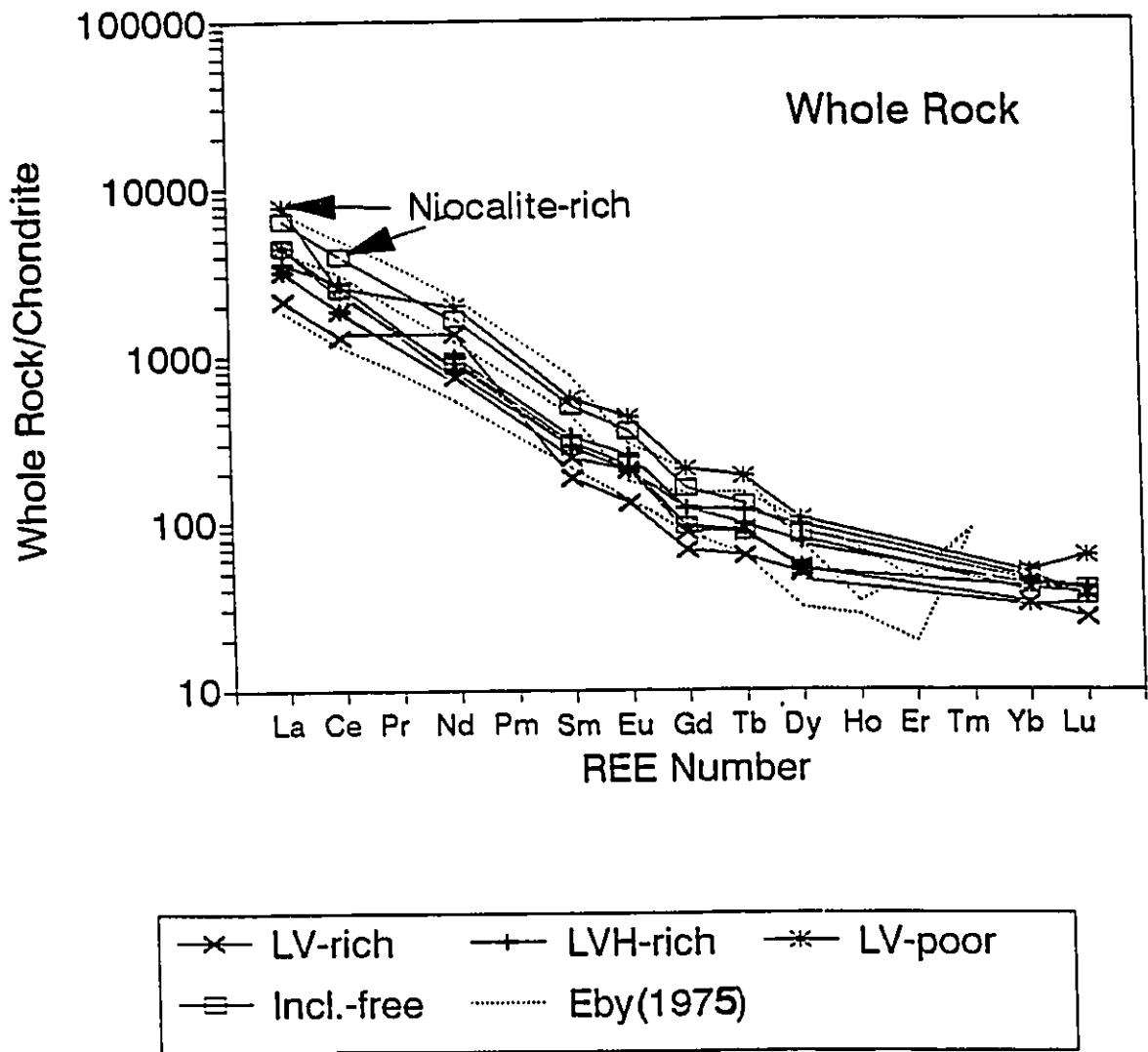


Figure 7.1. Chondrite-normalized curves of whole rocks

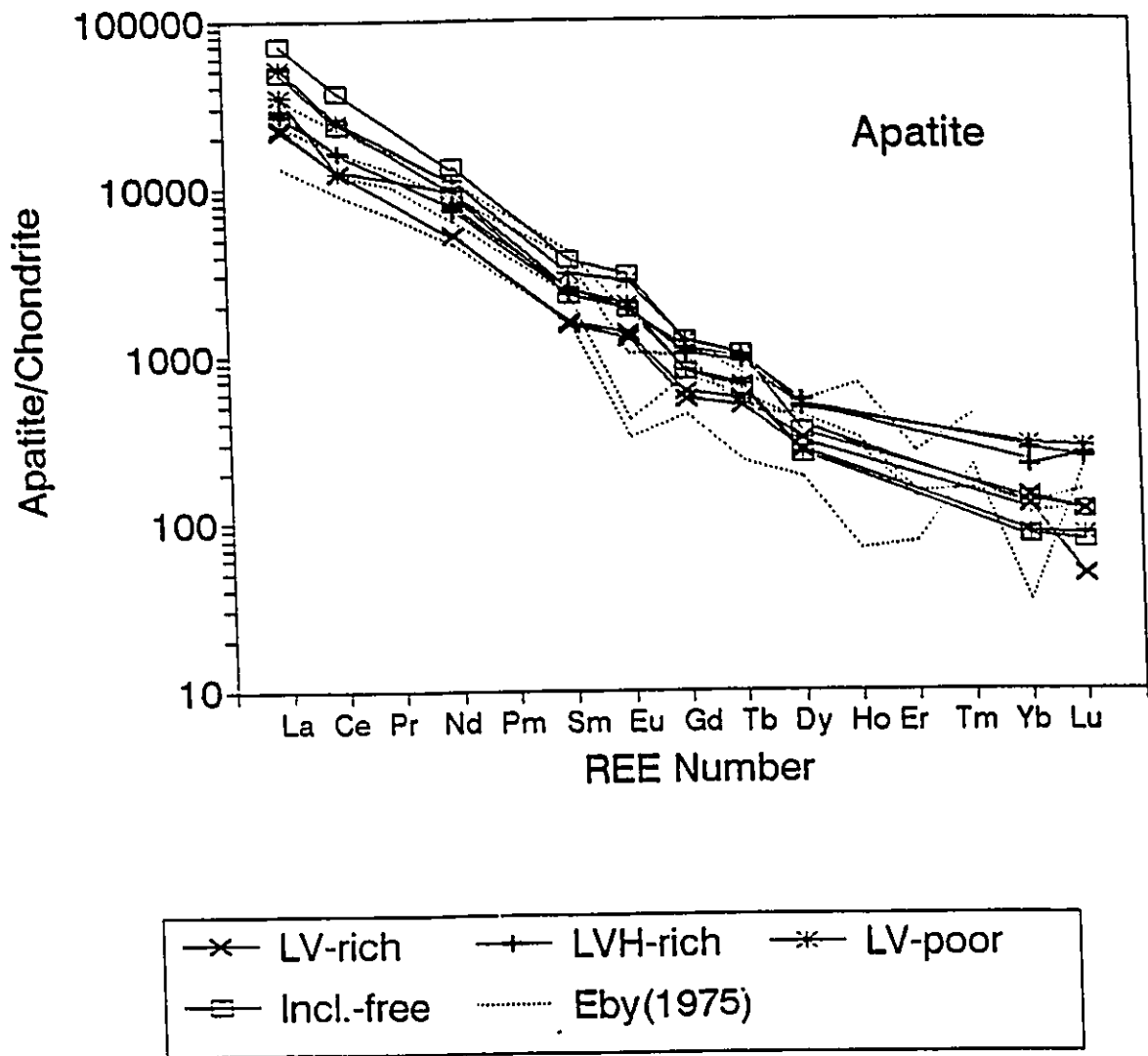


Figure 7.2. Chondrite-normalized curves of apatite.

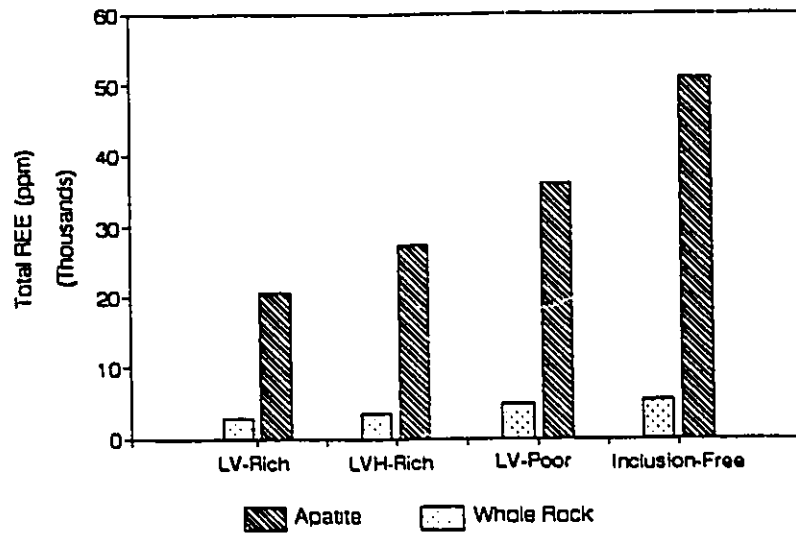


Figure 7.3. Total REE contents of whole rocks and apatites.

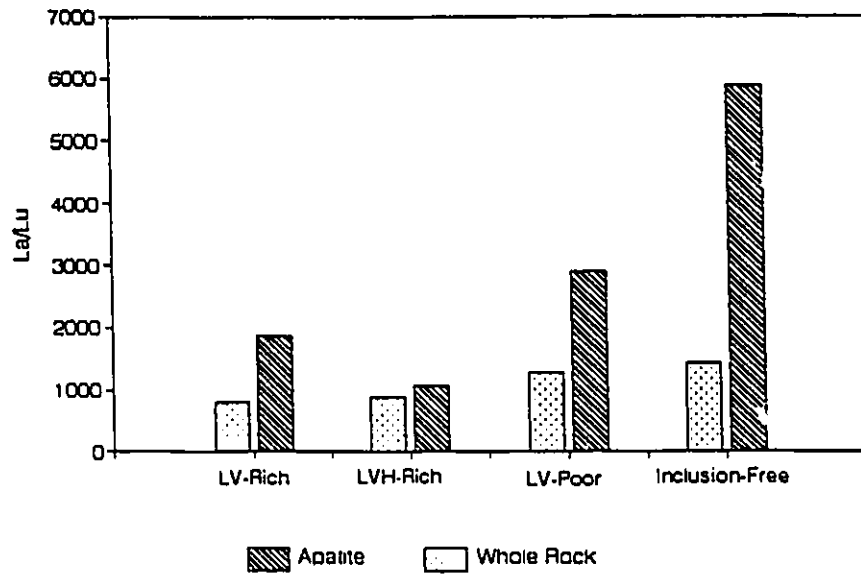


Figure 7.4. La/Lu ratios of whole rocks and apatites.

Table 7.6: Summary of EM data of apatites.

Sample	P2O5	SiO2	Al2O3	CaO	MgO	SrO	La2O3	Ce2O3	Nd2O3	F	Cl	Total
IS90-69-6*	37.9	2.49	n.a	51.8	0.01	0.67	1.06	1.36	0.16	2.98	0.01	98.4
IS90-69-7*	38.6	1.94	n.a	51.7	0.01	0.69	0.95	1.22	0.11	2.77	0.01	98.1
MA-1-1*	38.6	1.42	n.a	52.5	0.01	0.52	0.74	0.89	0.08	2.96	0.01	97.7
MA-1-2*	37.2	1.32	n.a	52.2	0.29	0.81	0.59	0.80	0.11	2.23	0.00	95.6
MA-1-3*	37.4	1.77	n.a	53.2	0.02	0.76	0.72	0.82	0.07	2.53	0.02	97.3
MA-1-4*	39.0	1.31	n.a	52.8	0.00	0.76	0.74	0.89	0.06	1.95	0.02	97.6
MA-4-2*	38.9	1.86	n.a	52.4	0.01	0.56	0.68	0.81	0.07	2.61	0.01	97.9
MA-4-4*	35.9	1.18	n.a	52.8	0.05	0.74	0.57	0.82	0.03	1.66	0.01	93.7
MA-4-9*	38.9	1.36	n.a	52.6	0.00	0.59	0.80	0.98	0.05	2.43	0.00	97.7
IS90-69-1**	35.0	2.88	0.60	55.4	n.a	n.a	1.16	2.06	0.48	2.00	0.00	99.6
IS90-69-2**	36.8	3.13	0.16	54.3	0.23	n.a	0.87	1.32	1.07	2.00	0.00	99.9
IS90-69-3**	32.5	2.82	0.14	59.2	0.26	n.a	0.68	1.30	0.73	2.00	0.07	99.7
IS90-69-4a**	34.6	2.72	0.23	56.8	n.a	n.a	1.15	1.63	0.54	2.00	0.09	99.8
IS90-69-4b**	33.1	2.25	0.00	59.2	0.28	n.a	0.94	1.71	0.44	2.00	0.00	100.0
IS90-69-4c**	31.4	2.91	0.28	58.9	0.64	n.a	1.20	1.87	0.71	2.00	0.00	99.9
IS90-69-4d**	32.5	2.28	0.35	59.7	0.48	n.a	0.49	1.08	1.13	2.00	0.00	100.0
IS90-69-5a**	36.7	2.86	0.17	54.5	0.73	n.a	1.16	1.15	0.76	2.00	0.00	100.0
IS90-69-5b**	34.7	2.58	0.00	57.7	0.15	n.a	0.92	1.69	0.00	2.00	0.18	99.9
MA-4-1a**	39.3	2.26	0.27	55.5	n.a	n.a	0.37	0.95	0.31	1.00	0.07	100.0
MA-4-1b**	38.0	1.96	0.00	56.2	0.18	n.a	0.37	0.90	0.35	2.00	0.00	100.0
MA-4-1c**	37.2	2.23	0.18	56.2	0.17	n.a	0.84	1.18	0.00	2.00	0.00	100.0
B12-1-2ap***	29.6	1.60	0.00	54.0	0.02	0.23	0.63	1.20	0.08	2.22	0.00	89.6
IS90-68-1ap***	29.2	2.38	0.00	51.3	0.02	0.39	1.16	1.34	0.66	2.64	0.00	89.1
IS90-68-2ap***	33.0	2.55	0.00	52.3	0.05	0.32	0.78	1.11	0.36	2.68	0.00	93.2
IS90-69-2ap***	31.0	1.84	0.00	47.8	0.04	0.28	0.85	1.62	0.38	2.89	0.01	86.7
IS90-79-1ap***	30.9	0.33	0.00	54.3	0.05	0.57	0.51	0.74	0.35	2.35	0.00	90.1
IS90-79-2ap***	33.0	0.10	0.00	56.5	0.04	0.61	0.42	0.78	0.20	2.14	0.00	93.8
L91-5-1ap***	32.5	0.55	0.00	53.7	0.04	0.61	0.75	1.09	0.36	2.70	0.00	92.3
MA-4-1ap***	27.9	1.48	0.00	53.0	0.02	0.18	0.63	1.10	0.37	2.10	0.00	86.8

Table 7.5 (continued)

Sample	Cations Based on 50 Oxygen								
	P	Si	Al	Ca	Mg	Sr	La	Ce	Nd
IS90-69-6*	11.3	0.87	n.a	19.5	0.01	0.14	0.14	0.17	0.02
IS90-69-7*	11.5	0.68	n.a	19.4	0.01	0.14	0.12	0.15	0.02
MA-1-1*	11.5	0.50	n.a	19.8	0.00	0.11	0.09	0.11	0.01
MA-1-2*	11.3	0.48	n.a	20.1	0.16	0.17	0.08	0.10	0.02
MA-1-3*	11.2	0.62	n.a	20.2	0.01	0.15	0.09	0.10	0.01
MA-1-4*	11.5	0.46	n.a	19.8	0.00	0.15	0.09	0.11	0.01
MA-4-2*	11.5	0.65	n.a	19.6	0.01	0.11	0.08	0.10	0.01
MA-4-4*	11.2	0.43	n.a	20.8	0.03	0.16	0.08	0.11	0.00
MA-4-9*	11.5	0.47	n.a	19.7	0.00	0.12	0.10	0.13	0.01
IS90-69-1**	10.4	1.01	0.25	20.8	n.a.	0.11	0.15	0.26	0.06
IS90-69-2**	10.8	1.08	0.07	20.1	0.12	n.a.	0.11	0.17	0.14
IS90-69-3**	9.8	1.00	0.06	22.6	0.14	n.a.	0.09	0.17	0.10
IS90-69-4a**	10.3	0.96	0.09	21.5	n.a.	n.a.	0.15	0.21	0.07
IS90-69-4b**	10.0	0.80	0.00	22.6	0.15	n.a.	0.12	0.22	0.05
IS90-69-4c**	9.6	1.05	0.12	22.7	0.35	n.a.	0.16	0.24	0.10
IS90-69-4d**	9.8	0.81	0.15	22.8	0.25	n.a.	0.06	0.14	0.15
IS90-69-5a**	10.7	0.98	0.07	20.1	0.37	n.a.	0.14	0.14	0.09
IS90-69-5b**	10.3	0.91	0.00	21.8	0.08	n.a.	0.12	0.21	0.00
MA-4-1a**	11.2	0.76	0.11	20.0	n.a.	n.a.	0.04	0.12	0.04
MA-4-1b**	11.0	0.67	0.00	20.7	0.09	n.a.	0.05	0.11	0.04
MA-4-1c**	10.9	0.76	0.07	20.7	0.08	n.a.	0.11	0.15	0.00
B12-1-2ap***	10.0	0.64	0.00	23.0	0.01	0.05	0.09	0.17	0.01
IS90-68-1ap***	9.9	0.95	0.00	22.0	0.01	0.09	0.17	0.20	0.09
IS90-68-2ap***	10.4	0.95	0.00	20.9	0.03	0.07	0.11	0.15	0.05
IS90-69-2ap***	10.6	0.75	0.00	20.7	0.02	0.07	0.13	0.24	0.06
IS90-79-1ap***	10.4	0.13	0.00	23.1	0.03	0.13	0.07	0.11	0.05
IS90-79-2ap***	10.6	0.04	0.00	22.9	0.03	0.13	0.06	0.11	0.03
L91-5-1ap***	10.6	0.21	0.00	22.2	0.02	0.14	0.11	0.15	0.05
MA-4-1ap***	9.8	0.61	0.00	23.5	0.01	0.04	0.10	0.17	0.05

Samples with * and ** were analyzed using WDS and EDS at McGill University;

Samples with *** were analyzed using WDS at the University of Michigan;

n.a.: not analyzed

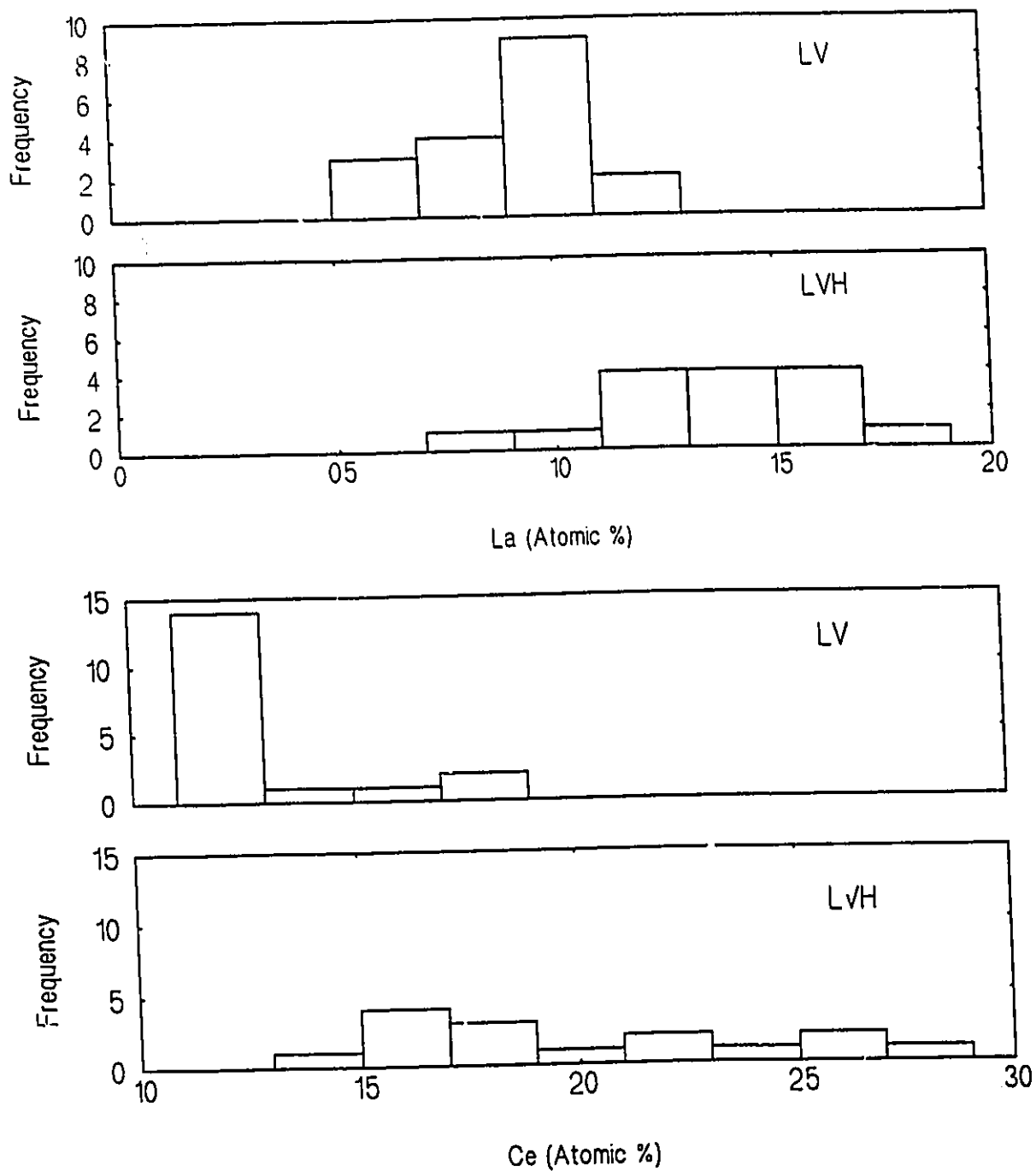


Figure 7.5. Comparison of LREE contents in two types of apatites (containing LV and LVH inclusions).

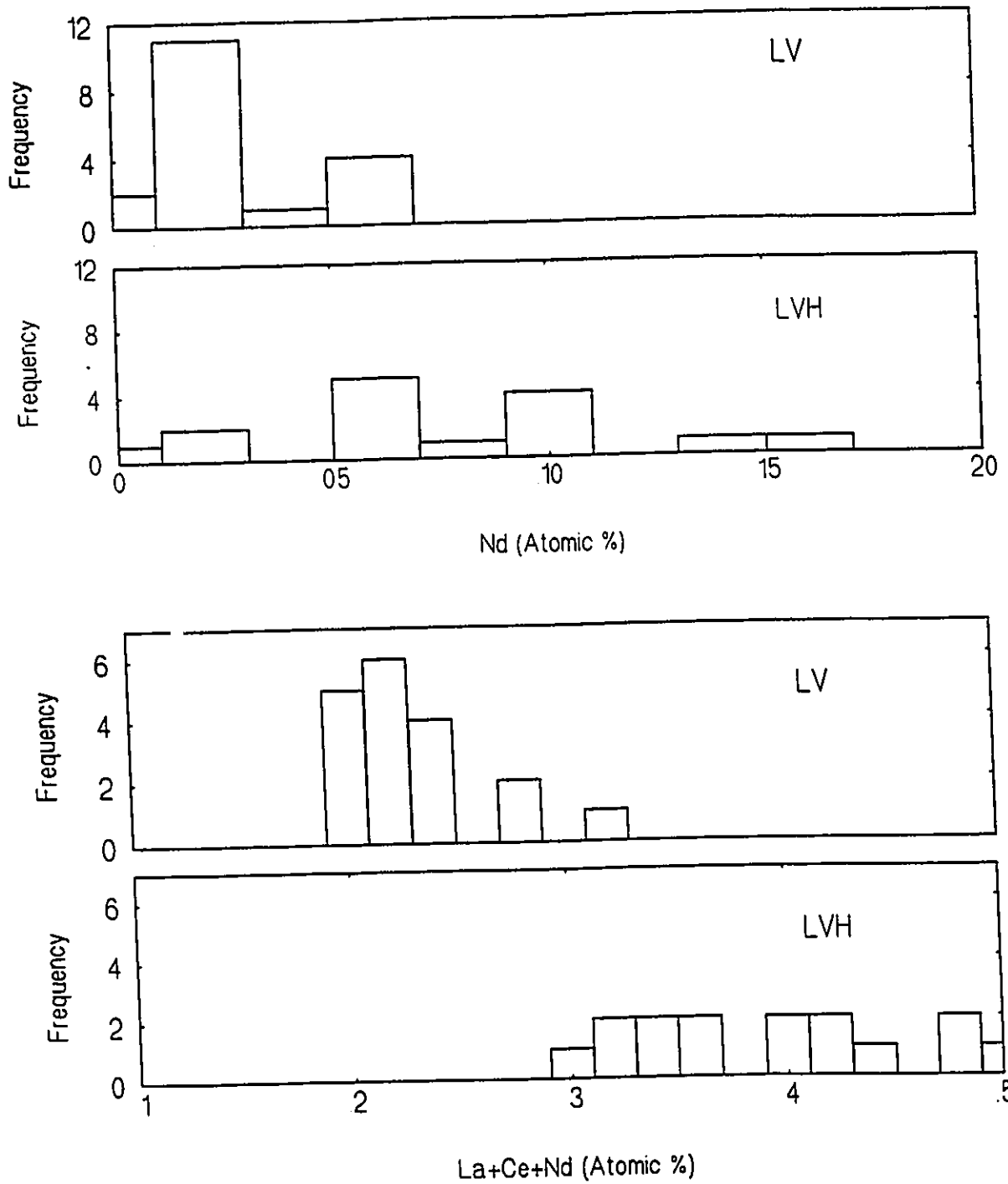


Figure 7.5 (continued)

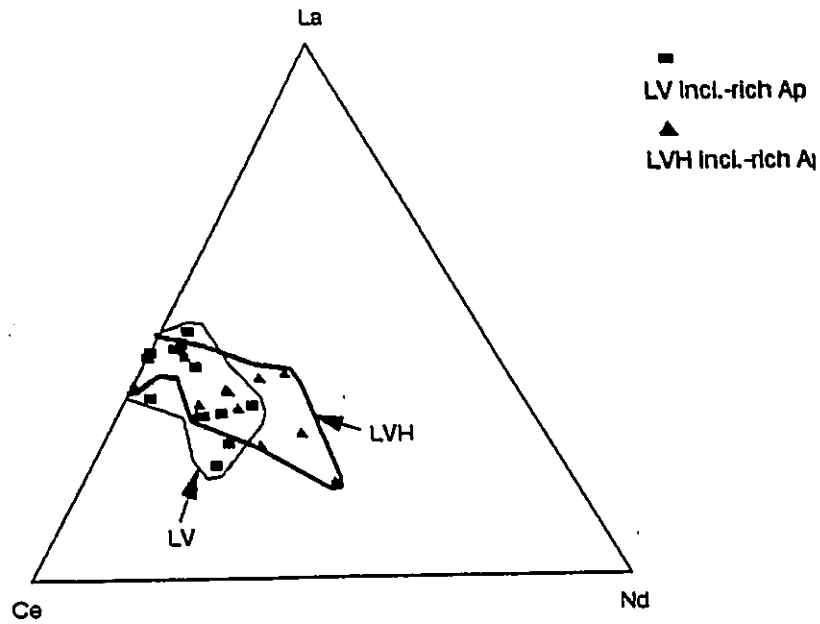


Figure 7.6. La-Ce-Nd plot for LV inclusions-bearing and LVH inclusion-bearing apatites.

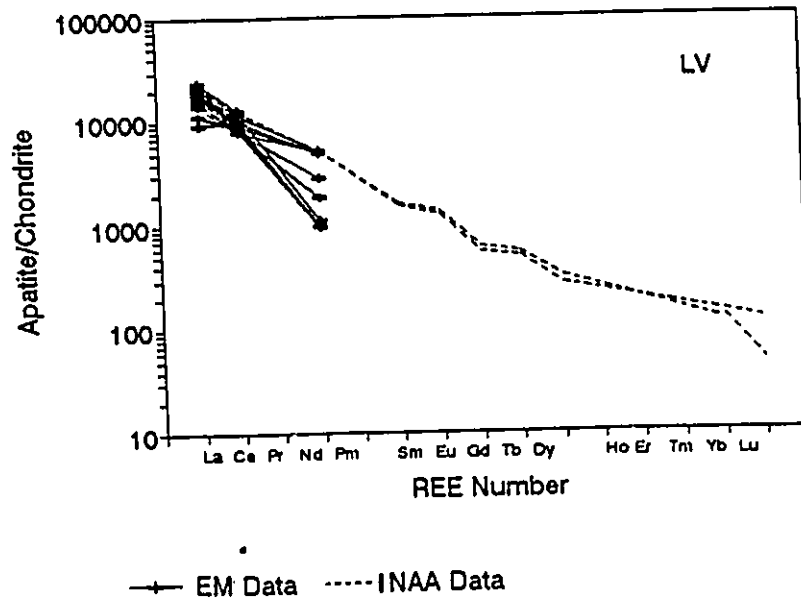


Figure 7.7. Chondrite-normalize curves of apatites containing LV-inclusions.

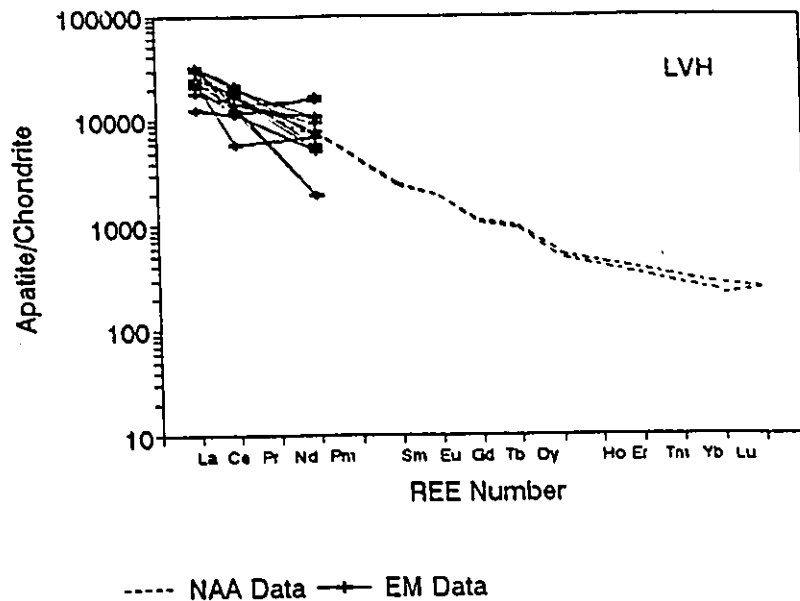


Figure 7.8. Chondrite-normalize curves of apatites containing LVH-inclusions.

Apatite data

The results of apatite analyses are given in Table 7.5. The data show that the apatites are LREE-enriched (Figure 7.2). Σ REE and La/Lu ratios are very variable, from 20562 to 61501 ppm and from 1022 to 6024 respectively, and are much higher than the rocks from which they came (Figures 7.3 and 7.4). The apatites from the Bond Zone have the highest Σ REE and La/Lu ratios. The apatites from the Manny Zone have lower Σ REE and higher La/Lu ratios than the apatites from the Mine. Σ REE and La/Lu ratios decrease with increasing inclusion abundances in the apatites (Figures 7.3 and 7.4). The LV-inclusion-rich apatites contain less REE but have higher La/Lu ratios than the LVH-inclusion-rich apatites (Figure 7.3 and 7.4). Chondrite-normalized patterns show small positive Eu anomalies for all apatite, but the curves given by Eby (1975) show small negative Eu anomalies (Figure 7.2).

7.3.2 Electron microprobe analyses

The results of the EM analyses on apatites are summarized in Table 7.6. The data indicate that, in addition to CaO and P₂O₅, the apatites contain significant amounts of

F, SiO₂, SrO, La₂O₃, Ce₂O₃ and Nd₂O₃. In most of the analyses, Ce is the dominant REE. The apatites containing LVH-inclusions have higher LREE contents and slightly lower La/Nd and Ce/Nd ratios than the apatites containing LV-inclusions (Figure 7.5 and 7.6). These two types of apatites show similar REE distribution on the chondrite-normalized curve (Figure 7.7 and 7.8).

7.4 Discussion

7.4.1 Substitutions involving REE in apatite

According to Clark (1984), REE substitute for Ca in the apatite structure. Hughes & Cameron (1991) undertook structural refinements on four natural apatites, two of which came from the Oka carbonatite. Their results demonstrate that LREE show a marked preference for the 7-fold coordination sites over the 9-fold coordination sites. Coupled substitution is required for the REE³⁺ substitution for Ca²⁺ in order to maintain charge balance. Two coupled substitution mechanisms involving REE have been established (Hogarth, 1984; Roedder et al., 1987; Ronsbo, 1989; Hughes & Cameron, 1991):

1. $\text{Na}^+ + \text{REE}^{3+} \rightarrow \text{Ca}^{2+} + \text{Ca}^{2+}$
2. $\text{REE}^{3+} + \text{Si}^{4+} \rightarrow \text{Ca}^{2+} + \text{P}^{5+}$

Figure 7.9 and 7.10 show that Si contents increase and P contents decrease with REE content, which suggests that the REE substitution for Ca is accompanied by Si addition and P removal. A plot of Ca+P versus REE+Si (Figure 7.11) reveals that the chemistry of the apatites may be explained by mechanism 2. Figure 7.12 and 7.13 show that REE contents and REE/Ca ratios decrease with Sr contents in apatite, which suggest that low Sr activity favours REE substitution for Ca.

7.4.2 Origin of LREE-rich hydrothermal fluids

Hydrothermal REE mineralization in carbonatites is characterized by LREE-enrichment (Gold, 1967; Balashov & Pozharitskays, 1969; Andersen, 1984 and 1986; and Williams-Jones, 1990). The hydrothermal fluids responsible for REE mineralization are believed to come from either orthomagmatic fluids (Lira & Ripley, 1990), or external waters or a mixture of orthomagmatic fluids and external waters

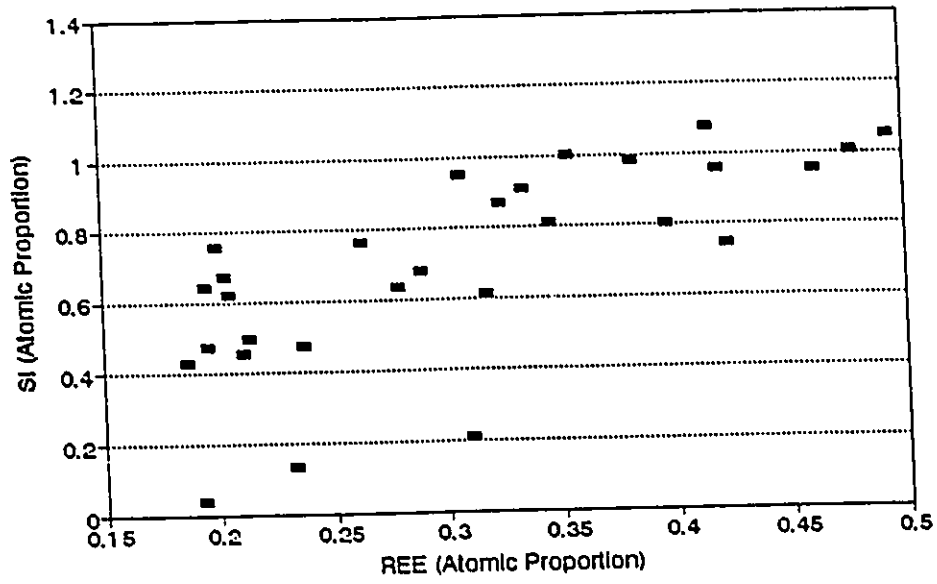


Figure 7.9. REE-Si plots of apatites.

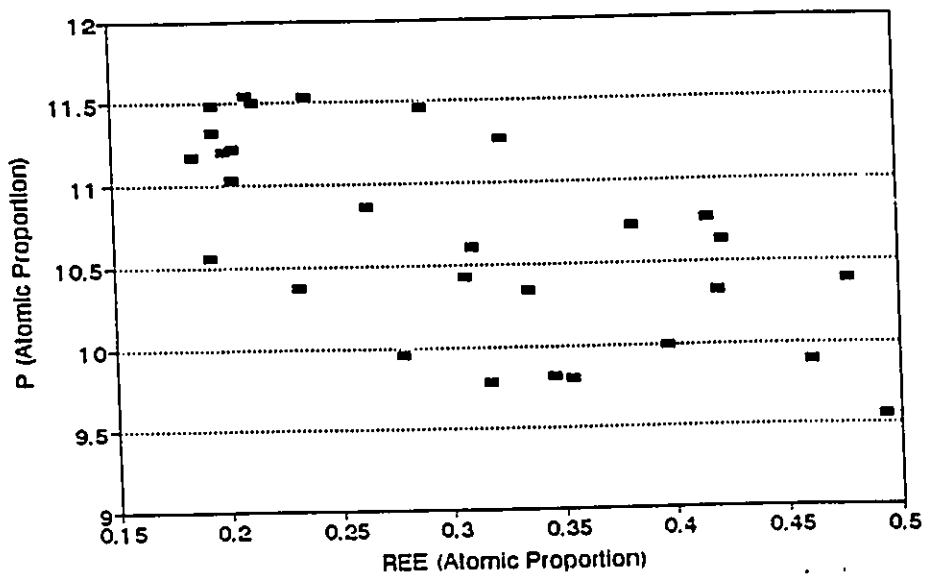


Figure 7.10. REE-P plots of apatites.

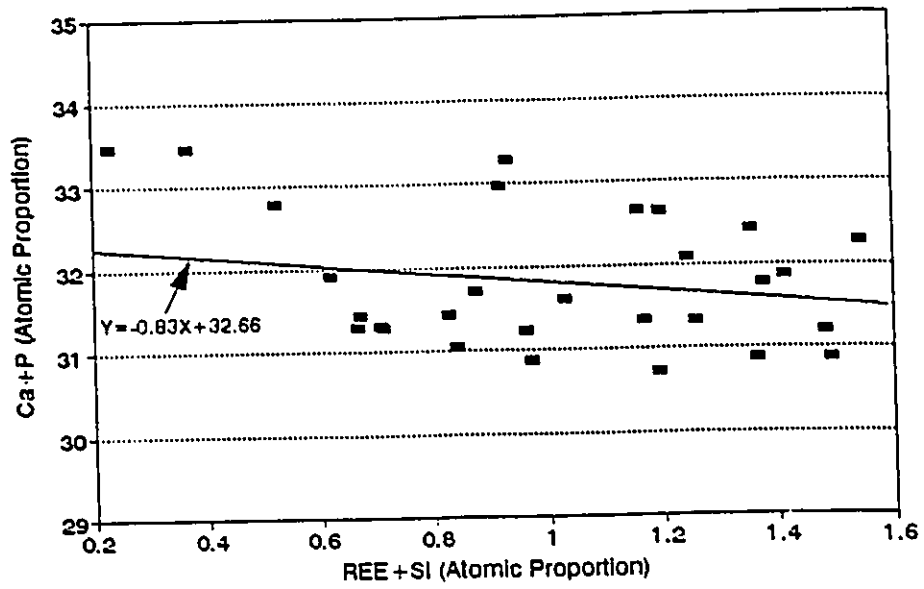


Figure 7.11. REE+Si - Ca+P plots of apatites.

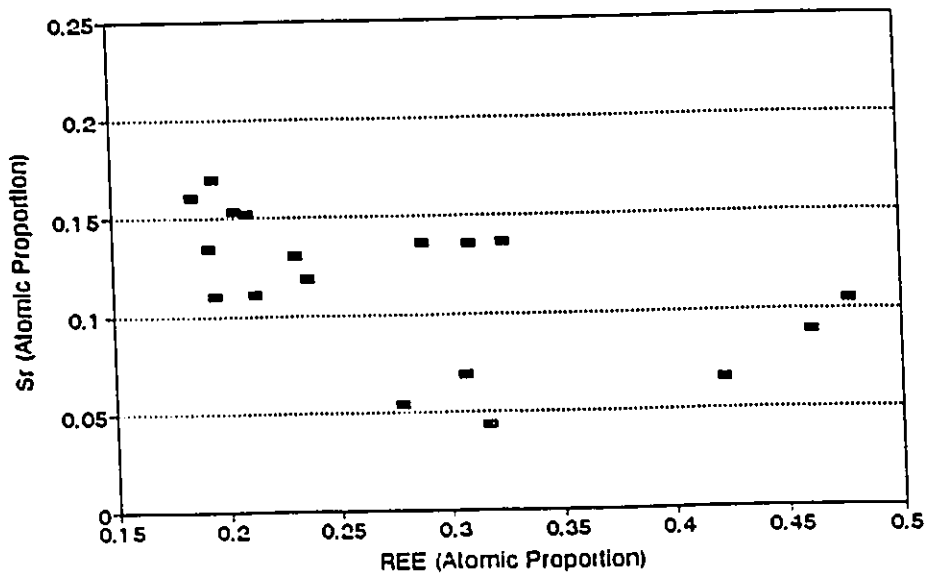


Figure 7.12. REE-Sr plots of apatites.

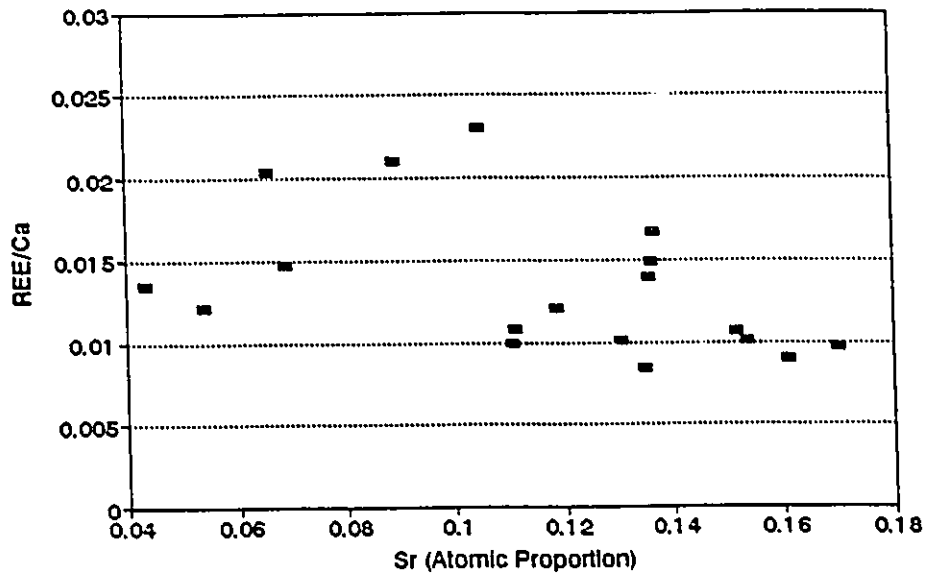


Figure 7.13. Sr-REE/Ca plots of apatites.

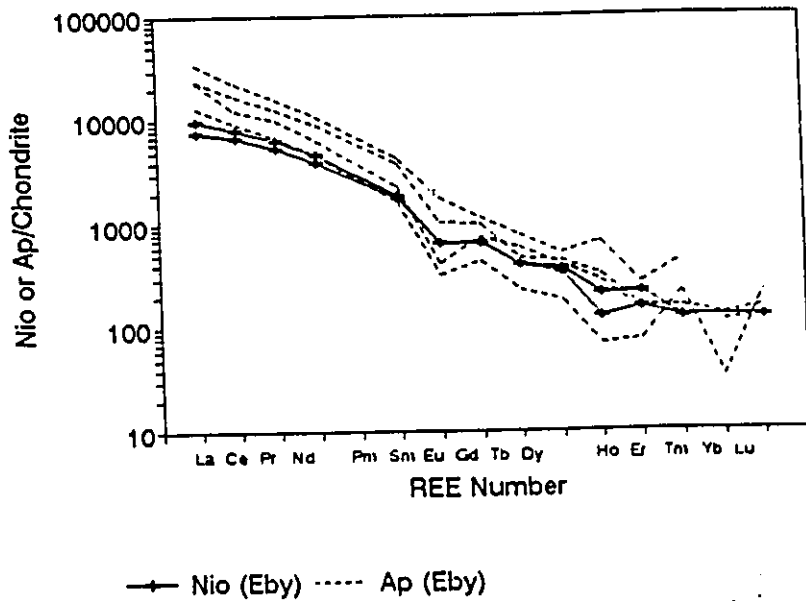


Figure 7.14. Chondrite-normalized curves of niocalites and apatites.

that have remobilized REE from primary phases (Andersen, 1986; Williams-Jones, 1990).

At Oka, LREE minerals, such as bastnaesite, synchisite and parisite occur in late hydrothermal carbonatite dikes or veins with pyrite and galena. In the early- and middle-stage carbonatites, REE are distributed principally in apatite, niocalite, calcite, pyrochlore and perovskite (Eby, 1975).

The highly variable REE concentration found in the Oka apatite may have been controlled by the following factors:

- 1) REE concentration of the magmas from which the apatite crystallized;
- 2) P-T conditions of the magma at which the apatite crystallized;
- 3) amounts of REE removed by crystallization of other REE-bearing minerals;
- 4) amounts of REE removed by hydrothermal fluids coexisting with the magmas.

REE concentrations in magma

If no hydrothermal fluids were evolved from the magma, REE concentrations in the magma are represented by REE concentrations of the whole rock. The REE concentrations in the Oka apatites increase with the REE concentrations in whole rocks, which suggests that the REE concentrations in the apatites were influenced by the REE concentrations in the magmas from which the apatites crystallized. However, there is evidence to suggest that hydrothermal fluids were present and influenced the REE distributions (see below).

P-T conditions of magmas

Experimental data on igneous rocks ranging in composition from basanite to granite (Watson & Green, 1981) indicate that the apatite/melt partition coefficients for REE increase with decreasing temperature, and that pressure has a minimal influence on the coefficients. Homogenization temperatures of the fluid inclusions in the Oka apatites are similar. If the apatites crystallized at similar pressure, their crystallization temperatures should be similar and the variation of REE concentrations in the apatites was not caused by the variation of magma's temperatures. If the apatite crystallized at different pressure, the REE concentration of the apatite may reflect the crystallization temperature of the apatites assuming that the magmas had the same REE concentrations.

Removal of REE by other minerals

The concentration of REE in calcite is one tenth of that in apatite, and most of the calcite crystallized later than apatite. Therefore crystallization of calcite could not affect the REE concentration of apatite. The REE concentrations in pyrochlore are twice that of apatite and perovskite has the same REE concentration as apatite. Only two of the samples which were used for INAA analyses contain minor pyrochlore and perovskite contents in the samples are less than 1%, therefore the crystallization of these two minerals will not have had much effect on the REE concentration of the magma.

REE concentrations in niocalite are slightly lower than in apatite. Niocalite shows almost the same REE pattern as apatite (Figure 7.14). Two samples from the Bond Zone contain 7% niocalite. In comparison to the niocalite-poor or -free samples from the same zone, one of the niocalite-rich samples has higher and another has lower REE concentrations. In addition, the REE variation in apatite from the niocalite-poor or -free samples cannot be explained by the niocalite contents. Therefore, niocalite content is probably not the main factor controlling REE concentrations in apatite.

Removal of REE by hydrothermal fluids in magmas

The results of the REE analyses on apatites show that REE concentrations in the apatites decrease with increasing fluid inclusion abundance in the apatites (Figure 7.3). If all the apatites crystallized from magmas with similar REE concentrations and the inclusion abundance reflects the amount of fluids exsolved from the magmas, the correlation of REE concentration with inclusion abundance suggests that the hydrothermal fluids may have removed large amounts of REE from the magmas and consequently decrease the REE concentration of the apatite which crystallized from the magma. If hydrothermal fluids were important in controlling the REE chemistry of the apatites, the lower La/Lu ratios in the inclusion-rich apatite, compared to the inclusion-poor or -free apatite (Figure 7.4), suggest that LREE are preferentially partitioned to the hydrothermal fluids relatively to HREE. The difference in REE concentration and La/Lu ratios between the LV-inclusion-rich apatites and the LVH-inclusion-rich apatites implies that fluid chemistry may have had an influence on the REE distribution in the apatites.

In summary, the REE concentration of magmas may have controlled the REE

concentration of the apatite which crystallized from the magmas. However, there is evidence which suggests that hydrothermal fluids may have removed LREE from the magmas during crystallization, and that the fluids may have become a source of late hydrothermal LREE mineralization in the Oka carbonatite.

7.4.3 Mineralizing potential of the Oka magmatic fluids

A study on REE geochemistry in hydrothermal solutions to 350°C by Wood (1990b) indicates that appreciable REE can be dissolved in hydrothermal fluids when complexed with suitable anionic species. Sulphate forms strong complexes with REE (Kosterin, 1959; Bandurkin, 1961; Menon et al., 1987; and Wood, 1990a, b) and chloride forms weaker complexes with REE (Wood, 1990b). As the hydrothermal fluids in the Oka carbonatite contain sulphate and chloride as major components, they have the potential to be mineralizing fluids, in which REE would primarily be transported as sulphate complex.

CHAPTER VIII

CONCLUSIONS

The detailed study of primary fluid inclusions in minerals from the Oka carbonatite and of REE geochemistry of the carbonatite allows the following conclusions to be made:

1. Primary fluid inclusions are present in calcite, apatite and monticellite from the Oka carbonatite. Monticellite is cut by apatite, and embayed and replaced by calcite. Apatite occurs as aggregates with interstitial calcite or as inclusions in calcite. These relationships indicate that the general crystallization sequence of these minerals is from monticellite through apatite to calcite. This is the same sequence that was established for the Magnet Cove carbonatite.
2. There are two types of primary inclusions in the carbonatite: 1) aqueous liquid-vapour (LV) inclusions which occur in all three minerals; and 2) aqueous liquid-vapour-halite (LVH) inclusions which occur in apatite and monticellite. No CO₂-rich inclusions were observed. These results suggest that hydrothermal fluids were present during crystallization of the calcite, apatite and monticellite from some of the carbonatite magmas and that these fluids were dominated by H₂O, and had low CO₂ concentrations. This is opposite to the results of Girault (1966) and Girault & Chaigneau (1967), which indicated that the hydrothermal fluids were dominated by CO₂. Most of the gases that they measured did not come from fluid inclusions, but from calcite inclusions in apatite as a result of decarbonation.
3. Trapped halite, apatite, calcite, nahcolite, mirabilite, strontianite, magnetite and silicate minerals are present in the inclusions. The presence of these minerals suggests that in addition to Na and Cl, Ca, carbonate, sulphate, silicate and phosphate are present in the inclusions. These are the first reported occurrence of mirabilite and strontianite in fluid inclusions from carbonatites.
4. All of the LV inclusions homogenized to the liquid phase between 95 and 435°C. Salinities and densities range from 4.3 to 24.7 wt. % and from 0.75 to 1.04 g/cm³

respectively. Most of the LVH inclusions in apatite homogenized to the liquid phase by halite dissolution between 248 and 340°C. Salinities and densities range from 34.5 to 43.3 equiv. wt. % NaCl and from 1.04 to 1.25 g/cm³ respectively. These data include the first obtained from monticellite.

5. Salinities of the LV inclusions decrease and their densities increase from monticellite through apatite to calcite, which suggests that the hydrothermal fluids in equilibrium with the carbonatite magmas evolved from high to low salinity and probably from high to low temperature during the crystallization of the minerals. These are the first empirical data to show that the salinities and densities of orthomagmatic fluids in equilibrium with carbonatite magmas change systematically with crystallization and the first data to show the nature of this change.
6. The minimum pressure in the magma chamber during crystallization of the inclusion-bearing minerals is estimated to be about 6 to 10 kb.
7. Results of leachate analyses and decrepitate analyses indicate that the fluids in equilibrium with carbonatite magmas are mainly composed of Na, Cl and S (sulphate?), and subordinate amounts of Ca, K, Mg and Si (silicate?). The low salinity fluids have higher Ca/Na, K/Na and Mg/Na ratios and lower Fe/Na ratios than the high salinity fluids. Phase equilibria also indicates that some fluids contained high concentrations of carbonate. These are the first semi-quantitative data obtained on cations other than Na and K, and on anions. These data will allow us to perform more precise tests on the involvement of orthomagmatic fluids in hydrothermal REE mineralization by obtaining similar data on the chemistry of the mineralizing fluids.
8. The apatites in the carbonatite are enriched in LREE relative to HREE. The rare earth elements substitute for Ca in the apatite structure through the coupled substitution:
$$\text{REE}^{3+} + \text{Si}^{4+} \rightarrow \text{Ca}^{2+} + \text{P}^{5+}$$
This is consistent with the models of Hogarth (1984), Roedder et al. (1987), Ronsbo (1989) and Hughes and Cameron (1991).

9. REE concentrations and La/Lu ratios in apatite increase with decreasing inclusion abundance in the apatites, which suggests that the hydrothermal fluids in equilibrium with the carbonatite magmas and the apatites may have removed LREE from the magmas and become a source for the late LREE mineralization in the carbonatite. Differences in REE concentrations and La/Lu ratios between LV inclusion-rich apatite and LVH inclusion-rich apatite suggest that fluid chemistry may have had an effect on the REE distribution in the apatite. In addition, these data shows that when studying the REE chemistry of igneous rocks, the possible role of hydrothermal fluids must be considered.

REFERENCES

- Andersen, T., 1984. Secondary processes in carbonatites: petrology of "rodberg" (hematite-calcite-dolomite carbonatite) in the Fen central complex, Telemark (South Norway). *Lithos*, 7: 227-248.
- Andersen, T., 1986a. Compositional variation of some rare earth minerals from the Fen Complex (Telemark, SE Norway): implications for the mobility of rare earths in a carbonatite system. *Min. Mag.*, 50: 503-509.
- Andersen, T., 1986b. Magmatic fluids in the Fen carbonatite complex, S.E. Norway: Evidence of mid-crustal fractionation from solid and fluid inclusions in apatite. *Contrib. Mineral. Petrol.*, 93: 491-503.
- Andersen, T., 1987. Mantle and crustal components in a carbonatite complex, and the evolution of carbonatite magma: REE and isotopic evidence from the Fen Complex, southeast Norway. *Chemical Geology (Isotope Geoscience section)*, 65: 147-166.
- Armbrustmacher, T.J., 1979. Replacement and primary magmatic carbonatites from the Wet Mountains area, Fremont and Custer Counties, Colorado. *Econ. Geol.*, 74: 888-901.
- Aspden, J.A. 1980. The mineralogy of primary inclusions in apatite crystals extracted from Alno ijolite. *Lithos*, 13: 263-68.
- Balashov, Y.A. and Pozharitskaya, L.K., 1969. Factors governing the behavior of rare-earth elements in the carbonatite process. *Geochem. Inter.*, 5: 271-288.
- Bandurkin, G.A., 1961. Behaviour of the rare earths in fluorine-bearing media. *Geochem. Inter.*, 6: 159-167.
- Barber, C., 1974. The geochemistry of carbonatites and related rocks from two carbonatite complexes, South Nyonza, Kenya. *Lithos*, 7: 53-63.
- Brown, P.E. and Lamb, W.M., 1989. P-V-T properties of fluids in the system $H_2O \pm CO_2 \pm NaCl$: new graphical presentations and implications for fluid inclusion studies. *Geochim. Cosmochim. Acta*, 53: 1209-1221.
- Brown, P.E., 1989. FLINCOR: A microcomputer program for the reduction and investigation of fluid inclusion data. *Am. Mineral.*, 74: 1390-1393.
- Clark, A.M., 1984. Mineralogy of the rare earth elements. *Rare earth element*

- geochemistry, Henderson, P. (editor). Elsevier, Amsterdam-Oxford-New York-Tokyo, 33-63.
- Conway, C.M. and Taylor H.P., 1969. O^{18}/O^{16} and C^{13}/C^{12} ratios of coexisting minerals in the Oka and Magnet Cove carbonatite bodies. *J. Geol.*, 7: 618-26.
- Crawford, M.L., 1981. Phase equilibria in aqueous fluid inclusions. *Fluid inclusions: applications to petrology*, MAC short course notes V, Hollister, L.S. and Crawford, M.L. (editors), 75-100.
- Cullers, R. L. and Medaris, L.G., 1977: Rare earth elements in carbonatite and cogenetic alkaline rocks: example from Seabrook Lake and Callander Bay, Ontario. *Contrib. Mineral. Petrol.*, 65: 143-153.
- Cullers, R.L. and Graf, J.L., 1984: Rare earth elements in igneous rocks of the continental crust: Predominantly basic and ultrabasic rocks: Rare earth element geochemistry, Henderson P. (editor). Elsevier, Amsterdam-Oxford-New York-Tokyo, 237-275.
- Dhamelincourt, P., Beny, J.M., Dubessy, J. and Poty, B., 1979. Analyse d'inclusions fluids a la microsonde MOLE a effet Raman. *Bull. Mineral*, 102: 600-610.
- Eby, G.H., 1975: Abundance and distribution of the rare earth elements and yttrium in the rocks and minerals of the Oka carbonatite complex, Quebec. *Geochim. Cosmochim. Acta*, 39: 597-620.
- Eadington, P.J., 1974. Microprobe analysis of the non-volatile constituents in fluid inclusions. *N. Jahrb. Mineral. Monatsh.*, 11: 518-525.
- Fairbairn, H.W., Aare, G., Pison, W.H., Hurley, P.M., and Powell, J.L., 1963. Initial ratio of Strontium 87 to Strontium 86, wholerock age, and discordant biotite in the Montereian Igneous Province, Quebec. *J. Geophys. Res.*, 68: 6515-6522.
- Girault, P.J., 1966. Genese et geochimie de l'apatite et de la calcite dans les rockes liees au complexe carbonatitique et hyperalcalin d'Oka (Canada), *Bull. Soc. franc. Miner. Crist*, LXXXIX: 496-513.
- Girault, P.J. et Chaigneau, M., 1967. Sur les inclusions fluides presentes dans les cristaux d'apatite des roches de la region d'Oka (Canada). *C. R. Acad. Sc. Paris*, 264 (D): 529-532.
- Gittins, J., Beckett, M.F. and Jago, B.C., 1990. Composition of the fluid phase

- accompanying carbonatite magma: A critical examination. *Am. Mineral.*, 75: 1106-1109.
- Gold, D.P., 1963. The relationship between the limestones and the alkaline igneous rocks of Oka and St. Hilaire, Quebec. Unpub. Ph.D Thesis, McGill University, Montreal.
- Gold, D.P., 1972. The Monteregean Hills: ultra-alkaline rocks and the Oka carbonatite complex. 24th International Geological Congress, Excursion Guide, B-II: 1-47.
- Gold, D.P., Vallee, M. and Charette, J.P., 1967. Economic geology and geophysics of the Oka alkaline complex, Quebec. *Canadian Mining and Metallurgy Bulletin*, 60: 1131-44.
- Freestone I.C. and Hamilton D.L., 1980. The role of liquid immiscibility in genesis of carbonatites-An experimental study. *Contrib. Mineral. Petrol.* V73: p105-117.
- Haapala, I., 1980. Fluid inclusions in the apatite of the Sokli carbonatite, Finland - A preliminary report. *Geoloci*, 32: 83-87.
- Haynes, F.M., Sterner, S.M. and Bodnar, R.J., 1988. Synthetic fluid inclusions in natural quartz: IV. Chemical analysis of fluid inclusions by SEM/EDA: Evaluation of method. *Geochim. Cosmochim. Acta.*, 52: 969-977.
- Haskin, L.A., 1984. Petrogenetic modelling -use of rare earth elements. Rare earth element geochemistry. Henderson P. (editor). Elsevier, Amsterdam-Oxford-New York-Tokyo, 115-152.
- Heinrich, E.W., 1966: The geology of carbonatites. Rand McNally & Company, Chicago.
- Hogarth, D.D., 1984. Pyrochlore, apatite and amphibole: distinctive minerals in carbonatites. *Carbonatites: Genesis and Evolution*. Keith Bell (editor), Unwin Hyman, London, 105-149.
- Hughes, J.M. and Cameron, M., 1991. Rare-earth-element ordering and structural variations in natural rare-earth-bearing apatites. *Am. Mineral.*, 76: 1165-1173.
- Jones, J.D. and Kesler, S.E., 1992. Fluid inclusion gas chemistry in east Tennessee Mississippi Valley-type districts: Evidence for immiscibility and implications for depositional mechanisms. *Geochim. Cosmochim. Acta*, 56: 137-154.
- Kapustin, Y.L., 1966. Geochemistry of rare earth elements in carbonatites. *Geochem. Inter.*, 3: 1054-1054.

- Kogarko, L.N. and Romanchev, B.P., 1977. Temperature, pressure, redox conditions, and mineral equilibria in agpaitic nepheline syenites and apatite-nepheline rocks. *Geochem. Inter.*, 14, 113-128.
- Koster van Groos, A.F. and Wyllie, P.J., 1973. Liquid immiscibility in the join $\text{NaAlSi}_3\text{O}_8$ - $\text{CaAl}_2\text{Si}_2\text{O}_8$ - Na_2CO_3 - H_2O . *Am. J. Sci.*, 272: 465-487.
- Kosterin, A.V., 1959. The possible modes of transport for the rare earths by hydrothermal solutions. *Geochem. Inter.*, 4: 381-387.
- Krauskopf, K. B., 1979. Introduction to geochemistry. McGraw-Hill Book Company, New York, 617p..
- Kretz, R. 1983. Symbols for rock-forming minerals. *Am. Mineral.*, 68: 277-279.
- Linke, W.F., 1965. Solubilities of inorganic and metal-organic compounds. (4th ed.) 2, Am. Chem. Soc.
- Lira, R. and Ripley, E.M., 1990. Fluid inclusion studies of the Rodeo de Los Molles REE and Th deposit, Las Chacras Batholith, Central Argentina. *Geochim. Cosmochim. Acta*, 54: 663-671.
- Loubet, M., Bernat, M., Javoy, M., and Allegre, C.J., 1972. Rare earth contents in carbonatites. *Earth Planet. Sci. Lett.*, 14: 226-232.
- Mariano A.N., 1989. Nature of economic mineralization in carbonatites and related rocks. *Carbonatites: Genesis and Evolution*. Keith Bell (editor), Unwin Hyman, London, 580-600.
- Maurice, O.D., 1956, Geology of Oka Hill. *Canadian Mining Journal*, 83: 70-73.
- Menon, M.P., James, J., and Jackson J.D., 1987. Studies on the solubility and complexation of lanthanum and neodymium fluoride-water systems. *Lanthinide Actinide Res*, 2: 49-66.
- Mitchell, R.H. and Brunfelt, A.O., 1975. Rare earth geochemistry of the Fen alkaline complex, Norway. *Contrib. Mineral. Petrol.*, 52: 247-259.
- Nesbitt, B.E. and Kelly, W.C., 1977, Magmatic and hydrothermal inclusions in carbonatite of the Magnet Cove Complex, Arkansas, *Contrib. Mineral. Petrol.*, 63: 271-94.
- Oakes, C.S., Bodnar, R.J. and Simonson, J.M., 1990. The system NaCl - CaCl_2 - H_2O : I. The ice liquidus at 1 atm total pressure. *Geochm. Cosmochim. Acta*, 54: 603-610.
- Phillips, R.S. and Campbell, A.R., 1990. Geochemistry of magmatic REE-Th-U

- quartz/fluorite veins from the Capitan pluton, Capitan Mountains, south-central New Mexico. GSA abstr. with prog., 22, #7: A159.
- Rankin, A.H., 1975. Fluid inclusion studies in apatite from carbonatites of the Wasaki area of western Kenya. *Lithos*, 8: 123-136.
- Rankin, A.H., 1977. Fluid inclusion evidence for the formation conditions of apatite from the Tororo carbonatite complex of eastern Uganda. *Mineral. Mag.*, 41: 155-164.
- Rankin, A.H and Le Bas, M.J., 1974. Nahcolite (NaHCO₃) in inclusions in apatites from some E. African ijolites and carbonatites. *Mineral. Mag.*, 39: 564-570.
- Roedder, E., 1973. Fluid inclusions from the fluorite deposits associated with carbonatite of Amba dongar, India, and Okorusu, south West Africa. *Inst. Mining Metall. Trans., Sect. B*, 82: B35-B39.
- Roedder, E., 1984. Fluid inclusions, *Reviews in Mineralogy*, Vol. 12. Mineralogical Society of America, 644p.
- Roedder, E., 1990. Fluid inclusion analysis-Prologue and epilogue. *Geochem. Cosmochim. Acta*, 54: 495-507.
- Roedder, P.L., Macarthur, D., Ma, X., and Palmer, G.R., 1987. Cathodoluminescence and microprobe study of rare-earth elements in apatite. *Am. Mineral.*, 72: 801-811.
- Romanchev, B.P., 1972. Inclusion thermometry and the formation condition of some carbonatites complexes in East Africa. *Geochim. Inter.* 9: 115-20.
- Romanchev, B.P. and Sokolov, S.V., 1979. Liqation in the production and geochemistry of the rocks in carbonatite complexes. *Geochem. Inter.*, 16: 125-135.
- Ronsbo, J.G., 1989. Coupled substitutions involving REEs and Na and Si in apatites in alkaline rocks from the Ilimaussaq intrusion, South Greenland, and the petrological implications. *Am. Mineral.*, 74: 896-901.
- Rowe, R.B., 1955. Notes on columbium mineralization, Oka District, Two Mountains County, Quebec. Canadian Geological Survey, Paper 54-22.
- Rowe, R.B., 1958. Niobium (columbium) deposits of Canada. *Can. Geol. Surv. Econ. Geol. Ser.* 18.
- Salvi, S. and Williams-Jones A.E., 1990. The role of hydrothermal processes in the granite-hosted Zr, Y, REE deposit at Strange Lake, Quebec/Labrador:

- Evidence from fluid inclusions. *Geochim. Cosmochim. Acta*, 54: 2403-2418.
- Schofeild, A. and Haskin, L., 1964. Rare-earth distribution patterns in eight terrestrial materials. *Geochim. Cosmochim. Acta*, 28: 437-446.
- Semenov, E.I., 1974. Economic mineralogy of alkaline rocks. *The alkaline rocks*, Sorensen, H. (editor), Wiley, 543-552.
- Shafiqullah, M., Tupper, W.M., and Cole, T.J.S., 1970. K-Ar age of the carbonatite complex, Oka, Quebec. *Can. Mineral.*, 10: 541-552.
- Stansfield, J., 1923. Extensions of the Monteregian petrographical province to the west and north-west. *Geol. Mag.*, 60: 433-453.
- Sterner, S.M., Hall, D.L. and Bodnar, R.J., 1988. Synthetic fluid inclusions. V. Solubility relations in the system NaCl-KCl-H₂O under vapour-saturated conditions. *Geochim. Cosmochim. Acta*, 52: 989-1005.
- Treiman, A.H. and Essene, E.J., 1984. A periclase-dolomite-calcite carbonatite from the Oka complex, Quebec, and its calculated volatile composition. *Contrib. Mineral. Petrol.*, 85: 149-157.
- Watson, E.B and Green, T.G., 1981. Apatite/liquid partition coefficients for the rare earth elements and strontium. *Earth Planet. Sci. Lett.*, 56: 405-421.
- White, W.B., 1974. The carbonate minerals. The infrared spectra of minerals, Farmer, V.C (editor), *Min. Soc. Monograph*, 4: 227-284.
- Williams-Jones, A.E., 1991. The genesis of LREE mineralization in carbonatites: A case study of the St-Honore deposit, Quebec. *Research Agreements Program, Energy, Mines and Resources Canada*: 128.
- Wood, S.A., 1990a. The aqueous geochemistry of the rare-earth elements and yttrium, 1. Review of available low-temperature data for inorganic complexes and the inorganic REE speciation of natural waters. *Chem. Geol.*, 82: 159-186.
- Wood, S.A., 1990b: The aqueous geochemistry of the rare-earth elements and yttrium, Theoretical predictions of speciation in hydrothermal solutions to 350°C at saturated water vapor pressure. *Chem. Geol.*, 88: 99-125.
- Wyllie, P.J. and Tuttle, O.F., 1960. The System CaO-CO₂-H₂O and the origin of carbonatites. *J. Petrol.*, 1: 1-46.

APPENDIX I

Summary of the Mineralogy of the Main Rock Types in the Oka Carbonatite (Gold, 1972)

- I. Carbonate Rocks: sovites (calcite), and rauhaugites (dolomite).
 1. Flow-layered calcite rock with accessory pyroxene, biotite, magnetite.
 2. Layered soda pyroxene-biotite-magnetite-calcite rock, with pyrochlore.
 3. Monticellite calcite rock, with accessory perovskite.
 4. Coarse-grained calcite rock (relatively pure).
 5. Very coarse-grained "pegmatitic" calcite rock.
 6. Soda amphibole calcite rock, with accessory pyrochlore.
 7. Melilite calcite rock.
 8. Niocalite calcite rock, commonly with accessory melilite and magnetite.
 9. Nepheline calcite rock, commonly with minor melanite and pyroxene.
 10. Forsterite calcite rock (rare), with accessory pyrochlore and magnetite.
 11. Fine-grained apatite calcite rock.
 12. Dolomite rock, locally with accessory pyrochlore.

- II. Okaite-Jacupirangite Series:

melilites and pyroxenites, commonly with accessory magnetite, apatite and perovskite.

 1. Okaite:

60-90% melilite; 40-10% nepheline, hauynite, apatite, perovskite, magnetite, biotite.
 2. Nepheline okaite:

40% nepheline; 40% melilite; 20% hauynite, calcite, magnetite, biotite.
 3. Hauynite-titanaugite:

30% melilite; 10% titanaugite; 40% hauynite; 10% biotite, apatite, calcite.
 4. Jacupirangite:

60-70% titanaugite; 20-15% nepheline; 10-2% magnetite; 10-15% apatite, biotite, perovskite.

5. Magnetite-apatite rock:

60-90% magnetite; 30-10% apatite, 10-5% calcite.

III. Ijolite-Urtite Series:

nephelinites, with accessory calcite, apatite.

1. Melteigite:

65% soda pyroxene; 35% nepheline.

2. Calcite melteigite:

65% soda pyroxene; 30-5% nepheline; 5-30% calcite.

3. Ijolite:

50% soda pyroxene; 50% nepheline.

4. Melanite ijolite:

30% melanite; 40% nepheline; 30% pyroxene.

5. Melanite-wollastonite ijolite:

25% melanite; 25% wollastonite; 25% nepheline; 25% soda pyroxene.

6. Calcitic ijolite:

50% pyroxene; 40-20% nepheline; 10-30% calcite.

7. Urtite:

70-90% nepheline; 30-10% soda pyroxene

8. Wollastonite urtite:

55% nepheline; 20% wollastonite; 25% soda pyroxene, melanite.

IV. Lamprophyres

1. Alnoite:

phenocrysts: olivine, augite, biotite, lamprobolite.

matrix: magnetite, melilite, calcite, melanite apatite, perovskite, glass.

2. Alnoite breccia:

polymict fragments in an alnoitic matrix.

3. Carbonatitic breccia:

phlogopite, ilmenite, magnetite, augite, phenocrysts in a carbonate matrix.

4. Biotite fourchite:

titanaugite, barkevikite, tinanomagnetite and biotite phenocrysts in a analcite or glassy matrix.

V. Replacement Rocks

1. Glimmerite:

50-80% biotite; 40-20% calcite; 20-10% zeolites, magnetite, rare earth carbonates.

2. Fenites:

allochemically metamorphosed quartzofeldspathic gneisses, minor anorthosites.

APPENDIX II MICROTHERMOMETRY DATA

Table 1: Microthermometry data for LVH inclusions.

Sample	Min	Fr	Gr	No	Orig	T _e (°C)	T _{dH} (°C)	T _{dI} (°C)	T _{dV} (°C)	T _D (°C)	Descrip
Mine											
ES90-68	Ap	10	1	1	P	-45	1.5	277	297		3-0
ES90-68	Ap	10	1	2	P	-50	2.3	291	371		3-0
ES90-68	Ap	11	1	1	P			243	214		3-0
ES90-68	Ap	11	1	2	P	-41	-0.1	414	309		3-0
ES90-69	Ap	1	1	1	P	-35	0.3	340	214		3-0
ES90-69	Ap	1	2	1	P	-39	0.2		211	399	3-0
ES90-69	Ap	3	1	1	P		0.5	343	162		3-0
ES90-69	Ap	3	1	2	P	-39	1.6	319	154		3-0
ES90-69	Ap	4	1	1	P	-50	4.6			270	3-0
ES90-69	Ap	5	1	1	P		3.0	360	182		bol
ES90-69	Ap	6	1	1	P	-35			172		bol
ES90-69	Ap	7	1	1	P	-45	3.1	335	157		3-0
ES90-69	Ap	9	1	1	P	-47	-0.5	291	146		3-0
ES90-69	Ap	10	1	1	P	-50	2.1	285	99		3-0
ES90-69	Ap	11	1	1	P	-35	-2.1	341	178		3-0
ES90-69	Ap	11	2	1	P			353	178		3-0
ES90-69	Ap	11	2	2	P			325	139		3-0
ES90-69	Ap	12	1	1	P	-50	4.1	322	177		3-0
ES90-69	Ap	12	1	2	P	-48	0.3	302	203		3-0
ES90-69	Ap	12	1	3	P			291			3-0
ES90-69	Ap	12	1	4	P	-45	2.1	353	205		3-0
ES90-69	Ap	12	1	5	P			300	206		3-0
ES90-69	Ap	12	1	6	P			343	189		3-0
ES90-69	Ap	13	1	1	P	-40	1.5	340	160		3-0
ES90-69	Ap	13	1	2	P	-40	-0.1	355	143		3-0
ES90-69	Ap	13	1	3	P			329	135		3-0
ES90-69	Ap	13	1	4	P			342	151		3-0
ES90-69	Ap	15	1	1	P			341	179		3-0
ES90-69	Ap	15	1	2	P	-40	0.1	340	186		3-0
ES90-69	Ap	15	1	3	P			304	161		3-0
ES90-69	Ap	15	1	4	P			348	274		3-0
ES90-69	Ap	15	1	5	P			336			3-0

Table 1 (continued)

Sample	Mn	Fr	Gr	No	Orig	T _e (°C)	T _{dH} (°C)	T _{dI} (°C)	T _{dV} (°C)	TD (°C)	Descrip
ES90-69	Ap	15	2	1	P	-35	2.1	343	265		3-D
L91-5	Ap	1	1	1	P	-40	3.1	276	203		3-D
L91-5	Ap	1	1	2	P			260	155		3-D
L91-5	Ap	1	1	3	P			261	152		3-D
L91-5	Ap	1	1	6	P	-35	0.2	330	162		3-D
L91-5	Ap	1	1	8	P			286	192		3-D
L91-5	Ap	2	1	1	P			248	128		3-D
L91-5	Ap	3	1	2	P			277	142		3-D
L91-5	Ap	3	1	3	P			283	150		3-D
Marry Zone											
MA-1	Mtc	8	1	1	P			175	460		bol
MA-1	Mtc	8	2	1	P	-26	0.5	146	468		bol

Mtc mineral; Fr: fragment; Gr: co-genetic group; No: number of inclusions;
 Orig: origin of inclusions; Descrip: description

Table 2: Microthermometry data for LV inclusions.

Sample	Min	Frag	Gr	No	Orig	T _e (°C)	T _m (°C)	T _{dv} (°C)	Descrip
Bond Zone									
B12-1	Ap	6	1	1	p		-19.7	302	3-D
B12-1	Ap	6	1	2	p	-45	-22.8	360	3-D
B12-1	Ap	6	1	3	p		-19.3	410	3-D
B12-1	Ap	6	1	4	p	-43	-24.1	371	3-D
B12-1	Ap	6	1	5	p			351	3-D
B12-1	Ap	6	2	1	p			315	3-D
B12-1	Ap	6	2	2	p			301	3-D
B12-1	Ap	6	2	3	p			345	3-D
B12-1	Cal	2	1	1	p	-38	-7.1	91	Isol
B12-1	Cal	2	2	1	p	-28	-3.0	126	Isol
B12-1	Cal	3	1	1	p	-28	-6.9	102	Isol
B12-1	Cal	4	1	1	p	-30	-9.2	114	Isol
B12-1	Cal	5	1	1	p	-30	-10.6	129	Isol
B12-1	Cal	5	2	1	p		-2.5	107	Isol
B12-1	Cal	5	3	1	p	-30	-8.0	117	Isol
B4-2	Ap	1	2	1	p	-35	-21.8	227	3-D
B4-2	Ap	1	2	2	p	-35	-22.4	264	3-D
B4-2	Ap	1	2	3	p	-35	-26.1	276	3-D
B4-2	Ap	1	2	4	p	-35	-24.0	416	3-D
B4-2	Ap	1	2	5	p			304	3-D
B4-2	Ap	1	2	6	p	-35	-21.2	288	3-D
B4-2	Ap	1	2	7	p			389	3-D
B4-2	Ap	1	3	1	p		-20.4	315	3-D
B4-2	Ap	1	3	2	p	-35	-19.3	384	3-D
B4-2	Ap	1	3	3	p			389	3-D
B4-2	Ap	2	1	1	p	-50	-15.8	280	3-D
B4-2	Ap	2	1	2	p		-19.1	361	3-D
B4-2	Ap	2	1	3	p	-50	-19.3	364	3-D
B4-8	Cal	3	1	1	p	-50	-21.7	261	Isol
B4-8	Cal	3	2	1	p			295	Isol
B4-9	Cal	1	1	1	p	-26	-14.9	231	Isol
B4-9	Cal	2	1	1	p	-25	-14.0	274	Isol
Mine									
IS90-72	Cal	1	1	1	p		-10.2	241	3-D
IS90-72	Cal	1	1	2	p		-10.6	238	3-D
IS90-72	Cal	2	1	1	p	-27	-9.6	233	3-D
IS90-72	Cal	2	1	2	p		-7.2	214	3-D
IS90-72	Cal	2	1	3	p	-31	-8.7	217	3-D
IS90-72	Cal	2	1	4	p	-31	-8.7	227	3-D
IS90-72	Cal	2	1	5	p		-9.2	228	3-D
IS90-79	Ap	1	1	1	p	-24	-10.5	267	3-D
IS90-79	Ap	1	1	2	p	-23	-4.9	159	3-D
IS90-79	Ap	1	1	3	p	-26	-6.9	252	3-D
IS90-79	Cal	1	1	1	p			267	3-D
IS90-79	Cal	1	1	2	p			204	3-D
IS90-79	Cal	1	1	3	p			192	3-D

Table 2 (continued)

Sample	Min	Frag	Gr	No	Orig	Te (°C)	Tml (°C)	Tdv (°C)	Descrip
S90-79	Cal	1	1	4	p			248	3-D
S90-79	Cal	1	1	5	p			189	3-D
S90-79	Cal	1	1	6	p			246	3-D
S90-79	Cal	1	1	7	p			286	3-D
S90-79	Cal	1	2	1	p			229	3-D
S90-79	Cal	1	2	2	p			240	3-D
S90-79	Cal	1	2	3	p			213	3-D
S90-79	Cal	1	2	4	p			233	3-D
L91-1	Cal	1	1	1	p		-12.2	173	3-D
L91-1	Cal	1	1	2	p			191	3-D
L91-1	Cal	1	1	3	p		-9.2	101	3-D
L91-6	Cal	1	1	1	p		-10.3	173	3-D
L91-6	Cal	1	1	2	p			189	3-D
L91-6	Cal	1	2	1	p		-9.1	101	isol
Manny Zone									
MA-1	Ap	4	1	1	p	-53	-19.3	273	3-D
MA-1	Ap	4	1	2	p	-56	-22.6	269	3-D
MA-1	Ap	4	1	3	p	-58	-20.8	268	3-D
MA-1	Ap	4	1	4	p	-51	-19.7	266	3-D
MA-1	Ap	5	1	1	p	-58	-23.4	310	isol
MA-1	Ap	5	2	1	p	-46	-14.3	286	3-D
MA-1	Ap	5	2	2	p	-49	-17.3	286	3-D
MA-1	Ap	5	2	3	p			263	3-D
MA-1	Ap	5	2	4	p			259	3-D
MA-1	Ap	5	2	5	p			287	3-D
MA-1	Ap	7	1	1	p	-53	-23.4	261	3-D
MA-1	Ap	7	1	2	p	-53	-18.3	253	3-D
MA-1	Ap	7	2	1	p	-31	-21.0	330	isol
MA-1	Ap	8	1	1	p		-13.0	328	3-D
MA-1	Ap	8	1	2	p			316	3-D
MA-1	Ap	8	1	3	p			302	3-D
MA-1	Ap	9	1	1	p	-55	-15.6	336	3-D
MA-1	Ap	9	1	2	p	-55	-19.1	342	3-D
MA-1	Ap	9	2	1	p		-19.9	268	3-D
MA-1	Ap	9	2	2	p			263	3-D
MA-1	Ap	9	2	3	p	-51	-23.5	267	3-D
MA-1	Ap	9	2	4	p			255	3-D
MA-1	Ap	9	2	5	p			252	3-D
MA-1	Ap	9	3	1	p		-12.4	295	3-D
MA-1	Ap	9	3	2	p	-53	-9.2	294	3-D
MA-1	Ap	9	3	3	p	-51	-10.5	313	3-D
MA-1	Mtc	8	3	1	ps			22.5	370
MA-1	Mtc	8	3	2	ps	-39	-23.7	388	S-P
MA-1	Mtc	8	3	3	ps			422	S-P
MA-1	Mtc	8	4	1	ps		-22.7	393	S-P

Table 2 (continued)

Sample	Min	Frag	Gr	No	Orig	Ta (°C)	Tml (°C)	Tdv (°C)	Descrip
MA-1	Mtc	8	4	2	ps	-31	-23.7	475	S-p
MA-1	Mtc	8	5	1	ps			395	S-p
MA-1	Mtc	8	5	2	ps			393	S-p
MA-1	Mtc	8	6	1	p	-32	-24.0	378	Isol
MA-1	Mtc	9	1	1	p	-59	-12.3	373	Isol
MA-3	Ap	1	2	1	p			348	3-D
MA-3	Ap	1	3	1	p	-35	-23.3	404	3-D
MA-3	Ap	1	3	2	p	-35	-19.5	367	3-D
MA-3	Ap	1	3	3	p	-35	-23.0	406	3-D
MA-3	Ap	1	3	4	p			378	3-D
MA-3	Ap	1	4	1	p	-29	-23.7	377	3-D
MA-3	Ap	1	4	2	p			385	3-D
MA-3	Ap	1	4	3	p	-29	-19.2	385	3-D
MA-3	Ap	1	4	4	p			387	3-D
MA-3	Ap	1	4	5	p			385	3-D
MA-4	Ap	4	1	1	p		-11.4	191	3-D
MA-4	Ap	4	1	2	p		-11.9	276	3-D
MA-4	Ap	4	1	3	p	-29	-21.1	262	3-D
MA-4	Ap	4	1	4	p		-13.3	272	3-D
MA-4	Ap	4	1	5	p		-13.5	273	3-D
MA-4	Ap	4	2	1	p		-17.3	270	3-D
MA-4	Ap	4	3	1	p	-51	-18.2	283	3-D
MA-4	Ap	4	3	2	p	-51	-14.1	288	3-D
MA-4	Ap	5	1	1	p	-36	-8.1	286	3-D
MA-4	Ap	5	1	2	p	-37	-13.5	283	3-D
MA-4	Ap	5	1	3	p		-16.1	269	3-D
MA-4	Ap	6	1	1	p		-11.4	244	3-D
MA-4	Ap	6	1	2	p		-8.5	195	3-D
MA-4	Ap	9	1	1	p	-25	-18.2	260	3-D
MA-4	Ap	9	1	2	p		-12.7	268	3-D
MA-4	Ap	9	1	3	p			259	3-D
MA-4	Ap	9	2	1	p	-25	-9.0	257	3-D
MA-4	Ap	9	2	2	p		-9.9	266	3-D
MA-4	Cal	2	1	1	p			149	Isol
MA-4	Cal	2	2	1	p			179	Isol
MA-4	Cal	2	3	1	p			162	Isol
MA-4	Cal	2	4	1	p			177	Isol
MA-4	Cal	2	5	1	p			197	Isol
MA-4	Cal	2	5	2	p		-11.1	174	Isol
MA-4	Cal	2	6	1	p			172	Isol
MA-4	Cal	2	7	1	p			200	3-D
MA-4	Cal	2	7	2	p			140	3-D
MA-4	Cal	2	7	3	p		-4.7	257	3-D
MA-4	Cal	2	8	1	p			216	Isol
MA-4	Cal	2	9	1	p	-28	-10.1	209	Isol
MA-4	Cal	2	10	1	p	-25	-12.5	205	Isol

Table 2 (continued)

Sample	Min	Frag	Gr	No	Orig	Te (°C)	Tmi (°C)	Tdv (°C)	Descrip
MA-4	Cal	2	11	1	p	-28	-7.5	208	Isol
MA-4	Mtc	7	1	1	p		-19.6	342	3-D
MA-4	Mtc	7	1	2	p	-27	-18.4	352	3-D
MA-4	Mtc	7	1	3	p			331	3-D
MA-4	Mtc	7	1	4	p		-17.7	332	3-D
MA-4	Mtc	7	2	1	p	-30	-21.9	350	Isol
MA-4	Mtc	7	3	1	p			359	3-D
MA-4	Mtc	7	3	2	p			374	3-D
MA-4	Mtc	10	1	1	p		-17.2	376	3-D
MA-4	Mtc	10	1	2	p			388	3-D
MA-4	Mtc	10	2	1	p			379	Isol
MA-5	Ap	1	1	1	p			428	3-D
MA-5	Ap	1	1	2	p			418	3-D

Min: mineral; Frag: fragment; Gr: co-genetic group; No: number of inclusions;
 Orig: origin of inclusions; Descrip: description

APPENDIX III
RAW DATA FOR DECREPITATE ANALYSES

Table 1: Raw data for decrepitates and their host apatite.

Method	Sample	Dec	Compositions of decrepitate+mineral(wt. %)								
			Ca	Mg	Fe	K	Na	Si	P	S	Cl
			LV Inclusions								
SEM	MA4	1	38.7	0.02	n.a.	0.5	6.1	0.6	17.6	2.1	0.2
SEM	MA4	2	30.6	0.03	n.a.	1.0	11.6	0.7	15.9	5.4	0.1
SEM	MA4	3	29.6	0.05	n.a.	1.2	12.1	0.6	15.0	6.2	0.2
SEM	MA4	4	38.1	0.14	n.a.	0.3	5.8	1.1	17.1	2.4	0.0
SEM	MA4	5	24.5	0.06	n.a.	1.0	15.5	0.8	12.0	5.7	0.1
SEM	MA4	6	33.3	0.00	n.a.	0.5	5.3	1.0	16.5	1.9	0.0
SEM	MA4	7	25.4	0.00	n.a.	1.2	11.0	1.2	13.9	5.2	0.2
SEM	MA1	1	38.6	0.72	n.a.	0.8	2.8	2.6	18.5	0.3	0.6
SEM	MA1	3	24.6	0.00	n.a.	1.2	16.2	0.2	13.8	4.5	8.0
SEM	MA1	4	34.8	0.16	n.a.	0.9	6.1	1.0	17.4	2.2	2.2
SEM	MA1	5	39.4	0.00	n.a.	0.3	5.5	0.8	18.6	1.7	0.9
SEM	IS90-79	1	14.6	6.73	n.a.	12.9	9.4	0.2	7.1	0.9	23.9
SEM	IS90-79	2	21.6	0.04	n.a.	0.6	22.6	0.1	11.8	4.6	7.9
SEM	IS90-79	3	20.9	0.00	n.a.	3.0	19.7	0.2	10.6	6.0	8.8
EM	MA-4	1	22.5	0.00	0.03	2.9	13.1	0.5	7.0	1.2	6.0
EM	IS90-79	1	25.2	0.01	0.02	1.5	30.5	0.1	10.1	0.6	4.8
EM	IS90-79	2	31.6	0.01	0.05	0.4	11.1	0.2	11.3	0.5	1.4
EM	B12-1	1	12.5	0.00	0.02	7.3	15.6	0.4	5.9	4.7	0.9
EM	B12-1	2	29.2	0.00	0.00	2.0	7.5	0.5	7.2	2.1	1.1
	Average		28.2	0.42	0.02	2.1	12.0	0.7	13.0	3.1	3.5
	Std.		7.7	1.50	0.02	3.0	6.7	0.6	4.1	2.0	5.6
			LVH Inclusions								
SEM	IS90-69	1	16.9	0.12	n.a.	0.7	23.9	0.7	8.8	3.6	17.5
SEM	IS90-69	2	13.7	0.00	n.a.	0.1	27.5	0.5	7.3	6.8	11.5
SEM	IS90-69	3	27.1	0.00	n.a.	0.5	17.1	0.7	12.4	5.4	4.1
SEM	IS90-69	4	6.6	0.00	n.a.	0.8	32.3	0.3	3.3	6.4	24.3
SEM	IS90-69	5	34.3	0.00	n.a.	0.1	10.0	1.0	17.6	0.9	5.6
SEM	IS90-69	6	29.8	0.00	n.a.	0.5	13.7	1.0	14.7	3.8	3.8
SEM	IS90-69	7	33.2	0.10	n.a.	0.4	11.2	1.2	16.5	1.5	5.3
SEM	IS90-69	8	12.5	0.00	n.a.	1.4	27.5	0.4	6.0	8.2	12.2
EM	L91-5	1	28.6	0.03	0.01	0.3	15.7	0.7	10.8	1.3	0.1
EM	L91-5	2	28.6	0.04	0.23	0.4	15.4	0.5	10.1	1.4	0.0
EM	L91-5	3	25.6	0.18	0.22	0.8	17.5	1.6	8.5	3.7	0.1
EM	IS90-69	1	14.9	0.02	0.08	0.1	33.0	1.0	7.5	0.1	31.2
EM	IS90-69	2	31.7	0.01	0.01	0.2	5.1	0.8	10.3	0.3	0.0
EM	IS90-69	3	30.7	0.07	0.13	0.2	2.7	1.6	9.1	1.1	0.1
EM	IS90-68	1	28.1	0.03	0.21	0.8	7.3	2.0	11.7	1.2	0.1
EM	IS90-68	2	29.0	0.01	0.05	0.2	11.4	2.2	11.3	0.9	0.0
	Average		24.5	0.04	0.12	0.5	17.0	1.0	10.4	2.9	7.2
	Std.		8.3	0.05	0.09	0.4	9.1	0.6	3.6	2.5	9.4

Table 1 (continued)

Method	Sample	Dec	Compositions of mineral (%)								
			Ca	Mg	Fe	K	Na	Si	P	S	Cl
			LV Inclusions								
SEM	MA4	1	37.0	0.09	n.a.	0.3	0.5	0.8	18.6	0.0	0.2
SEM	MA4	2	37.0	0.09	n.a.	0.3	0.5	0.8	18.6	0.0	0.2
SEM	MA4	3	37.0	0.09	n.a.	0.3	0.5	0.8	18.6	0.0	0.2
SEM	MA4	4	37.0	0.09	n.a.	0.3	0.5	0.8	18.6	0.0	0.2
SEM	MA4	5	37.0	0.09	n.a.	0.3	0.5	0.8	18.6	0.0	0.2
SEM	MA4	6	37.0	0.09	n.a.	0.3	0.5	0.8	18.6	0.0	0.2
SEM	MA4	7	37.0	0.09	n.a.	0.3	0.5	0.8	18.6	0.0	0.2
SEM	MA1	1	44.5	0.00	n.a.	0.0	0.3	0.9	23.0	0.0	0.1
SEM	MA1	3	44.5	0.00	n.a.	0.0	0.3	0.9	23.0	0.0	0.1
SEM	MA1	4	44.5	0.00	n.a.	0.0	0.3	0.9	23.0	0.0	0.1
SEM	MA1	5	44.5	0.00	n.a.	0.0	0.3	0.9	23.0	0.0	0.1
SEM	IS90-79	1	43.6	0.13	n.a.	0.2	0.7	0.0	23.3	0.0	0.0
SEM	IS90-79	2	43.6	0.13	n.a.	0.2	0.7	0.0	23.3	0.0	0.0
SEM	IS90-79	3	43.6	0.13	n.a.	0.2	0.7	0.0	21.6	0.0	0.0
EM	MA-4	1	36.0	0.01	0.14	0.0	0.1	0.6	11.5	0.1	0.0
EM	IS90-79	1	38.6	0.03	0.03	0.0	0.2	0.0	13.6	0.0	0.0
EM	IS90-79	2	38.6	0.03	0.03	0.0	0.2	0.0	13.6	0.0	0.0
EM	B12-1	1	36.7	0.01	0.08	0.0	0.1	0.7	12.2	0.1	0.0
EM	B12-1	2	36.0	0.02	0.00	0.0	0.1	0.8	11.4	0.1	0.0
		Average	39.7	0.06	0.06	0.1	0.4	0.6	18.5	0.0	0.1
		Std.	3.5	0.05	0.05	0.13	0.21	0.34	4.13	0.04	0.1
			LVH Inclusions								
SEM	IS90-69	1	43.3	0.04	n.a.	0.4	0.5	1.3	21.6	0.0	0.2
SEM	IS90-69	2	43.3	0.04	n.a.	0.4	0.5	1.3	21.6	0.0	0.2
SEM	IS90-69	3	43.3	0.04	n.a.	0.4	0.5	1.3	21.6	0.0	0.2
SEM	IS90-69	4	43.3	0.04	n.a.	0.4	0.5	1.3	21.6	0.0	0.2
SEM	IS90-69	5	43.3	0.04	n.a.	0.4	0.5	1.3	21.6	0.0	0.2
SEM	IS90-69	6	43.3	0.04	n.a.	0.4	0.5	1.3	21.6	0.0	0.2
SEM	IS90-69	7	43.3	0.04	n.a.	0.4	0.5	1.3	21.6	0.0	0.2
SEM	IS90-69	8	43.3	0.04	n.a.	0.4	0.5	1.3	21.6	0.0	0.2
EM	L91-5	1	36.4	0.02	0.05	0.0	0.2	0.4	13.2	0.0	0.0
EM	L91-5	2	34.7	0.02	0.19	0.0	0.2	0.3	12.1	0.0	0.0
EM	L91-5	3	36.6	0.02	0.00	0.0	0.3	0.2	13.4	0.0	0.0
EM	IS90-69	1	32.3	0.02	0.01	0.0	0.3	0.8	12.7	0.1	0.0
EM	IS90-69	2	33.8	0.01	0.00	0.0	0.3	0.8	10.7	0.2	0.0
EM	IS90-69	3	32.6	0.18	0.03	0.1	0.1	1.4	9.2	1.1	0.0
EM	IS90-68	1	35.5	0.03	0.15	0.0	0.1	1.1	13.6	0.2	0.0
EM	IS90-68	2	34.6	0.01	0.10	0.0	0.2	1.0	12.0	0.2	0.0
		Average	38.9	0.04	0.07	0.2	0.3	1.0	16.8	0.1	0.1
		Std.	4.5	0.04	0.07	0.17	0.14	0.37	4.8	0.26	0.1

VITA AUCTORIS

PERSONAL DATA

Name: Weining Liu
Place of Birth: Nanning, P.R. China
Date of Birth: July 28, 1960

EDUCATION

Master of Science (Economic Geology/Geochemistry)
University of Windsor, Windsor, Ontario, Canada, 1990-92
Master of Science (Structural Geology/Economic Geology)
Kunming Institute of Technology, Kunming, China, 1982-84
Bachelor of Science (Geology)
Kunming Institute of Technology, Kunming, China, 1977-81

WORK HISTORY

Teaching and Research Assistant
University of Windsor, Windsor, Ontario, Canada, 1990-92
Lecturer
Kunming Institute of Technology, Kunming, China, 1985-88

PUBLICATIONS

- Liu, W., Samson, I.M. and Williams-Jones, A.E., 1992: Hydrothermal fluid evolution and LREE chemistry of apatites in the Oka carbonatite, Quebec. Annual Meeting of GSA, Abstract: Vol 24, No. 7, p210.
- Liu, W., Samson, I.M. and Williams-Jones, A.E., 1991: The nature of hydrothermal fluids in carbonatites: Evidence from primary fluid inclusions in apatite, Oka, Quebec. Annual Meeting of GSA, Abstract: Vol 23, No. 5, p148.
- Liu, W., and Liang, Y., 1988: The structural-geochemical characteristics of the Yunlong tin deposit, West Yunnan, China. *Geochimica*, No. 1, p62-68.